Elsevier Editorial System(tm) for Lithos
Manuscript Draft

Manuscript Number: LITHOS5851R1

Title: The P-Fe diagram for K-feldspars: a preliminary approach in the discrimination of pegmatites

Article Type: Regular Article

Keywords: K-feldspar, pegmatites, perthite, trace elements, LA-ICP-MS data, P-Fe diagram

Corresponding Author: Dr. Luis Sanchez-Munoz, PhD

Corresponding Author's Institution: CSIC

First Author: Luis Sanchez-Munoz, PhD

Order of Authors: Luis Sanchez-Munoz, PhD; Axel B Müller, Dr.; Sol López Andrés, Dra.; Robert F Martin, Prof.; Peter J Modreski, Prof.; Odulio De Moura

Abstract: Pegmatites are extremely coarse-grained and heterogeneous rocks in which quantitative measurements of mineral proportions and chemical compositions of the whole rock are virtually impossible to acquire. Thus, conventional criteria such as bulk compositions and modal mineralogy used for the classifications of igneous rocks simply cannot be applied for pegmatites. An alternative is to use the mineralogical and chemical attributes of K-rich feldspars, the only mineral that is omnipresent in pegmatites. We have used this approach to test a possible discriminant among four groups of pegmatites on the basis of major petrological features, such as the abundance of quartz, feldspars, micas and phosphates. Group I is represented by relatively flux-poor, and silica-poor pegmatites, in most cases with hypersolvus feldspars, devoid of quartz and with minor biotite, which are common in rift settings as in the Coldwell Alkaline Complex in northwestern Ontario, Canada. Group II comprises relatively flux-poor, silica-rich pegmatites with quartz, subsolvus feldspars and biotite as major primary minerals, typically occurring in the asymmetric collisional Grenville Orogeny. Group III comprises relatively flux-rich, silica-rich P-poor pegmatites with quartz, subsolvus feldspars, and muscovite as the major primary minerals. Finally, group IV consists of relatively flux-rich, silica-rich, P-rich pegmatites with the same previous major minerals as in group III but with abundant phosphates. Group III and IV are found in most symmetric collisional orogens, such as in the Eastern Brazilian Pegmatite Province as the result of the collision of cratons mainly formed by igneous and metamorphic rock of Archean and Early Proterozoic age. We have selected specimens of blocky perthitic K-rich feldspar from the inner part of thirty-one pegmatites belonging to these four categories occurring worldwide to cover a wide range of mineralogy, geological age, geotectonic setting and geographical positions. Concentrations of major elements (Si, Al, K, Na, Ca, Fe, Mg, Mn, Ti and P) were obtained by X-ray fluorescence (XRF), and those of minor and trace elements (P, Fe, Li, Ge, Ga, Rb, Sr, Ba, Tl, Pb, Y, Cs, Ba, La, Ce, Pr, Nd, Sm, Eu, Gd, Tb, Dy, Ho, Er, Tm, Yb, and Lu) were established by laser-ablation inductively coupled plasma - mass spectrometry (LA-ICP-MS), in areas free of coarse

Na-feldspar veins or patches. We show that the four groups have very different average values of the minor and trace elements. However, only the cations occupying tetrahedral sites, particularly the Fe and P, are sufficiently immobile to show distinct differences among pegmatites. Hence, we propose a P-Fe diagram to discriminate among the four groups of pegmatites, as a possible criterion with which to classify pegmatites.

Dear Editor

Pegmatites are extremely coarse grained and heterogeneous rocks in which quantitative mineral and chemical analyses of the whole rock can hardly be achieved. Thus, conventional criteria such as bulk chemistries and modal mineralogy used for the classifications of igneous rocks cannot simply applied for pegmatites. An alternative is the use of mineralogical and chemical features of feldspars, the only mineral that is omnipresent in pegmatites. We have made great efforts for sampling in fieldtrips and selecting “pristine” feldspars from well-known pegmatites around the world to do this work. Textural and chemical features are correlated in pegmatitic K-feldspars for the first time. It allows classifying pegmatites in four categories, by using the P-Fe diagram. We hope this work will be of interest for our entire community.

Best regards,

Luis Sánchez Muñoz

ICV-CSIC

Conflict of Interest Statement and Funding Source Declaration

We certify that there's no financial/personal interest or belief that could affect our objectivity, and no any other kind of potential conflicts with our work. We certify that all authors have seen and approved the final version of the manuscript being submitted. We warrant that the article is the authors' original work, hasn't received prior publication and isn't under consideration for publication elsewhere.

Luis Sánchez Muñoz

ICV-CSIC

Dear Editor-in-Chief and reviewers,

Thanks you very much for your comments and suggestions. We agree with most of your suggestions to improve our article, but not all of them. Below, we explain in detail what we have done. The new text is in green color in the new MS. Some figures and tables are now as Supplementary Materials, as suggested. In addition, an Electronic Appendix is included with an example for each specimen of the areas selected for LA-ICP-MS.

A) Comments from editor-in-chief

a) …. the data set is [are] relatively sparse, but that as a first stab at a new idea it is adequate.

OK, we have changed the title of the article and we have incorporated many comments indicating that this is a preliminary study.

b) … the availability of such data in the literature ….

Our article shows that the geochemistry of K-rich feldspar (with crypto- and micro-perthitic textures) and of Na-feldspar as large albite veins can be strikingly different. In other words, the main source of dispersion in data from bulk analyses in literature is a result of the lack of discrimination between the two different domains, as a result of dealing with pulverized samples. In addition, no data about the degree of alteration is included in literature, but it is clear that hydrothermal fluids do change the chemical compositions drastically. We have described now in the new MS the twin patterns and the perthitic texture in much more detail (with a new figure 2 and new text with reference to other articles in which these patterns are resolved) to demonstrate that we have performed selected-area laser-ablation inductively coupled plasma – mass spectrometry (LA–ICP–MS) analyses in parts of the specimen with a

pristine character. Finally, most chemical analyses in literature have been performed with totally different experimental techniques. The literature contains information on pegmatites of group IV, i.e., those pegmatites with an economic interest. Our results are totally compatible with these published data. Thus, we believe it inadvisable to compare the datasets in the literature with our results. We have been concentrated on a discussion of our own results. Note that these comments are also related to those of Reviewers 2, where he considers the petrography of the perthitic feldspars and the scale of the perthitic patterns, in order to have areas with perthite-free K-feldspar. To analyze perthite- free "K-feldspar" is almost impossible by conventional geochemistry techniques. The only thing we can do is to analyze "K-rich feldspar" with a pristine character. That is why Table 2 is very important. In the same way, Electronic Appendix 1 is now included to show an example of the selected-areas for LA–ICP–MS analyses carried out in all specimens.

c) Aside from the Fe–P diagram, most of the other trace element diagrams do not yield meaningful results. They could be eliminated with the simple statement that no meaningful distinctions were observed.

OK, only the Eu–Ce and Fe–P diagrams are used in the revised MS. Most of the chemical data and the diagrams with no discrimination are in Supplementary Materials.

d) One also wonders why does the Fe and P content of feldspars act as a discriminator.

This is explained in the paper, and it is related with the crystal structure of feldspars, because chemical elements in the framework tetrahedral T sites of the crystal structure are much more stable (i.e.,much lower rates of diffusion) than chemical elements in the cavity M sites. There are no other elements in such high concentrations as Fe and P that can be used as

discriminants. In addition, Fe and P can be correlated with lower continental crust and upper continental crust, respectively, as source materials.

e) Additionally have you considered elemental ratios which are often more useful than simple element comparisons?

In feldspars, elemental ratios are mainly used for alkali elements, like Rb/K, Cs/K, Rb/Cs, etc. We have found that alkali atoms are not stable in the crystal structure of the feldspars because of the ordering and twinning processes that develop during the subsolidus stage. Other ratios like those of the diagrams of Pearce et al. (1984) are based in statistical analysis to develop nice representations from the numerical point of view from bulk rocks, i.e., a mixture of minerals with very different geochemical signatures and different behaviors in terms of trace elements. Thus, the fields they obtain in those representations have no crystallochemical significance. In our case, we have tried to simplify as much a possible; we can do this as we work with a single mineral. Thus a simple linear relationship is found in a conventional log–log plot in the Eu–Ce and Fe–P diagrams, with crystallochemical significance, as both atoms are occupying the T sites of the structure and the two atoms will be lost more or less at the same rate with Si/Al ordering on cooling.

f) Comma between author names and year in citations frequently lacking. Other errors in citations. Please correct.

OK, thank you.

g) Random errors in References. Proof reading required.

OK, thank you.

h) Tables 4 - 9 should be submitted as supplemental electronic data tables.

We think that previous tables 4, 6, 7, 8 and part of table 9 could be as supplemental electronic data tables. However, the previous Table 5 (averages and pegmatite groups) and part of Table 9 (i.e., the Fe and P contents) could be in the main text, close to the figure of the P-Fe diagram (see Electronic Appendix 2).

i) To the key words add "P–Fe diagram"

OK, thank you.

B) Comments from Reviewer 1.

1. The classification of pegmatites into 4 Types may be too simplified to appeal to many pegmatologists as much of the established chemical characteristics of pegmatites is ignored.

OK, yes, our approach is very simplified, and much work has to be done now because pegmatites exhibit a huge mineralogical and petrological diversity. The main suggestion is to divide the NYF-LCT duality into four categories.

2. A lack of data to enable a statistical evaluation of the Fe-P diagram. There are only about 8 points for each field.

OK, we have changed the title and other parts of the paper to be considered only as a preliminary approach.

3.- Whether figures 2 and 3 a, b & c should be published. They are not at all useful in discriminating between pegmatite Types.

It is important to note that in literature most geochemical representations are related to chemical elements that substitutes the K atom in the crystal structure, i.e., the alkali and alkaline-earth elements. These types of correlations (new as Figure SM1) is what one can expect.

4. On page 13 & 14, specific examples of pegmatites would be helpful: African pegmatites of Grenville age, are typical LCT pegmatites, whereas the northeast American and south Scandinavian pegmatites of the same age are typical NYF bodies. Typical examples are most of the pegmatites of Minas Gerais in Brazil formed during the Braziliano Orogeny.

OK, examples are now cited in the new MS.

5. Table 3 is missing samples TM2, FB34, UL1 & ETT1.

OK, thank you, Table 3 now has been corrected. I cut the table unintentionally.

6. On Page 19 - I recommend removing the analytical data for the contaminated feldspars S5C5 & S10C12 that are contaminated with amphibole which certainly affects the Fe content and MMG2 which is contaminated with muscovite.

It is true than contamination exists in data from powder (bulk) X-ray fluorescence, but not that much in data from selected-area laser-ablation inductively coupled plasma – mass

spectrometry (LA–ICP–MS). We have now an Electronic Appendix 1 to show that the selected-area technique is useful to avoid this and other similar problems.

7. Note that only 31 samples are presented - not 32.

OK, thank you.

8. I recommend that that field (green on the plot) be eliminated from Figure 3d.

OK, the green field has been eliminated in the Eu–Ce diagram.

9. There are several errors in the references indicated on the manuscript.

OK, thank you very much for your help !!!!!

10. I recommend eliminating Figures 2 & 3a, b, & c. If they are not eliminated, the Y-axis labels must be enlarged - the exponents are too small.

OK, thank you. The Y-axis labels and exponents have been enlarged in these figures now in Supplementary Materials.

11. Figure 3d should have the green field eliminated as it is not defined by any data.

OK, the green field has been eliminated in the Eu–Ce plot.

12. It would be very desirable to show the error bars for figures 4 & 5.

OK, thanks, an error band is used in the figures.

13. In Table 3 - Only 27 feldspars are listed. Samples TM2, FB34, UI1, and ETT1 are missing. It would seem that twinning features of all of the feldspars analyzed should be listed in this table. Add description of samples TM2, FB34, UI1, and ETT1.

OK, thank you, now it is corrected.

14. In Table 4 CLM is incorrectly listed as CLM1. This needs to be corrected. Also 6 of the OrxAbyAnz values have apparent rounding errors and don't sum to exactly 100 - The value for sample TM2 is misreported.

OK, thank you, Table 4 is totally corrected.

C) Comments from Reviewer 2.

1. With only 32 samples from 29 localities it is also clear that this is a preliminary approach to a new classification method and that hundreds of analysis remain to be done before their conclusions are settled. To even approach that goal, a much more comprehensive database must be assembled. Tentatively 5-10 localities should be sampled at each pegmatite-field with a couple of samples from each pegmatite. However, that is a daunting task and It should be appreciated that the authors in this study has sketched a method that may be tested in future studies of granitic pegmatites throughout the world.

OK, *yes it is very simplified, and much work has to be done now because pegmatites exhibit a huge mineralogical and petrological diversity. The main suggestion is to divide the NYF–LCT duality into four categories. That is all. The main text has been modified to consider this comment in several parts. We have changed the title and other parts of the paper to be considered only as a preliminary approach. On the other hand, we have used the word "discrimination" more than "classification", as we did in the title of the first MS.*

2. The authors should have included literature data on P and Fe analysis of pegmatitic K-feldspar. Unless literature data are unavailable this is a serious shortcoming of the study. Probably P and Fe are normally analysed as major elements i.e. would be close to or below their respective LOD's and good data are unavailable? Did the authors check this potential source of data? If they did they should explain in the paper why they did not use this source of data; if not a literature search is required to see if data from elsewhere support their method. *As you can see in our article, the geochemistry of K-rich feldspars and N-feldspars can be extremely different. However, most of the information in the literature pertains to minor and trace elements; it has been acquired by means of bulk powdered samples. In addition, no data about the degree of alteration are included in literature. We know that hydrothermal and deuteric fluids change drastically the chemical compositions. We have described the twin patterns and the perthitic texture to demonstrate that we have performed selected-area laser-ablation inductively coupled plasma – mass spectrometry (LA–ICP–MS) analyses in parts of the specimen characterized by a pristine character. Finally, most chemical analyses in literature have been performed with totally different experimental techniques. The data in the literature are presented mostly for pegmatites of group IV, i.e., those pegmatites with an economic interest. Our results are totally compatible with these published data. Thus, we believe that it is inadvisable compare the datasets in literature with our results. Therefore, we have*

concentrated in "our paper" in the discussion of "our own results". This is not a lack of respect of the previous works.

3. TITLE - the title promises too much. The application of the P-Fe method to discriminate pegmatites is in its infancy, even after publication of this study. A sentence such as "a promising approach" "possible method" or similar should be added.
OK, *the title has been revised.*

4. PREVIOUS WORK - In the discussion of previous work, they refer to many studies including some on pegmatitic K-feldspar, however they should also refer to the quite successful applications of the quartz-chemistry in the classification and genetic interpretations of granitic pegmatites. Not least since the 2nd author, Prof. Axel Müller is involved in several such quartz studies.

OK, thank you. New comments about the applications of the quartz compositions in the classification and genetic interpretations of granitic pegmatites are now included.

5.- PETROGRAPHY - Not a single SEM-image of perthitic feldspar is included. This is a serious shortcoming of the paper. With an analytical area of 300 x 150 microns it must be difficult to find areas with perthite free K-feldspar let alone re-locating the areas for LA-analysis unless calibrated coordinate systems were used. Please document how this is accomplished and show SEM-images or similar to document the analytical approach. A comprehensive electronic appendix showing SEM- Microscope images of feldspar should also be included.

This is an extremely important comment. Most of the improvements of the previous MS have been done to give a consistent answer to this one, as perhaps readers can think in a similar way.

We never try to obtain chemical data from K-feldspars, but K-rich feldspars. That is why we present an extended section about petrography. In the new MS, this section is extended including also some SEM images. An analytical area of 300 x 150 micrometers is more than enough to discriminate pristine areas from those with important chemical changes associated to albite veins. Instead of an electronic appendix with those images, we prefer to explain to the readers in detail which are the "size scales of perthitic textures" by means of the new Fig. 2 and the Electronic Appendix 1, in which we present the optical images of the thick sections used in the LA–ICP–MS analyses. To analyze perthite-free "K-feldspars" is almost impossible by conventional geochemistry techniques, the only thing we can do is to analyze "K-rich feldspars" with a pristine character. The analyses of perthite-free "K-feldspars" have neither petrological significance nor usefulness when considering the conventional modern technology at present. What we do is to analyze areas of crypto- and microperthitic feldspars with pristine character, as exsolution took place in "isochemical condition" at the size of the laser probe. Problems related to the dispersion of data are related to albite veins and turbidity, not to fine perthitic textures (fortunately).

6.- With an analytical area that large the authors may as well analyze bulk feldspar to obtain the original feldspar compositions - that would probably produce more representative analysis and limit some of the scatter in the discrimination plots.

Unfortunately, bulk analyses from coarse perthitic K-rich feldspars like those from most pegmatites used in this article cannot be analyzed by this method, as our figures demonstrate, because of the scales of the perthitic intergrowths. But it is possible to discriminate between

the chemical composition mainly from pristine K-rich perthitic feldspars and from large albite veins with associated turbidity. This is more than enough, and is being done for the first time (as far as we know) with such large number of samples with extended pristine areas. That is why we should not compare our findings with published data. We wish to avoid comparing apples and oranges.

7. REE - ANALYSIS - how many samples are analysed for the REE? I get the impression that only 4 samples are included. This would be inadequate; if indeed they analysed all the samples then please show the REE spectrum for all the samples.

All samples have been analyzed for the REE, in the two parts, i.e., in the K-rich matrix and in the Na-feldspars veins. However, most experimental values are below the LOD. We have selected some examples in which we have determined a concentration high enough to represent the data as in the new Fig. SM2.

ABSTRACT

Pegmatites are extremely coarse-grained and heterogeneous rocks in which quantitative measurements of mineral proportions and chemical compositions of the whole rock are virtually impossible to acquire. Thus, conventional criteria such as bulk compositions and modal mineralogy used for the classifications of igneous rocks simply cannot be applied for pegmatites. An alternative is to use the mineralogical and chemical attributes of K-rich feldspars, the only mineral that is omnipresent in pegmatites. We have used this approach to test a possible discriminant among four groups of pegmatites on the basis of major petrological features, such as the abundance of quartz, feldspars, micas and phosphates. Group I is represented by relatively flux-poor, and silica-poor pegmatites, in most cases with hypersolvus feldspars, devoid of quartz and with minor biotite, which are common in rift settings as in the Coldwell Alkaline Complex in northwestern Ontario, Canada. Group II comprises relatively flux-poor, silica-rich pegmatites with quartz, subsolvus feldspars and biotite as major primary minerals, typically occurring in the asymmetric collisional Grenville Orogeny. Group III comprises relatively flux-rich, silica-rich P-poor pegmatites with quartz, subsolvus feldspars, and muscovite as the major primary minerals. Finally, group IV consists of relatively flux-rich, silica-rich, P-rich pegmatites with the same previous major minerals as in group III but with abundant phosphates. Group III and IV are found in most symmetric collisional orogens, such as in the Eastern Brazilian Pegmatite Province as the result of the collision of cratons mainly formed by igneous and metamorphic rock of Archean and Early Proterozoic age. We have selected specimens of blocky perthitic K-rich feldspar from the inner part of thirty-one pegmatites belonging to these four categories occurring worldwide to cover a wide range of mineralogy, geological age, geotectonic setting and geographical positions. Concentrations of major elements (Si,

Al, K, Na, Ca, Fe, Mg, Mn, Ti and P) were obtained by X-ray fluorescence (XRF), and those of minor and trace elements (P, Fe, Li, Ge, Ga, Rb, Sr, Ba, Tl, Pb, Y, Cs, Ba, La, Ce, Pr, Nd, Sm, Eu, Gd, Tb, Dy, Ho, Er, Tm, Yb, and Lu) were established by laser-ablation inductively coupled plasma - mass spectrometry (LA-ICP-MS), in areas free of coarse Na-feldspar veins or patches. We show that the four groups have very different average values of the minor and trace elements. However, only the cations occupying tetrahedral sites, particularly the Fe and P, are sufficiently immobile to show distinct differences among pegmatites. Hence, we propose a P-Fe diagram to discriminate among the four groups of pegmatites, as a possible criterion with which to classify pegmatites.

ABSTRACT

Pegmatites are extremely coarse grained and heterogeneous rocks in which quantitative mineral and chemical analyses of the whole rock can hardly be achieved. Thus, conventional criteria such as bulk chemistries and modal mineralogy used for the classifications of igneous rocks cannot simply applied for pegmatites. An alternative is the use of mineralogical and chemical features of feldspars, the only mineral that is omnipresent in pegmatites. We have used this approach to test a possible discrimination of pegmatites in four types based on major petrological features as the abundance of quartz, micas and phosphates. Type I is represented by relatively dry silica-poor pegmatites in most cases with hypersolvus feldspars, absent quartz and minor biotite, which are common in rift settings. Type II comprises relatively dry silica-rich pegmatites with quartz, subsolvus feldspars and biotite as major primary minerals, typically occurring in the asymmetric collisional Grenville Orogeny. Type III comprises relatively wet silica-rich P-poor pegmatites with quartz, subsolvus feldspars and muscovite as major primary minerals. And type IV consists of relatively wet silica-rich P-rich pegmatites with the same previous major minerals of type III but with abundant phosphates. Type III and IV are found in most symmetric collisional orogenies. We have selected blocky perthitic K-rick feldspars from the inner part of thirty-two pegmatites of these four types occurring worldwide to cover a wide range of mineralogy, geological age, geotectonic setting and geographical positions. Major elements (Si, Al, K, Na, Ca, Fe, Mg, Mn, Ti and P) were obtained by X-ray fluorescence (XRF), and minor/trace elements (P, Fe, Li, Ge, Ga, Rb, Sr, Ba, Tl, Pb, Y, Cs, Ba, La, Ce, Pr, Nd, Sm, Eu, Gd, Tb, Dy, Ho, Er, Tm, Yb, and Lu) by laser ablation inductively-coupled plasma mass spectrometry (LA-ICP-MS). It is shown that the four types have very different average values in the minor/trace elements. However, only cations occupying tetrahedral sites are stable to show distinct

differences between pegmatites, particularly the Fe and P contents. Hence, a P-Fe diagram is built up to discriminate the four types of pegmatites, as a possible criterion to classify pegmatites.

Graphical Abstract (for review)

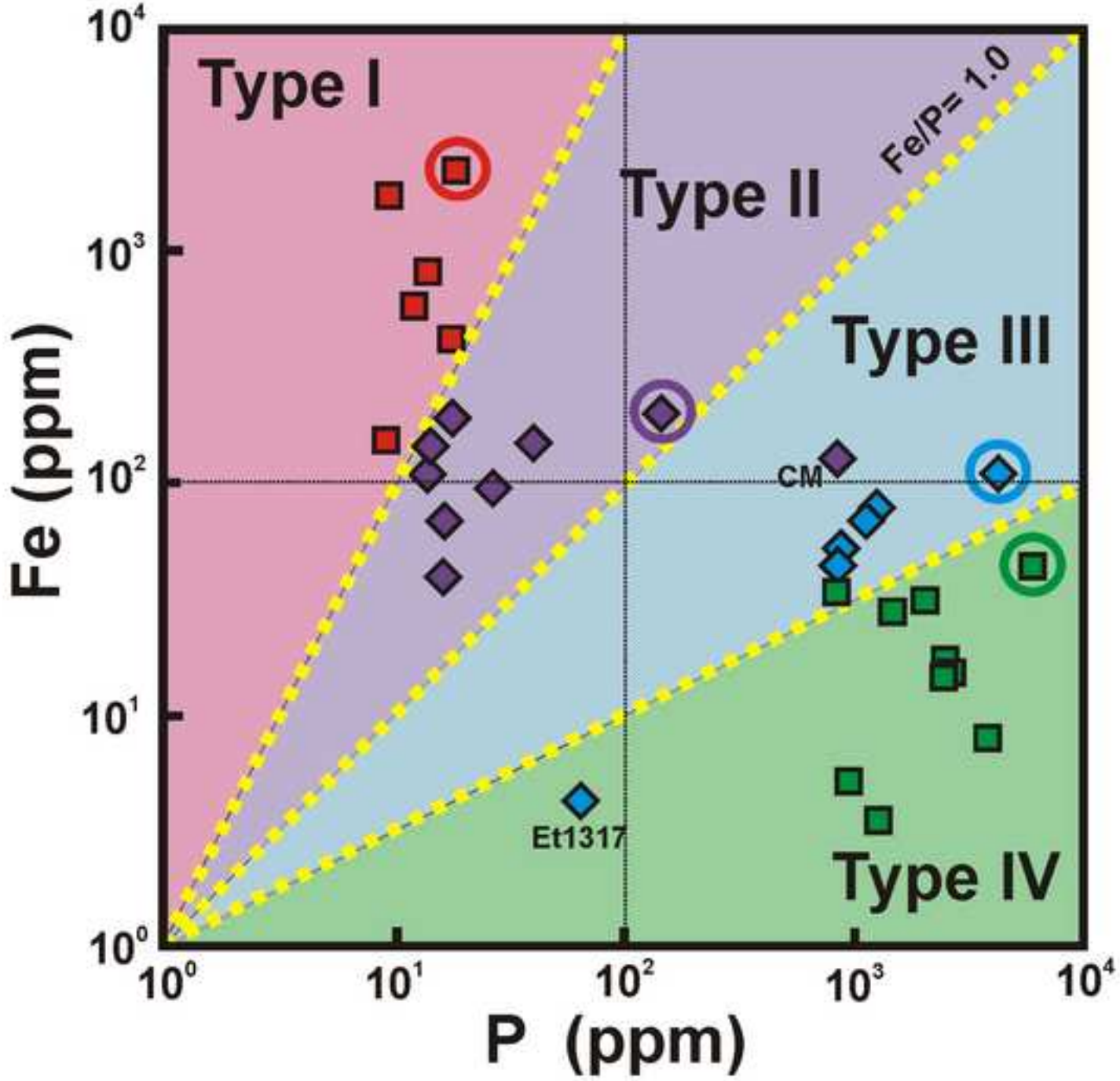

***Highlights (for review)**

Pegmatites can be classified using the geochemical features of K-feldspars.

Four general categories of pegmatites are described from the geological and mineralogical points of view.

The four categories of pegmatites can be represented in the P-Fe diagram of K-feldspars.

The P-Fe diagram of K-feldspars for the discrimination of pegmatites

Luis Sánchez-Muñoz[a]*, Axel Müller[b,c], Sol López Andrés[d], Robert Martin[e], Peter J. Modreski[f], Odulio J.M. de Moura[g]

[a] Instituto de Cerámica y Vidrio – CSIC, Madrid (Spain),*lsm@icv.csic.es

[b] Natural History Museum, University of Oslo (Norway),

[c] Natural History Museum, London (UK)

[d] Facultad de Ciencias Geológicas, Universidad Complutense de Madrid (Spain)

[e] Earth and Planetary Science, McGill University, Montreal, Quebec (Canada)

[f] U.S. Geological Survey, Federal Center Denver, CO 80225-0046 (USA)

[g] Governador Valadares, Minas Gerais (Brazil)

ABSTRACT

Pegmatites are extremely coarse grained and heterogeneous rocks in which quantitative mineral and chemical analyses of the whole rock can hardly be achieved. Thus, conventional criteria such as bulk chemistries and modal mineralogy used for the classifications of igneous rocks cannot simply applied for pegmatites. An alternative is the use of mineralogical and chemical features of feldspars, the only mineral that is omnipresent in pegmatites. We have used this approach to test a possible discrimination of pegmatites in four types based on major petrological features as the abundance of quartz, micas and phosphates. Type I is represented by relatively dry silica-poor pegmatites in most cases with hypersolvus feldspars, absent quartz and minor biotite, which are common in rift settings. Type II comprises relatively dry silica-rich pegmatites with quartz, subsolvus feldspars and biotite as major primary minerals, typically occurring in the asymmetric collisional Grenville Orogeny. Type III comprises relatively wet silica-rich P-poor pegmatites with quartz, subsolvus feldspars and muscovite as major primary minerals. And type IV consists

of relatively wet silica-rich P-rich pegmatites with the same previous major minerals of type III but with abundant phosphates. Type III and IV are found in most symmetric collisional orogenies. We have selected blocky perthitic K-rick feldspars from the inner part of thirty-two pegmatites of these four types occurring worldwide to cover a wide range of mineralogy, geological age, geotectonic setting and geographical positions. Major elements (Si, Al, K, Na, Ca, Fe, Mg, Mn, Ti and P) were obtained by X-ray fluorescence (XRF), and minor/trace elements (P, Fe, Li, Ge, Ga, Rb, Sr, Ba, Tl, Pb, Y, Cs, Ba, La, Ce, Pr, Nd, Sm, Eu, Gd, Tb, Dy, Ho, Er, Tm, Yb, and Lu) by laser ablation inductively-coupled plasma mass spectrometry (LA-ICP-MS). It is shown that the four types have very different average values in the minor/trace elements. However, only cations occupying tetrahedral sites are stable to show distinct differences between pegmatites, particularly the Fe and P contents. Hence, a P-Fe diagram is built up to discriminate the four types of pegmatites, as a possible criterion to classify pegmatites.

Keywords: K-feldspars, pegmatites, perthites, trace elements, LA-ICP-MS

1. Introduction

One of the challenges of studying any rock with a pegmatitic texture is the lack of information on bulk composition of an intrusive body owing to the exceptionally coarse grain-size and textural heterogeneity. For these reasons, conventional schemes of classification of igneous rocks using modal proportions or bulk compositions are not applicable. Furthermore, in the case of pegmatites of granitic composition, the intrusive bodies are commonly zoned vertically and horizontally, such that modal proportions of essential minerals may show extreme variability and thus significant departures from the bulk composition of the pegmatite-forming

magma. Yet there is an urgent need to classify granitic pegmatites, in order to properly assess their economic potential and the geological information they can provide, including the tectonic context of their emplacement.

Existing classifications are largely based on qualitative criteria applied mainly to mineralized pegmatites, and do not lead to broadly defined or accepted categories. After a brief review of these schemes of classifications, we present analytical results of representative alkali feldspar from 32 carefully evaluated pegmatite localities covering a wide range of mineralogy, age, geotectonic setting at the time of emplacement, and geographic position. These specimens have been characterized by selected-area chemical analysis using laser-ablation – inductively coupled plasma – mass spectrometry (LA–ICP–MS) in order to obtain the concentration of 33 minor elements in pristine areas of K-rich feldspar making up the blocky perthite from the voluminous intermediate zone of zoned bodies of granitic and syenitic pegmatites. Our simplified approach to a complex problem targets an essential mineral common to all pegmatites of granitic-syenitic composition, and yields several new insights that are useful to the geologist mapping uncharted territory in a pegmatite district. Our aim in this research is to test whether the trace-element signature of K-rich feldspar can be used as a measurable criterion for pegmatite discrimination, and to suggest elements that are best suited to accomplish this purpose.

2. Brief review of the literature

Because of the exceptionally large size of some crystal and an overall textural heterogeneity (London, 2014), conventional schemes of classification, for example using quantitative estimates of modal mineralogy plotted in QAP and APF diagrams, are not possible. Likewise, an approach based of bulk chemical composition plotted in a TAS diagram cannot

succeed. Several other criteria have been proposed. Index minerals have been applied, as well as characteristically enriched groups of elements, especially where tied in to tectonic setting, for example using the S-I-A-M classification of granitic suites (Simmons and Webber 2008). However, the recognition of key minerals commonly depends on the level of exposure in any zoned body of granitic pegmatite. Petrogenetic aspects and tectonic setting are difficult or impossible to evaluate from field observations, and their interpretation depends on current models, which evolve with time and increasing knowledge. Genetic classifications thus involve subjective criteria and interpretations. An easily and widely applicable classification should be based on objective (measurable) criteria only.

Most pegmatite investigators use a classification scheme based on the depth of pegmatite formation (pressure and temperature), inspired from the Russian literature (e.g., Ginsburg and Rodionov 1960, Ginsburg 1984) and refined by Petr Černý and collaborators (Černý 1991, Černý and Ercit, 2005). In addition to the depth-zone classification of pegmatite classes (abyssal, muscovite, muscovite rare element, rare element, and miarolitic classes), Černý (1991) established a geochemical subdivision of the rare-element class into three families: the Niobium–Yttrium–Fluorine (NYF), the Lithium–Caesium–Tantalum (LCT) and the mixed NYF–LCT family. Currently, however, the NYF–LCT subdivision has been applied to distinguish also pegmatites of the other four depth-zone classes. The family classification is more widely used than the depth-zone classification because it is useful for the study and description of pegmatites having an economic interest, enriched in Li, Be, Sn, Nb, Ta and gemstones. Basically, the family approach involves a bimodal approach for the discrimination between pegmatite-forming melts derived from the middle and upper crust (i.e., with an LCT geochemical signature) and melts

97 arising from melting in the lower crust, in some cases with mantle contributions (i.e., with the
98 NYF geochemical signature).
99
100 Numerous pegmatites have no temporal and obvious genetic relationship with a parental
101 pluton. In those cases, anatectic melts arising from ultrametamorphism in the deep crust can
102 evidently crystallize with a pegmatitic texture (Ercit 2005, Müller et al., 2012, Müller et al.,
103 2015). In addition, bodies of pegmatite may well exhibit features of both NYF and LCT suites,
104 with the LCT overprinting the NYF assemblages. Such an overprint is attributed to hydrothermal
105 activity involving an acidic fluid and contamination from the exocontact area (Martin and De
106 Vito, 2014). One must appreciate that not every mineral in granitic pegmatites crystallized from
107 a silicate magma; everything gets reworked to some degree after the magma has crystallized, and
108 especially so in large bodies.
109 It is important to note that many pegmatite occurrences do not contain rare minerals, and
110 a clear geochemical affiliation cannot be identified. Consequently, proposals for classification
111 have recently been suggested that focus on the rare elements and volatiles in addition to depth of
112 emplacement (Zagorsky et al. 2003), the geochemistry of micas and feldspars (Webber et al.
113 1999, Wise 2013), and the microtextural and microstructural characteristics of perthitic K-rich
114 feldspars (Marmo, 1971; Sánchez-Muñoz et al., 2011a). Note that feldspars are the only
115 constituents that occur in all occurrences of granitic pegmatite; quartz and micas can be absent.
116 Actually, the presence of “amazonite” (blue-green variety of K-feldspar) in pegmatites has been
117 considered a hallmark of pegmatites of the NYF family (Martin et al., 2008).
118 Although feldspars are heterogeneous minerals that are very sensitive to chemical
119 changes during the subsolidus and hydrothermal-deuteric stages, the bulk chemical composition

of feldspars is commonly used in the study of pegmatites. Previous studies have led to a better understanding of their variability, with applications in the exploration for rare elements (e.g., Alfonso, 2003; Černý et al., 1984; Černý et al., 1985; Larsen, 2002; London, 1990; London, 1992; Marchal et al., 2014; Müller et al., 2008; Neiva, 1995; Oyarzábal et al., 2009; Rhodes, 1969; Sánchez-Muñoz et al., 2011b, Shmakin, 1979; Shearer et al., 1985; Wise, 2013). However, most research has been done in pegmatites of the LCT affiliation, using a single province in many cases, in samples with rather limited microtextural and microstructural characterization, without consideration of location of the samples within zoned pegmatites, and in most cases using bulk data (from powdered samples) on the alkalis and the alkaline earths only.

3. The relation of pegmatites to orogenic and anorogenic settings.

The map in Figure 1 shows the distribution of the major pegmatite provinces and districts in the world. In most cases, these are spatially related to orogenic belts associated with areas of crustal convergence, i.e., a compressional regime. Granitic pegmatites can also form in environments marked by tectonic quiescence, i.e., an extensional regime. Most of the large and mineralized pegmatites are associated with collisional orogens. Pegmatite fields are lacking in non-collisional environments, as in the western part of the American continent and in the East of the Australian continent, because a thickened continental crust is needed to create the heat and pressure necessary for melt generation (e.g., Tkachev, 2011). In Figure 1, granitic pegmatites are mainly classified according to the conventional NYF–LCT bimodal approach, although some provinces and districts are known to have hybrid pegmatites. From this literature analysis and the field experience of the authors in many of these provinces, it was possible to distinguish four types of pegmatites (Table 1) to be discriminated by the mineralogical and geochemical

143 signatures of the perthitic K-rich feldspar. The identification of distinct features to distinguish
144 among bodies or groups of pegmatites is extremely challenging because exceptions are the rule.
145 However, the relative proportions of the major minerals can be used as starting point for
146 discrimination using only general "trends", to test our initial hypothesis (i.e., the usefulness of
147 mineralogical and geochemical features of perthitic K-feldspar for pegmatite discrimination).

148 The main distinction is based on the proportion of hydrous minerals in the pegmatitic
149 rocks. A first category, which we label "High-T, low-flux", consists of pegmatites with rare
150 micas or amphiboles (type I) and pegmatites that contain hydrous minerals (biotite) as minor
151 phases (type II). These are pegmatites derived from syenitic magmas, or hosted in granulitic
152 terranes without obvious genetic relationship to a parental pluton (anatectic pegmatites). Such
153 pegmatite-forming magmas are likely to have crystallized at a temperature largely above the
154 upper thermal stability of the ferroan hydrous phases, from a magma relatively poor in fluxing
155 components. A second category, which we label "Low-T, high-flux", consists of granitic
156 pegmatites that contain abundant micas (including muscovite). Two types are further
157 distinguished by the abundance and diversity of phosphate minerals, which are much higher in
158 type IV than in type III. This bimodal partition parallels the NYF–LCT approach, but it is not
159 based on geochemical affiliations or index minerals.

160 The silica-poor pegmatites of type I contain in most cases two feldspars that have a
161 hypersolvus texture (Tuttle & Bowen, 1958); biotite and fayalite are rare, whereas quartz is
162 absent in some cases. They are common in rift settings associated with syenites and nepheline
163 syenites, as well as anatectic melts in high-grade metamorphic terranes, without a clear genetic
164 relationship to a parental pluton (Table 1). Phosphates are very rare, in comparison with types III
165 and IV, although accessory apatite and monazite do occur.

166 The silica-rich pegmatites of type II consist of quartz, two feldspars that have a subsolvus
167 texture, and biotite as major primary minerals (Table 1). They are typically found in anorogenic
168 environments related to A-type granites, for example in the Grenville orogen of northeastern
169 North America and in southern Scandinavia. The Grenville orogen was a locus of repeated
170 collisions of two crustal blocks over the period 1400–1000 Ma, each followed by delamination
171 and extension accompanying the diapiric rise of an asthenospheric mantle (McLelland et al.
172 2010, Dickin et al. 2010). The same scenario applies to the Himalayas today. The juxtaposition
173 of hot fertile mantle undergoing decompression-induced melting below the lowermost of the
174 stacked crusts provided the setting for wholesale anatexis and production of relatively hot
175 granitic magma. As in type I, pegmatites generally cannot be genetically linked to a parental
176 pluton.
177 In contrast to type II, types III and IV are typically found in collisional orogens with a
178 symmetrical structure, initially as the product of subduction of an oceanic plate underneath a
179 thickened continental crust and ending with the collision of two continental cratons. The
180 resulting calc-alkaline magmas are metaluminous to peraluminous, and relatively oxidizing
181 except where the protolith is organic-matter-rich. The presence of a metasedimentary protoliths
182 is responsible for phosphate enrichment. Typical examples (Fig. 1) are the Grenville pegmatites
183 in Africa (Kokonyangi et al. 2006, Dewaele et al. 2011) and West Australia (Sheppard et al.
184 2007) derived from crustal peraluminous melts. Thus, the African pegmatites of Grenville age
185 are typical LCT pegmatites, whereas the northeast American and south Scandinavian pegmatites
186 of the same age are typical NYF bodies.
187 The silica-rich P-poor pegmatites of type III have quartz, subsolvus feldspars and
188 muscovite as major primary minerals, and minor phosphates. These pegmatites are commonly

189 formed during the late- to post-orogenic relaxation in an extensional environment, typically in
190 the form of long and regular tabular bodies.
191
192 Type IV is similar to type III but is rich in phosphates (Table 1). High-phosphorus
193 pegmatites typically develop via fractionation from voluminous granitic melts formed by melting
194 of a thick crust in a syn- to late-orogenic setting. Typical examples are most of the pegmatites of
195 Minas Gerais in Brazil formed during the Braziliano Orogeny (Pedrosa-Soares et al. 2011).
196 (Table 1. Main features of the four types of pegmatites used in this work.)
197
198 **4. Experimental procedure**
199 *4.1. Samples*
200 Fresh megacrystic (blocky) perthitic K-rich feldspar samples were taken from the
201 intermediate zone of selected pegmatite bodies of the four defined pegmatite types, having
202 distinct (001) and (010) cleavages. Table 2 provides details about the origin of the investigated
203 samples. As the content of impurities of feldspars changes from border to core in zoned bodies of
204 pegmatites, only blocky feldspars from the intermediate zone was sampled, in order acquire
205 comparable data.
206 (Table 2. Selected pegmatites, sample codes and some important geological features.)
207
208
209 *4.2. Methods.*
210 *4.2.1. Polarized light optical microscopy (PLOM).*
211 The feldspar samples were studied using surface-polished thin sections of 30 and 300 μm
212 thickness mounted on standard glass slides parallel to the (001) cleavage. Surfaces were polished
213 up to an average roughness Ra value less than 0.5 □m. A Nikon Eclipse LV100 POL was used,

using 1x to 100x objectives that allow observations at five orders of magnitude in the same petrographic preparation, from 10-2 to 10-7 m. Pristine areas without turbidity (i.e., fluid and mineral inclusions, e.g., clay minerals from deuteric and hydrothermal alterations) were selected and marked for the in situ trace-element analyses by LA-ICP-MS. The detail of the experimental procedure for textural and microtextural characterization of the samples can be found in Sánchez-Muñoz et al. (2012).

4.2.2. X-ray fluorescence (XRF).

The concentrations of major elements (Si, Al, K, Na, Ca, Fe, Mg, Mn and Ti) were established at the Technical Assistance Center in Earth Science Research of the Complutense University (Madrid, Spain) using a Bruker S2 Ranger energy-dispersive X-ray fluorescence (EDXRF) spectrometer equipped with a Pd anticathode X-ray tube of 50 W in a vacuum atmosphere. Sample preparation was made by the flux-fusion technique with 10 g flux [mix of $Li_2B_4O_7$ (99.5%) and LiI (0.5%)] and 0.5g sample at 1050ºC (maximum temperature), and pressed cylindrical pellets of 4 cm in diameter (9.5 g of dry sample and 0.5 g of Hoechst wax C micropowder as binding agent). Quantification was made by the software provided with the equipment (Spectra Plus/Bruker AXS) through empirical calibration of the system, by using six certified reference materials (NCS DC 71313, FKN, GA, GH, NIM-G and SY3). The limits of detection (%) of the analyzed elements are: SiO_2 0.23 and Al_2O_3 0.05 to fused beads, and Fe_2O_3 0.007, MnO 0.01, MgO 0.02, CaO 0.02, Na_2O 0.02, K_2O 0.03, TiO_2 0.01 and P_2O_5 0.003 to pressed cylindrical pellets. The chemical compositions was expressed as OrxAbyAnz (x+y+z = 100) (Table 4), with Or, Ab and An expressing the molar content of $KAlSi_3O_8$, $NaAlSi_3O_8$ and $CaAl_2Si_2O_8$ components.

4.2.3. Laser-ablation inductively coupled plasma mass spectrometry (LA-ICP-MS).

The analyses were performed at the Geological Survey of Norway, Trondheim (Norway) on the double-focusing sector field mass spectrometer, model ELEMENT XR, from Thermo Scientific, which is combined with the excimer-based NewWave UP193FX laser probe. The analyses were done on the 300-μm-thick sections. The 193-nm laser had a repetition rate of 20 Hz, a spot size of 75 μm, and an energy fluence of 5.5 to 6.5 mJ/cm2 on the sample surface. A continuous raster ablation (laser speed 15 μm/s) on an area of approximately 300 × 150 μm was applied. For each sample, two analyses of the K-feldspar matrix and one of the Na-rich feldspar in the veins of the perthite intergrowth were carried out. The isotope 29Si was used as the internal standard, applying the concentration of Si determined by XRF. An Ar blank was run before every sample and standard measurement to determine the background signal. In order to avoid memory effects between samples, the background signal was subtracted from the instrumental response of the standard before normalization against the internal standard. External multistandard calibration was performed using five silicate glass reference materials produced by the National Institute of Standards and Technology, USA (NIST SRM 610, 612, 614, 616, 1830) and the certified reference material silica glass BCS CRM 313/1 from the Federal Institute for Material Research and Testing in Germany. Certified, recommended, and proposed values for these reference materials were taken from Jochum et al. (2011), Flem and Bédard (2002) and from the certificates of analysis where available. The limits of detection (LOD) are based upon 3x standard deviation (3σ) of 10 NIST SRM 616 measurements. The LODs for the individual elements are: Li 0.14 ppm, P 5.01 ppm, Fe 0.88 ppm, Ga 0.26 ppm, Ge 0.04 ppm, Rb 0.02 ppm, Sr 11.46 ppm, Y 0.01 ppm, Cs 0.01 ppm, Ba 0.53 ppm, La 0.012 ppm, Ce 0.007 ppm, Pr 0.004

ppm, Nd 0.009, Sm 0.009, Eu 0.004 ppm, Gd 0.009 ppm, Tb 0.005 ppm, Dy 0.007 ppm, Ho 0.008 ppm, Er 0.004 ppm, Tm 0.005 ppm, Yb 0.009 ppm, Lu 0.006 ppm, Tl 0.006 ppm, and Pb 0.16 ppm. Data provided in Tables 6 to 9 represent a single value for Na-feldspar veins and the average of two analyses for K-feldspar in each sample.

5. Petrographic features

The microstructures developed resulting from the monoclinic-to-triclinic inversion and recrystallization-induced twinning in the K-feldspar and the perthitic microtextures resulting from K–Na exsolution for the four categories of pegmatite s are shown in Table 3. The nomenclature employed to describe the twin patterns and to identify microcline and orthoclase using Raman spectra measured directly on the thin sections is explained in detail in Sánchez-Muñoz et al. (2012).

Pegmatite bodies of category I typically show first-generation twins of microcline, and albite veins in a wide range of sizes. Albite in fine mesoperthitic microtextures only occurs in the hypersolvus feldspars of this type, i.e., in specimens S5C2, S10C12 and FH1. Extremely coarse veins of albite in large mesoperthitic textures, visible with the naked eye, occur in sample TL from Perth (Ontario, Canada), i.e., the type locality of perthite.

First-generation twins in tartan and parquet configurations in microcline are the most common feature in pegmatite bodies of category II. These configurations commonly involve irrational twins, as well as diffuse cross-hatched microstructures. In some cases, one can observe several microtextures resulting from the recrystallization of Albite- (A) and Pericline- (P) twinned microcline to single-orientation microcline. All examples studied in this category exhibit a subsolvus texture, in which perthitic grains contain albite veins narrower than 100 μm, as well

as thin films of albite. Residual orthoclase with an intermediate degree of local order can be found in this group, as for instance in specimen WC1.

Single-orientation microcline is the most characteristic microstructure in pegmatites of category III, as well as intermediate steps in achieving to that pattern. The perthitic textures often consist of albite veins of variable from a few micrometers to tens of micrometers in width. Orthoclase can be found in cases, specifically where the K-rich feldspar s of this category has a relatively high content of phosphorus, as in specimen MMG2.

The twin patterns of microcline in pegmatites of category IV are extremely variable, but single-orientation microcline has not been found in any case. Orthoclase is common in these pegmatites, mainly because of chemical effect of impurities as kinetic hinderers, mainly phosphorus (Sánchez-Muñoz et al. 2012). Second-generation twins that arise by recrystallization and directed coarsening of the first generation of twins from interfaces between the K-feldspar matrix and albite veins are very common. Perthitic textures trend to be bimodal in size, having fine films that are well preserved if orthoclase is not recrystallized in to microcline. The development of recrystallization units from interfaces involves albite films with zigzag interfaces (serrated albite) related to mechanical polysynthetic A± twinning arising from tectonic stresses. Large veins from coalescence of albite are the most common feature, often having also last stages of coarsening resulting from interactions with fluids migrating along interfaces, giving rise to a patch morphology.

(Table 3. Petrographic features of samples selected by PLOM observations.)

6. Bulk geochemistry

The 32 samples consist of K-rich feldspar with a perthitic texture. There is thus a greater proportion of K-feldspar than of Na-feldspar in the bulk, except in samples S5C5 and S10C12,

where there is a greater proportion of the sodic component. These samples are also rich in inclusions of amphiboles that could not be separated when preparing the powders for bulk chemical analysis, resulting into a high Fe_2O_3 content. Most of the other samples have Na_2O content between 2 and 3 % wt. Samples with Na_2O lower specimen Et1317, than approximately 2.2 wt.%, such as specimen Et1317, do not have large veins of albite, a typical characteristic of K-rich feldspar of post-orogenic granites (Marmo 1971). In sample MMG2, the high Al_2O_3 value is caused by the presence of many fine inclusions of muscovite that cannot be separated. Data have been normalized to give a total of 100%.

(Table 4. Bulk chemical analyses of the thirty-two samples by XRF (wt. %))

7. Minor and trace elements

The structure of alkali feldspars consists of three-dimensionally linked SiO_4 and AlO_4 tetrahedral units. There are four spectroscopically non-equivalent tetrahedrally coordinated (T) sites in each ring of tetrahedra, which are arranged in double crankshaft chains (Taylor, 1965). The alkali A^{+} and alkaline earth A^{2+} elements are located at the M sites inside the irregular cavity formed by the framework of tetrahedra; these ensure local electrostatic neutrality forming medium-range order schemes (Sánchez-Muñoz et al., 2013). The Si and Al atoms of the framework sites can be replaced by other 5+, 4+ and 3+ cations, such as Ga^{3+}, Ge^{4+}, P^{5+} and Fe^{3+}, during crystallization of the magma. Their concentration in the feldspar will reflect the availability of these elements in the pegmatite-forming magma and the relevant partition-coefficients. Similarly, K and Na atoms of the cavity M sites can be occupied by other 1+, 2+ and 3+ cations as Li^{+}, Rb^{+}, Cs^{+}, Tl^{+}, Sr^{2+}, Ba^{2+}, Pb^{2+} and rare-earth elements as REE^{3+}, except for europium, that in reducing conditions can be present as Eu^{2+}.

When *averaged values* of the four categories of pegmatites are considered, the chemical characteristics of the four groups are found to be very different (Table 5). Lithium, Rb, Cs, Tl, Ge and P increase in concentration from categories I to IV, whereas Sr, Eu and Fe exhibit the contrary trend. Barium peaks in category II, and its concentration is higher in category I than in III and IV, a behaviour also found in Ga, Y, La and Ce. Lead also peaks in category III, but its concentration is higher in categories III and IV than in I. Thus, the coherent pattern of distribution of these elements indicates that the selection of samples and pegmatites was appropriate to attain our objectives.

(Table 5. Average values of minor and trace elements in ppm and ppb (only for Y, La, Ce and Eu) of the K- and Na-feldspars in the types of pegmatites by LA-ICP-MS.)

7.1. The M-site cations

Figure 2a shows correlations between the Rb content and other 1+ elements occupying the M sites of K- and Na-feldspars (Table 6). A tight linear relationship is found in the Rb-Tl diagram for K-rich feldspars, which becomes broader but still linear in the case of the Rb-Cs plot. The correlation is weakly developed in the Rb-Li graph. The fields are not well defined, and thus these diagrams are not useful for the discrimination of pegmatites. The contents of these elements in the albite veins of the perthitic microtexture are in most cases much lower than values in the K-feldspar matrix, indicating that important chemical changes must occur during exsolution and later growth of the albite veins. This effect is particularly strong in specimen TL1, with albite veins up to 2 mm thick, and also in specimens NH1, CM3, TC and BK2.

(Table 6. Alkalis and thallium contents in K- and Na-feldspars (ppm) by LA-ICP-MS.)

Figure 2b exhibits the correlation of Rb and 2+ elements also present at the M sites of the K-feldspar fraction (Table 7). In contrast to the Rb-A^{+} plots, no well-defined trend can be

observed. In addition, there are no separate fields that would allow a distinction of the four categories of pegmatites. Because of the high detection limit of Sr (11.5 ppm), the Rb-Sr plot not of much use. Moreover, the contents of these elements in the Na-feldspar do not follow any particular behavior. In many cases, these elements are lost with albite formation, particularly in samples TL1 and CM3, as was found to be the case with the alkalis.

(Table 7. Alkaline earth and lead contents in K- and Na-feldspars (ppm) by LA-ICP-MS)

7.2. Rare-earth elements

Rare-earth elements are allocated to the M sites of the structure (Zhang et al. 2009). Although La, Ce, Pr, Nd, Sm, Eu, Gd, Tb, Dy, Ho, Er, Tm, Yb, and Lu were sought in all samples, only Y, La, Ce and Eu have concentrations sufficient to be measured with the equipment used, particularly in feldspars of category I and II pegmatites (Table 8). Interestingly, the REE are mainly concentrated in the Na-feldspar of the albite veins in the perthitic microtexture, as shown in the REE patterns (Fig. 3). The highest contents in most of these elements are encountered in pegmatites of category I; these exhibit a pronounced Eu anomaly (Fig. 3a). Only in one sample (specimen LL1 from the Lone Lode pegmatite in the Pikes Peak, Colorado, USA) there is a sufficiently high concentration in the two feldspars to compare their REE patterns. In this case, the total REE content is higher in the K-rich feldspar, but its positive Eu anomaly is lower than in the Na-feldspar (Fig. 3b), and these anomalies are lower than in the sample C5S5 from a pegmatite ~~s~~ of category I. Figure 3c illustrates an example of a REE pattern in a category-III pegmatite, where no Eu anomaly is found, and a very low total REE content is recorded. In most samples of category-IV pegmatites, the concentration of REE is below the limit of detection.

With these data, it is possible to represent the variability among the categories of pegmatite as shown in Figure 3d. In this graph, where Eu and Ce contents have the same scale, three fields represent well the different geochemical affiliations. Pegmatites of category I exhibit Eu > Ce (pink field in Fig. 3d), in contrast to pegmatites of category II, where in most cases, Eu is less than Ce (violet field in Fig. 3d). Similar REE contents to pegmatites of category II have been found in K-feldspar from the Evje-Iveland and Froland pegmatite fields in southern Norway (Larsen, 2002). Only certain samples from pegmatites of category III have a sufficient content of these elements to be represented in the green field (Fig. 3d).

(Table 8. Rare-earth elements contents in K- and Na-feldspars (ppb) by LA-ICP-MS)

7.3. The T-site cations

Figure 4 shows the measured concentrations of Ga and Ge in K-feldspar, using a plot with the same values for both axes, and Table 6 has the numerical values. The Ge-Ga graph shows that pegmatites of category I can be clearly discriminated from the other types because they show a lower content in Ge. The pegmatites of category II can be distinguished only partially from the pegmatites of categories III and IV (the two groups of LCT pegmatites) by means of the ratio Ga/Ge. Note that in contrast with the behaviour of the M cations (including REE), there are no sharp differences in most cases between the values of the K-feldspar matrix and the Na-feldspar veins. The implication is that these elements remain where they are during the subsolidus transformations (Si–Al ordering, transformation twinning and recrystallization twinning, as described in Sánchez-Muñoz et al., 2012).

In sharp contrast with the previous graphs, the P-Fe plot of K-feldspars (Fig. 5) shows a very good discrimination between the four categories of pegmatite (see Table 9 for numerical

values). The plot is constructed using the same log scale for both elements. The transversal line expressing a Fe:P ratio equal to 1.0 perfectly separates the NYF pegmatites (category I in pink and II in violet) from the LCT pegmatites (category III in blue and IV in green). The only exception is sample CM3 from the Climax Mica pegmatite (sample CM, Fig. 5), which contains rare-earth minerals and a strongly peraluminous character having unusual large masses of cordierite (Heinrich, 1950) and abundant secondary muscovite (Hanley et al., 1950). Pegmatites of categories I and II are separated by a line starting at the origin (at a concentration of 1 ppm in the two cations) and ending at P = 10^2 ppm and Fe = 10^4 ppm. In the same way, pegmatites of categories III and IV can be separated by a similar line starting at the same point and ending at P = 10^4 ppm and Fe = 10^2 ppm, with an exception in sample Et1317 from East Transbaikalia (Russia), where extensive recrystallization caused single-orientation microcline to form (PLOM observations).

(Table 9. Ge, Ga, Fe and P contents in K- and Na-feldspars (ppm) by LA-ICP-MS)

8. Implications

Figure 5 shows that the four categories of pegmatite that we have defined can be discriminated using the contents of P and Fe. Any pegmatitic body thus can presumably be classified with this graph, independently of index minerals or the mineralization and economic potential (see Dill, 2015 for a recent review about the ore geology of pegmatites). Thus a purely petrochemical classification seems to be possible. This type of diagram is common in the geological literature, e.g., the discrimination diagrams used to infer the tectonic setting of granitic rocks, but the resulting shape and distribution of the chemical fields in plots are difficult to interpret, as they result from statistical studies from a data bank (Pearce et al. 1984). In our approach, we have selected a few representative pegmatites to obtain high-quality trace-element

data by selected-area chemical analyses of pristine regions of K-rich feldspar using LA-ICP-MS. Thus, conventional crystallochemical concepts can be employed to interpret the resulting radial fields of Figure 5.

Starting from the high-temperature crystallization of a pegmatite-forming melt, the first-formed alkali feldspar at the magmatic stage is sanidine, a disordered solid-solution with a composition close to $(Na,K)AlSi_3O_8$ that incorporates others cations in the framework T and cavity M sites as "chemical impurities". Goldsmith (1953) explained the crystallization with the Ostwald's rule of stages, i.e., the highest simplexity or most disordered stage should be the most easily formed from a random liquid system. In this initial step, the concentration of the minor and trace elements in feldspars depends mainly on their concentration in the melt, as well as on pressure, temperature and oxygen fugacity at the time of crystal growth.

However, as temperature decreases after emplacement, the feldspar system evolves to more equilibrated configurations by means of several processes, including atomic ordering, phase separation and impurity exclusion. The transformation and recrystallization affecting the sanidine solid solution to produce orthoclase or microcline (or both) and albite (Sánchez-Muñoz et al., 2012, 2013) involves a drastic decrease in the concentration of impurities. Thus, in most cases, orthoclase has a higher content of minor and trace elements than microcline in the same group of pegmatites, as shown by a circle in Figure 5. The trend shown by samples of each population trending toward the origin in the diagram can be explained as a progressive loss of impurities with its recrystallization of A± and P± twinned microcline first and the development of single-orientation microcline at later subsolidus stages.

Consequently, the concentrations that we measure in the feldspars are the result of two effects: the composition of the original melt, which depends on the source lithologies (upper

463 mantle, lower crust, upper crust), and the extent of recrystallization, which mainly depends on
464 the tectonic setting and local geological conditions as cooling rate, directed stresses [see Černý et
465 al. (2012) and Martin and De Vito (2005) for detailed discussions]. The K-feldspar records self-
466 organized non-equilibrium twin patterns at the subsolidus stage and ambient physical conditions
467 in each tectonic setting (Sánchez-Muñoz et al., 2012). It is clear that the original chemical
468 signatures involving the framework (T) sites are not totally released. However, when
469 hydrothermal and deuteric fluids interact with feldspars, dissolution-recrystallization phenomena
470 occur by catastrophic processes, typically at the last stages of vein perthite formation, to give
471 patches. Drastic chemical changes are likely to occur, as commonly seen in bulk compositions of
472 weathered feldspars in fine-grained granitic rocks.
473
474 **9. Conclusions**
475 Because of the large size of crystals and the exceptional textural heterogeneity of
476 pegmatites, it is not possible to use the standard methods of classification in petrology, like
477 modal mineralogy and bulk chemical compositions. An alternative approach is to use the
478 geochemical features of K-feldspar, an omnipresent mineral in pegmatites, to discriminate
479 among different types, having well-defined petrological features. With this objective, we have
480 selected 32 samples of blocky feldspar s from pegmatites that can be grouped into four different
481 categories according to the amount of hydrous minerals, the presence or absence of quartz, and
482 the abundance and variability of phosphates minerals (Table 1). The trace-element diagrams
483 based on cations at M sites (M vs M and M vs T) were found to be useless to discriminate among
484 the four categories in spite of average values in each population that are different. Elements
485 located at M site are easily released from the mineral structure during the subsolidus and

hydrothermal-deuteric stages. However, the T vs T plots are useful to represent different pegmatites in well-separated fields, as the T cations are much more firmly held in the structure. Specifically, the P–Fe graph, with four radially distributed fields, is found to be very useful in the division of four previously defined categories of pegmatite. Therefore, this methodology could be useful to help place the classification of pegmatites on a more objective basis than has been possible so far.

Acknowledgements

We thank B. Ronald Frost from University of Wyoming (Laramie, WY, USA) for his assistance in field works for sampling of Funny Hill pegmatite (specimen FH1) in Wyoming used in this work, to Victor Ye. Zagorsky (1942-2015) and V.M. Makagon from Vinogradov Institute of Geochemistry (Irkutsk, Russia) for samples ZAG and Et1317. We thank projects MAT2013-48009-C4-1-P, MAT2013-46452-C4-2-R, and CAM S2013/MIT-2753 for partial financial support.

References

Alfonso, P., 2003. Geochemistry of feldspars and muscovite in granitic pegmatite from Cap de Creus Field, Catalonia, Spain. The Canadian Mineralogist 41, 103-116.

Beurlen, H., Da Silva, M.R.R., Thomas, R., Soares, D.R., and Olivier, P., 2008. Nb–Ta–(Ti–Sn) oxide mineral chemistry as tracer of rare element granitic pegmatite fractionation in the Borborema Province, Northeastern Brazil. Mineralium Deposita 43, 207-228.

507 Beurlen, H., Thomas, R., Rodrigues da Silva, M.R., Müller, A., Rhede, D., Soares, D.R., 2014.
508 Perspectives for Li- and Ta-mineralization in the Borborema pegmatite province, NE-Brazil: A
509 review. Journal of South American eath Sciences 56, 110-127.
510 Černý, P., Smith, J.V., Mason, R.A., Delaney, J.S., 1984. Geochemistry and petrology of
511 feldspar crystallization in the Vezna pegmatite, Czechoslovakia. The Canadian Mineralogist 22,
512 631-651.
513 Černý, P., Mintzer, R.E., Anderson, A.J., 1985. Extreme fractionation in rare-element granitic
514 pegmatites: selected examples of data and mechanisms. The Canadian Mineralogist 23, 381-421.
515 Černý, P. 1991. Fertile granites of Precambrian rare-element pegmatite fields: is geochemistry
516 controlled by tectonic setting or source lithologies? Precambrian Research 51, 429-468.
517 Černý, P., Ercit, T.S., 2005. The classification of granitic pegmatites revisited. The Canadian
518 Mineralogist 43, 2005–2026.
519 Černý, P., London, D., Novak, M., 2012. Granitic pegmatites as reflections of their sources.
520 Elements 8, 257–261.
521 Dewaele, S., Henjes-Kunst, F., Melcher, F., Sitnikova, M., Burgess, R., Gerdes, A., Alonso
522 Fernandez, M., De Clercq, F., Muchez, P., Lehmann, B. 2011. Late Neoproterozoic overprinting
523 of the cassiterite and columbite-tantalite bearing pegmatites of the Gatumba area, Rwanda
524 (Central Africa). Journal of African Earth Sciences 61, 10–26.
525 Dickin, A.P., McNutt, R.H., Martin, C., Guo, A. 2010. The extent of juvenile crust in the
526 Grenville Province: Nd isotope evidence. GSA Bulletin 122, 870-883.
527
528 Dill, H.G., 2015. Pegmatites and aplites: Their genetic and applied ore geology. Ore Geology
529 Reviews 69, 417-561.

530 Ercit, T.S., 2005. REE-enriched granitic pegmatites, in: Linnen, R.L., Samson, I.M. (Eds.), Rare-
531 element geochemistry and mineral deposits. Geological Association of Canada, GAC Short
532 Course Notes 17, pp. 175-199.
533 Fanton J.J., Arioli E.A., Moura O.J.M., 1978. Pegmatitos da região de Galiléia-Mendes Pimentel,
534 MG. In: SBG, Anais do XXX Congresso Brasileiro de Geologia, Recife, 1770-1781.
535 Flem B., Bédard L.P., 2002. Determination of Trace Elements in BCS CRM 313/1 (BAS) and
536 NIST SRM 1830 by Inductively Coupled Plasma-Mass Spectrometry and Instrumental Neutron
537 Activation Analysis. Journal of Geostandards and Geoanalysis, 26, 287-300.
538 Galliski, M.A., Márquez-Zavalía, M.F., Martínez, V., Roquet, M.B., 2011. Granitic pegmatites
539 of the San Luis ranges. Field Trip Guidebook, 5th International Symposium on Granitic
540 Pegmatites. PEG2011. Argentina, pp. 44.
541 Ginsburg, A.I., Rodionov, G.G., 1960. On the depths of the granitic pegmatite formation.
542 Geologiya Rudnykh Mestorozhdenyi, Izd. Nauka, Moskva, l, pp. 45-54. (in Russian)
543 Ginsburg, A.I. (1984) The geological conditions of the location and the formation of granitic
544 pegmatites. 27Th International Geological Congress, 15: 245-260.
545 Goldsmith, J.R., 1953. A “simplexity principle” and its relations to “ease” of crystallization.
546 Journal of Geology 61, 439-451.
547
548 Hanley, J.B., Heinrich E.WM. and Page, L.R. (1950) Pegmatite investigations in Colorado,
549 Wyoming, and Utah 1942-1944. Geological Survey Professional Paper 227, 83p.
550 Hanson, S.L., Simmons, W.L., Webber, K.L., Falster, A.U., 1992. Rare-earth-element
551 mineralogy of granitic pegmatites in the Trout Creek Pass dictrict, Chaffee County, Colorado.
552 The Canadian Mineralogist 30, 673-686.

553 Harris, R.E., Hausel, W.D., 1986. Wyoming pegmatites. In: Colorado Pegmatite Symposium:
554 Colorado Chapter, Friends of Mineralogy, May 30th-June 2nd, p. 101-108.
555 Heinrich, E. WM. (1950) Cordierite in pegmatite near Micanite, Colorado. American
556 Mineralogist, 35, 173-184.
557 Jacobson, M.I., Calderwood, M.A., Grguric, B.A., 2007. Guidebook to the pegmatites of
558 Western Australia. Carlisle, Hesperian Press.
559 Jochum, K.P., Weis, U., Stoll, B., Kuzmin, D., Yang, Q., Raczek, I., Jacob, D.E., Stracke, A.,
560 Birbaum, K., Frick, D.A., Günther, D. and Enzweiler, J., 2011, Determination of reference
561 values for NIST SRM 610-617 glasses following ISO guidelines: Geostandards and
562 Geoanalytical Research, 35, p. 397–429.
563 Jolliff, B.L:, Papike, J.J., Shearer, C.K., 1992. Petrogenetic relationships between pegmatite and
564 granite based on geochemistry of muscovite in pegmatite wall zones, Black Hills, South Dakota,
565 USA. Ceochimica et Cosmochimica Acta 56, 1915-1939.
566 Jordt-Evangelista, H., Cesar-Mendes, J., Cosso Lima, A.L., 2000. Amazonitação em granito
567 resultante da intrusão de pegmatitos. Revista Brasileira de Geosciências 30, 693-698.
568
569 Kinnaird, J., Schneider, G., Nex, P., 2014. Namibian pegmatites and indsutrial minerals. 6-12
570 September. Post Conference Field Trips. 21st General Meeting of IMA South Africa 2014.
571 Kokonyangi, J.W., Kampunzu, A.B., Armtrong, R., Yoshida, M., Okudaira, T., Arima, M.
572 Ngulube, D.A. 2006. The Mesoproterozoic Kibaride belt (Katanga, SE D.R. Congo). Journal of
573 African Earth Sciences 46, 1–35.

574 Larsen, R.B., 2002. The distribution of rare-earth elements in K-feldspars as an indicator of
575 petrogenetic processes in granitic pegmatites: Examples from two pegmatite fields in Southern
576 Norway. The Canadian Mineralogist 40, 137-151.
577 London, D., 1990. Phosphorous in alkali feldspars of rare-element granitic pegmatites. The
578 Canadian Mineralogist 28, 771-786.
579 London, D., 1992. Phosphorus in S-type magmas: the P2O5 content of feldspars from
580 peraluminous granites, pegmatites, and rhyolites. American Mineralogist 77, 126–145.
581 London, D., 2014. A petrologic assessment of internal zonation in granitic pegmatites. Lithos
582 184-187, 74-104.
583 Lottermoser, B.G., Lu, J., 1997. Petrogenesis of rare-element pegmatites in the Olary Block,
584 South Australia, part 1. Mineralogy and chemical evolution. Mineralogy and Petrology 59, 1-19.
585 Marchal, K.L., Simmons, W.B., Falster, A.U., Webber, K.L., Roda-Robles, E., 2014.
586 Geochemistry, mineralogy, and evolution of Li-Al micas and feldspars from the Mount Mica
587 pegmatite, Maine, USA. The Canadian Mineralogist 52, 221-233.
588 Marmo, V. 1971. Granite petrology and the granite problem. Elsevier Publishing Company, New
589 York.
590 Martin, R.F., De Vito, C. 2005. The patterns of enrichment in felsic pegmatites ultimately
591 depend on tectonic setting. The Canadian Mineralogist 43, 2027-2048.
592 Martin, R.F., De Vito, C. 2014. The late-stage miniflood of Ca in granitic pegmatites: an open
593 system acid-reflux model involving plagioclase in the exocontact. The Canadian Mineralogist
594 52, 165-181.

595 Martin, R.F., De Vito, C., Pezzotta, F., 2008. Why is amazonitic K-feldspar an earmark of NYF-
596 type granitic pegmatites? Clues from hybrid pegmatites in Madagascar. American Mineralogist
597 93, 263-269.
598 McLelland, J.M., Selleck, B.W., Hamilton, M.A., Bickford, M.E., 2010. Late- to posttectonic
599 setting of some major Proterozoic anorthosite–mangerite–charnockite–granite (AMCG) suites.
600 The Canadian Mineralogist 48, 729-750.
601 Merino, E., Villaseca, C., Orejana, D., Jeffries, T., 2013. Gahnite, chrysoberyl and beryl co-
602 occurrence as accessory minerals in a highly evolved peraluminous pluton: The Belvís de
603 Monroy leucogranite (Cáceres, Spain). Lithos 179, 137-156.
604 Mitchell, R.H., Platt, R.G., 1978. Mafic mineralogy of ferroaugite syenite from the Coldwell
605 alkaline complex, Ontario, Canada. Journal of Petrology 19, 627-651.
606 Mitchell, R.H., Platt, R.G., 1982. Mineralogy and Petrology of Nepheline Syenites from the
607 Coldwell Alkaline Complex, Ontario, Canada. Journal of Petrology 23, 186-214.
608 Müller, A., Ihlen, P.M., 2012, Trace elements of pegmatitic quartz and their regional distribution
609 in two pegmatite fields of Southern Norway. Maarten A. T. M. Broekmans (ed.), Proceedings of
610 the 10th International Congress for Applied Mineralogy (ICAM), Springer-Verlag, Berlin
611 Heidelberg.
612 Müller, A., Seltmann, R., Kober, B., Eklund, O., Jeffries, T., Kronz, A., 2008. Compositional
613 zoning of rapakivi feldspars and coexisting quartz phenocrysts. The Canadian Mineralogist 46,
614 1417-1442.
615 Müller A., Ihlen P.M., Snook B., Larsen R., Flem B., Bingen B., Williamson B.J., 2015. The
616 chemistry of quartz in granitic pegmatites of southern Norway: Petrogenetic and economic
617 implications. Economic Geology 110, 137-157.

Neiva, A.M.R., 1995. Distribution of trace elements in feldspars granitic aplites and pegmatites from Alijó-Sanfins, northern Portugal. Mineralogical Magazine 59, 35-45.

Norton, J.J., Page, L.R., Brosbst, D.A., 1962. Geology of the Hugo pegmatite, Keystone, South Dakota. Geological Survey Professional Paper 297-P, 1-85.

Pearce, J.A., Harris, N.B.W., Tindle, A.G. (1984) Trace Element Discrimination Diagrams for the Tectonic Interpretation of Granitic Rocks. Journal of Petrology 25, 956-983.

Pedrosa-Soares, A.C., De Campos, C.P., Noce, C., Silva, L.C., Novo, T., Roncato, J., Medeiros, S., Castañeda, C., Queiroga, G., Dantas, E., Dussin, I., Alkmim, F., 2011, Late Neoproterozoic-Cambrian granitic magmatism in the Araçuaí orogen (Brazil), the Eastern Brazilian Pegmatite Province and related mineral resources. Geological Society, London, Special Publications 350, 25-51.

Ostrooumov, M., 2016. Amazonite: Mineralogy, crystal chemistry, and typomorphism. Amsterdam, Elsevier.

Oyarzábal, J., Galliski, M.A., Perino, E., 2009. Geochemistry of K-feldspar and Muscovite in Rare-element Pegmatites and Granites from the Totoral Pegmatite Field, San Luis, Argentina. Resource Geology 59, 315–329.

Palme, H., Jones, A., 2003. Solar system abundances of the elements, in: Meteorites, comets, and planets. Treatise on Geochemistry, vol. 1, Amsterdam, Elsevier, pp. 41-61.

Payne, J.G., 1968. Geology and geochemistry of the Blue Mountain nepheline syenite. Canadian Journal of Earth Sciences 5, 259-273.

Proctor, K., 1985. Gem pegmatites of Minas Gerais, Brazil: the tourmalines of the Governador Valadares district. Gems and Gemology 21, 86-104.

640 Rino, S., Kon, Y., Sato, W., Maruyama, S., Santosh, M., Zhao, D., 2008. The Grenvillian and
641 Pan-African orogens: World's largest orogenies through geologic time, and their implications on
642 the origin of superplume. Gondwana Research 14, 51–72.
643 Rhodes, J.M., 1969. On the chemistry of potassium feldspars in granitic rocks. Chemical
644 Geology 4, 373-392.
645 Sabina, A.P., 1971. Rocks and Minerals for the Collector: Ottawa to North Bay, Ontario, Hull to
646 Waltham, Quebec. Geological Survey of Canada. paper 70-50. Canada. pp. 130.
647 Sabina, A.P., 1983. Rocks and Minerals for the Collector: Kingston, Ontario to Lac St-Jean,
648 Quebec. Geological Survey of Canada Miscellaneous Reports 32. Canada. pp. 130.
649 Sánchez-Muñoz, L., García-Guinea, J., Zagorsky, V.Ye., de Moura, O.J.M., Modreski, P.J.,
650 2011a. K-feldspar minerals defined from their twin-structures: Application to a preliminary
651 classification of pegmatites. Asociación Geológica Argentina, Serie D, Publicación Especial 14,
652 175-178.
653 Sánchez-Muñoz, L., Modreski, P.J., Frost, B.R., 2011b. K-feldspar twin-structures from orogenic
654 and anorogenic granitic pegmatites in Central North America. Asociación Geológica Argentina,
655 Serie D, Publicación Especial 14, 179-183.
656 Sánchez-Muñoz, L., García-Guinea, J., Zagorsky, V.Ye., Juwono, T., Modreski, P.J., Cremades,
657 A., Van Tendeloo, G., De Moura, O.J.M., 2012. The evolution of twin patterns in perthitic K-
658 feldspar from granitic pegmatites. The Canadian Mineralogist 50, 989-1024.
659 Sánchez-Muñoz, L., Sanz, J., Sobrados, I., Gan, Z.-H., 2013. Medium-range order in disordered
660 K-feldspars by multinuclear NMR. American Mineralogist 98, 2112-2131.
661 Satterly, J. Hewitt, D.F., 1955. Some radioactive mineral occurrences in the Bancroft area.
662 Geological Circular nº 2 of the Ontario Department of Mines. Toronto, pp.76.

663 Scoates, J.S., Frost, C.D., Mitchell, J.N., Lindsley, D.H., Frost, B.R., 1996. A residual liquid
664 origin for monzonitic rocks in Proterozoic anorthosite complexes: The Sybille intrusion, Laramie
665 Anorthosite Complex, Wyoming. Geological Society of American Bulletin 108, 1357-1371.
666 Sheppard, S., Rasmussen, B., Muhling, J.R., Farrell, T.R., Fletcher, I.R., 2007. Grenvillian-aged
667 orogenesis in the Palaeoproterozoic Gascoyne Complex, Western Australia: 1030–950 Ma
668 reworking of the Proterozoic Capricorn Orogen. Journal of Metamorthic Geology 25, 477-494.
669 Shmakin, B.M., 1979. Composition and structural state of K-feldspars from some U.S.
670 pegmatites. American Mineralogist 64, 49-56.
671 Shearer, C.K., Papike, J.J., Laul, J.C., 1985. Chemistry of potassium feldspars from three zoned
672 pegmatites, Black Hills, South Dakota: Implications concerning pegmatite evolution.
673 Geochimica et Cosmochimica Acta 49, 663-673.
674 Simmons, Wm.B., Heinrich, E.Wm., 1980. Rare-earth pegmatites of the South Platte District,
675 Colorado. Colorado Geological survey, Resource Series 11, pp. 131.
676 Simmons, Wm.B., Lee, M.T., Brewster, R.H., 1987. Geochemistry and evolution of the South
677 Platte granite-pegmatite system, Jefferson County, Colorado. Geochimica et Cosmochimica Acta
678 51, 455-471.
679 Simmons, Wm.B., Webber, K.L., 2008. Pegmatite genesis: state of the art. European Journal of
680 Mineralogy 20, 421-438.
681 Sweetapple, M.T., Collins, P.L.F., 2002. Genetic Framework for the Classification and
682 Distribution of Archean Rare Metal Pegmatites in the North Pilbara Craton, Western Australia.
683 Economic Geology 97, 873-895.
684 Tkachev, A.V., 2011. Evolution of metallogeny of granitic pegmatites associated with orogens
685 throughout geological time. From: Sial, A. N., Bettencourt, J. S., De Campos, C. P. & Ferreira,

686 V. P. (eds) Granite-Related Ore Deposits. Geological Society, London, Special Publications 350,
687 7–23.
688 Taylor, W.H., 1965. The Feldspars, in: Bragg W.L. and Claringbull G.F. (Eds.), Crystal
689 Structure of Minerals, London, Bell and Sons.
690 Utsunomiya, A.; Ota, T., Windley, B.F., Suzuki, N., Uchio, Y., Munekata, K., Maruyama, S.,
691 2008. History of the Pacific superplume: Implications for Pacific paleogeography since the late
692 Proterozoic, in: Yuen, D.A. et al. (Eds.), Superplumes. Springer, pp. 363-408.
693 Vetrin, V.R., Rodionov, N.V., 2009. Geology and Geochronology of Neoarchean Anorogenic
694 Magmatism of the Keivy Structure, Kola Peninsula. Petrology 17, 578-600.
695 Wagener, G.F., 1989. Systematic variation in the tin content of pegmatites in western central
696 Namibia. Journal of Geochemical Exploration 34, 1-19.
697 Walker, R.J., Hanson, G.N., Papike, J.J., Oneil, J.R., Laul, J.C., 1986. Internal evolution of the
698 Tin Mountain pegmatite, Black Hills, South-Dakota. American Mineralogist 71, 440-459.
699 Walker, E.E., Sutcliffe, R.H., Shaw, C.S.J., Shore, G.T., 1993. Preliminary Report on the
700 Petrology and Chemistry of the Rare Metal Occurrences Hosted by the Coldwell Alkaline
701 Complex. Ontario Geological Survey, Open File Report 5840, 20p.
702 Webber, K.L., Simmons, W.B., Falster, A.U., 1999. Biotite as a tectonic discriminant for
703 anorogenic and orogenic pegmatites. Canadian Mineralogist 37, 839-841.
704 Wise, M.A., 1999. Characterization and classification of NYF-type pegmatites. The Canadian
705 Mineralogist 37, 802-803.
706 Wise, M.A., 2013. The discrimination of LCT and NYF granitic pegmatites using mineral
707 chemistry: A pilot study. Abstracts PEG 2013 New Hampshire (USA): The 6th International
708 Symposium on Granitic Pegmatites. 156-157.

709 Zagorsky, V.Ye., Makagon, V.M., Shmakin, B.M., 2003. Systematics of granitic pegmatites.
710 Russian Geology and geophysics 44, 422-435.
711 Zhang, C., Yang, J., Lin, C., Li, C., Lin, J. 2009. Reduction of Eu^{3+} to Eu^{2+} in $MAl_2Si_2O_8$ (M =
712 Ca, Sr,Ba) in air condition. Journal of Solid State Chemistry 182, 1673-1678.
713
714 **Footnotes**
715 Figure 1. Map of the world showing the geological distribution of 123 pegmatite provinces and
716 districts, distinguishing between LCT and NYF suites, as well as some with hybrid affiliation.
717 The map of orogenic belts bases on Utsunomiya et al (2007) and Rino et al. (2008). Legend: 1.
718 Bighorn Mt. (WY, USA); 2. Copper Mt. (WY, USA); 3. South Pass (WY, USA); 4. Black Hills
719 (SD, UDistrict (Country); 5. Haystack Range (WY, USA); 6. Routt Plutonic Suite (CO, USA); 7.
720 Trout Creek Pass (CO, USA); 8. White Picacho (AZ, USA); 9. Mohave Co (AZ, USA); 10.
721 Laramie Mt (WY, USA); 11. Berthoud Plutonic Suite (CO, USA); 12. Burro Mt (NM, USA); 13.
722 Adirondacks Highlands (NY, USA); 14. North New Mexico fields, (USA); 15. Rockford (AL,
723 USA); 16. Kings Mountain (NC, USA); 17. Spruce Pine (NC); 18. Amelia (Virginia, USA); 19.
724 New England districts (USA); 20. Brazil Lake (Nova Scotia, Canada); 21. Southern California
725 (USA); 22. Cat Lake – Winnipeg River (Manitoba, Canada); 23. Wekusko Lake (Manitoba,
726 Canada); 24. Yellowknive basin (NW Territories, Canada); 25. NW Ontario fields (Canada); 26.
727 Superior Lake (ON, Canada); 27. Lac Simard (QC, Canada); 28. Preissac – La Corne (QC,
728 Canada); 29. Birch Portage – Hanson Lake (SK, Canada); 30. Granville Lake (Manitoba,
729 Canada); 31. SW Grenville southern fields (ON, Canada); 32. SW Grenville northern fields (ON,
730 Canada); 33. Mt Laurier and Gatineau fields (QC, Canada); 34. Lac Turgeon Johan Beets (QC,
731 Canada); 35. Pikes Peak (CO, USA); 36. Llano-Burnet (TX, USA); 37-37. Sveconorwegian

Province in S Norway and SW Sweden (Evje-Iveland, Froland, Glamsland, Arendal, Søndeled, Kragerø, Tørdal, Østfold-Halland; 39. Uttö-Mysingen (Sweden); 40. Varuträsk (Sweden); 41. Bothnian Basin (Sweden); 42. Falun (Central Sweden); 43. Kemiö – Orijärvi (Finland); 44. Eräjärvi (Finland); 45. Seinäjorki (Finland); 46. Ladoga Lake (Russia - Finland); 47. Chupa-Ijona (Karelia, Russia); 48. Keivy Massif. Kola Peninsula (Russia); 49. Leinster (Ireland); 50. El Muerto pegmatites (Oaxacan Complex, Southern Mexico); 51. Borborema Province (RGN, PB, Brazil); 52. Eastern Brazilian Province (MG, BA, ES, Brazil); 53. Sta Maria de Itabira (MG, Brazil); 54. Damara province (Namibia); 55. Namaqualand (South Africa); 56. Kaapvaal (South Africa); 57. Natal districts (South Africa); 58. Panpean Pegmatite Province; 59. SW Nigeria province (Ago-Iwoye, Keffi, Nassarawa, Komu, Wamba districts); 60. Giraul (SW Angola); 61. Caxito (NW Angola); 62. Bikita, Zimbabwe; 63. Alto Ligonha, Mozambique; 64. Ruanda; 65. Burundi; 66. Kobokobo, Kamituga area, South Kivu (Congo); 67. Kapiri Mposhi, Zambia; 68. Lundazi, Zambia; 69. Chroma-Kalomo (Zambia) and Kamativi (Zimbabwe); 70. Itremo, Madagascar; 71. Southeastern Desert province (Egypt); 72. Manono-Kittolo (Shaba, Congo); 73. Pilbara (WA, Australia); 74. Lake Moore - Dalgaranda (WA); 75. King Leopold (WA); 76. Greenbushes (WA); 77. Coolgardie – Norseman (WA); 78. Mukinbudin (WA); 79. Gascoyne (WA); 80. Mt. Isa (QNL); 81. Olary and Broken Hill, Curnamona province (SA-NSW); 82. Bihar mica belt (India); 83. Nellore mica belt (India); 84. Tamil Nadu belt (india); 85. Bastar-Malkagiri belt India); 86. Rajasthan belt (India); 87. Nuuk region (Greenland); 88. Gardar province (Greenland); 89. Volta Grande, Sao Joao de Rei (Brazil); 90. Strange Lake, Labrador, Canada ; 91.Alakha (Russia); 92. Kolmozero-Voronya (Kola Peninsula, Russia); 93. Yenisei Ridge (Russia); 94. Highland Complex (Sri Lanka); 95. Ghaha-Cote d'Ivore; 96. Bohemian-Moldanubicum belt; 97. Taimyr fold belt (Russia); 98. Altai belt (China, Kazakhstan, Russia);

755 99. Mongol-Okhotsk fold belt; 100. East Sayan Mt. (Siberi, Russia); 101. Southern Tuva
756 (Kamar-Daba fold belt); 102. East Transbaikalia (Russia); 103. NW Baikal (Russia); 104.
757 Mama-Chuya, North Baikal Highland (Rissia); 105. Iberian Peninsula; 106. Creus Cap (Spain);
758 107. Hagendorf-Pleystein (Babaria, Germany); 108. Paranesti (NE Greece); 109. Koralpe
759 (Austria); 110. Afghanistan-Pakistan belt; 111. Little Nahanni (NW Territories, Canada); 112.
760 Jiajika, Kangdi, (Sichuan province, China); 113. Nanping, China; 114. Cattlin CreeK –
761 Cocanarup, Ravensthorpe, (WA); 115. Tak (Thailand); 116. Phuket (Thailand); 117. Lao Cai
762 and Phu Tho (Northern Vietnam); 118. Kenticha (Ethiopia); 119. Nimnyr block, Central Aldan
763 (Russia); 120. Middle Urals (Russia); 121. South Urals (Russia); 122. Southern Japan (Japan);
764 123 Central Alps.
765
766 Figure 2. a) Rb, Li, Cs and Tl contents by LA-ICP-MS as log-log plots of Rb vs Li, Rb vs Cs and
767 Rb vs Tl of the K-feldspars from the thirty-two pegmatites. b) Rb, Sr, Ba and Pb contents in the
768 same tipe of graphs with Rb vs Sr, RB vs Ba and Rb vs Pb plots of the K-feldspars from the
769 thirty-two pegmatites.
770
771 Figure 3. a) Distribution of rare-earth elements (REE) by LA-ICP-MS in the Na-feldspar from a
772 type I pegmatite using sample C5S5; b) idem in the K- and Na-feldspar from a type II pegmatite
773 using sample LL1; c) idem in the Na-feldspar from a type III pegmatite using sample Et1317;
774 and iv) Ce-Eu plot (ppb) with three fields, type I with Eu/Ce > 1.0, type II with Eu/Ce < 1.0, and
775 type III and IV with a low value in the two contents. Normalization values from Palme and Jones
776 (2005).
777

Figure 4. Ge-Ga plot by LA-ICP-MS in log-log scale of the K-feldspars of the thirty-two pegmatites, where three fields can be differentiated for type I (red squares), type II (violet lozenges), and a hybrid field for type III (blue lozenges) and IV (green squeres).

Figure 5. P-Fe plot by LA-ICP-MS measurements in a log-log scale of the thirty-two pegmatites, where four radial fields can be differentiated for each type of pegmatites: type I (red squares in a pink field), type II (dark violet lozenges in a violet field), type III (blue lozenges in a shy blue field) and type IV (green squares in a clear green field). A circle marks the samples in each population with a highest content of orthoclase. Sample CM is from a peraluminous pegmatite of type II that is represented in the field of type III. Sample Et1317 is from a type III pegmatite that is represented in the field of type IV pegmatites. The diagonal line of the diagram separates NYF pegmatites at the left side with Fe > P from LCT pegmatites at the right side with P > Fe.

The P-Fe diagram for K-feldspars: a preliminary approach in the discrimination of pegmatites

Luis Sánchez-Muñoz[a]*, Axel Müller[b,c], Sol López Andrés[d], Robert F. Martin[e], Peter J. Modreski[f], Odulio J.M. de Moura[g]

[a] Instituto de Cerámica y Vidrio – CSIC, Kelsen 5, E-28049 Madrid, Spain,*lsm@icv.csic.es

[b] Natural History Museum, University of Oslo, NO-0318 Oslo, Norway.

[c] Natural History Museum, London SW7 5BD, UK.

[d] Facultad de Ciencias Geológicas, Universidad Complutense de Madrid, E-28040, Spain.

[e] Earth and Planetary Science, McGill University, Montreal, Quebec, H3A 0E8, Canada.

[f] U.S. Geological Survey, Federal Center Denver, CO 80225-0046, USA.

[g] Governador Valadares, Minas Gerais, Brazil.

ABSTRACT

Pegmatites are extremely coarse-grained and heterogeneous rocks in which quantitative measurements of mineral proportions and chemical compositions of the whole rock are virtually impossible to acquire. Thus, conventional criteria such as bulk compositions and modal mineralogy used for the classifications of igneous rocks simply cannot be applied for pegmatites. An alternative is to use the mineralogical and chemical attributes of K-rich feldspars, the only mineral that is omnipresent in pegmatites. We have used this approach to test a possible discriminant among four groups of pegmatites on the basis of major petrological features, such as the abundance of quartz, feldspars, micas and phosphates. Group I is represented by relatively flux-poor, and silica-poor pegmatites, in most cases with hypersolvus feldspars, devoid of quartz and with minor biotite, which are common in rift settings as in the Coldwell Alkaline Complex

in northwestern Ontario, Canada. Group II comprises relatively flux-poor, silica-rich pegmatites with quartz, subsolvus feldspars and biotite as major primary minerals, typically occurring in the asymmetric collisional Grenville Orogeny. Group III comprises relatively flux-rich, silica-rich P-poor pegmatites with quartz, subsolvus feldspars, and muscovite as the major primary minerals. Finally, group IV consists of relatively flux-rich, silica-rich, P-rich pegmatites with the same previous major minerals as in group III but with abundant phosphates. Group III and IV are found in most symmetric collisional orogens, such as in the Eastern Brazilian Pegmatite Province as the result of the collision of cratons mainly formed by igneous and metamorphic rock of Archean and Early Proterozoic age. We have selected specimens of blocky perthitic K-rich feldspar from the inner part of thirty-one pegmatites belonging to these four categories occurring worldwide to cover a wide range of mineralogy, geological age, geotectonic setting and geographical positions. Concentrations of major elements (Si, Al, K, Na, Ca, Fe, Mg, Mn, Ti and P) were obtained by X-ray fluorescence (XRF), and those of minor and trace elements (P, Fe, Li, Ge, Ga, Rb, Sr, Ba, Tl, Pb, Y, Cs, Ba, La, Ce, Pr, Nd, Sm, Eu, Gd, Tb, Dy, Ho, Er, Tm, Yb, and Lu) were established by laser-ablation inductively coupled plasma - mass spectrometry (LA-ICP-MS), in areas free of coarse Na-feldspar veins or patches. We show that the four groups have very different average values of the minor and trace elements. However, only the cations occupying tetrahedral sites, particularly the Fe and P, are sufficiently immobile to show distinct differences among pegmatites. Hence, we propose a P-Fe diagram to discriminate among the four groups of pegmatites, as a possible criterion with which to classify pegmatites.

Keywords: K-feldspar, pegmatites, perthite, trace elements, LA-ICP-MS data, P-Fe diagram

1. Introduction

One of the challenges of studying any rock with a pegmatitic texture is the lack of information on bulk composition of an intrusive body, owing to the exceptionally coarse grain-size and textural heterogeneity. For these reasons, conventional schemes of classification of igneous rocks using modal proportions or bulk compositions are not applicable. Furthermore, in the case of pegmatites of granitic composition, the intrusive bodies are commonly zoned vertically and horizontally, such that modal proportions of essential minerals may show extreme variability and thus significant departures from the bulk composition of the pegmatite-forming magma. Yet there is a pressing need to classify granitic pegmatites, in order to properly assess their economic potential and the geological information they can provide, including the tectonic context of their emplacement.

Existing classifications are largely based on qualitative criteria applied mainly to mineralized pegmatites, and do not lead to broadly defined or accepted categories. After a brief review of these schemes of classifications, we present analytical results of representative alkali feldspar from 31 carefully evaluated pegmatite localities covering a wide range of mineralogy, age, geotectonic setting at the time of emplacement, and geographic position. These specimens have been characterized by selected-area chemical analysis using laser-ablation – inductively coupled plasma – mass spectrometry (LA–ICP–MS) in order to obtain the concentration of 33 minor elements in pristine areas of K-rich feldspar making up the blocky perthite from the voluminous intermediate zone of zoned bodies of granitic and syenitic pegmatites. Our simplified approach to a complex problem targets an essential mineral common to all pegmatites of granitic or syenitic composition, and yields several new insights that are useful to the

geologist mapping uncharted territory in a pegmatite district. Our aim in this research is to test whether the trace-element signature of K-rich feldspar can be used as a measurable criterion for pegmatite discrimination, and to suggest elements that are best suited to accomplish this purpose.

2. Brief review of the literature

Because of the exceptionally large size of some crystals and an overall textural heterogeneity (London, 2014), conventional schemes of classification, for example using quantitative estimates of modal mineralogy plotted in QAP and APF diagrams, are not possible. Likewise, an approach based of bulk chemical composition plotted in a TAS diagram cannot succeed. Several other criteria have been proposed. Index minerals have been applied, as well as characteristically enriched groups of elements, especially where tied into tectonic setting, for example using the S-I-A-M classification of granitic suites (Simmons and Webber, 2008). However, the recognition of key minerals commonly depends on the level of exposure in any zoned body of granitic pegmatite. Petrogenetic aspects and tectonic setting are difficult or impossible to evaluate from field observations, and their interpretation depends on current models, which evolve with time and increasing knowledge. Genetic classifications thus involve subjective criteria and interpretations. An easily and widely applicable classification should be based on objective (measurable) criteria only.

Most pegmatite investigators use a classification scheme based on the depth of pegmatite formation (pressure and temperature), inspired from the Russian literature (e.g., Ginsburg and Rodionov, 1960; Ginsburg, 1984) and refined by Petr Černý and co-authors (Černý, 1991; Černý and Ercit, 2005). In addition to the depth-zone classification of pegmatite classes (abyssal, muscovite, muscovite rare element, rare element, and miarolitic classes), Černý (1991)

93 established a geochemical subdivision of the rare-element class into three families: the Niobium–
94 Yttrium–Fluorine (NYF), the Lithium–Caesium–Tantalum (LCT) and the mixed NYF–LCT
95 family. Currently, however, the NYF–LCT subdivision has been applied to distinguish also
96 pegmatites of the other four depth-zone classes. The family classification is more widely used
97 than the depth-zone classification because it is useful for the study and description of pegmatites
98 having an economic interest, enriched in Li, Be, Sn, Nb, Ta and gemstones. Basically, the family
99 concept involves a bimodal approach for the discrimination between pegmatite-forming melts
100 derived from the middle and upper crust (i.e., with an LCT geochemical signature) and melts
101 arising from melting in the lower crust, in some cases with mantle contributions, i.e., with the
102 NYF geochemical signature. The NYF pegmatites have been subdivided into three groups,
103 peralkaline, metaluminous and peraluminous, based on the alumina saturation (Wise, 1999).

104 Numerous pegmatites have no temporal and obvious genetic relationship with a parental
105 pluton. In those cases, anatectic melts arising from ultrametamorphism in the deep crust can
106 evidently crystallize with a pegmatitic texture (Ercit, 2005; Müller et al., 2012; Müller et al.,
107 2015). In addition, bodies of pegmatite may well exhibit features of both NYF and LCT suites,
108 with the LCT overprinting the NYF assemblages. Such an overprint may be attributed to
109 hydrothermal activity involving an acidic fluid and contamination from the exocontact area
110 (Martin and De Vito, 2014), or it is a result of extreme, pegmatite-internal differentiation (e.g.
111 Müller et al., 2012). One must appreciate that not every mineral in granitic pegmatites
112 crystallized from a silicate magma; everything gets reworked to some degree after the magma
113 has crystallized, and especially so in large bodies.

114 It is important to note that many pegmatite occurrences do not contain rare minerals, and
115 a clear geochemical affiliation cannot be identified. Consequently, proposals for classification

have recently been suggested that focus on the rare elements and volatiles in addition to depth of emplacement (Zagorsky et al., 2003), the geochemistry of micas and feldspars (Webber et al., 1999; Wise, 2013), the trace element content of quartz (Müller et al., 2013; Müller, 2014), and the microtextural and microstructural characteristics of perthitic K-rich feldspars (Marmo, 1971; Sánchez-Muñoz et al., 2011a). The advantage of using feldspar for classification is that it is the only constituent that occurs in all types of pegmatites of the felsic composition, whereas quartz and micas can be absent. Actually, the presence of "amazonite" (blue-green variety of K-feldspar) in pegmatites has been considered a hallmark of pegmatites of the NYF family (Martin et al., 2008).

Although feldspars are heterogeneous minerals that are very sensitive to chemical changes during the subsolidus and hydrothermal-deuteric stages, the bulk chemical composition of feldspars is commonly used in the study of pegmatites. Previous studies have led to a better understanding of their variability, with applications in the exploration for rare elements (e.g., Alfonso, 2003; Černý et al., 1984; Černý et al., 1985; Larsen, 2002; London, 1990; London, 1992; Marchal et al., 2014; Müller et al., 2008; Neiva, 1995; Oyarzábal et al., 2009; Rhodes, 1969; Sánchez-Muñoz et al., 2011b; Shmakin, 1979; Shearer et al., 1985; Wise, 2013). However, most research has been done in pegmatites of the LCT affiliation, generally from a single province. In many cases, the samples selected for study have had a rather limited microtextural and microstructural characterization, without consideration of the location of the samples within zoned pegmatites, and in many cases using bulk data from powdered samples on the alkalis and the alkaline earths only.

3. The relation of pegmatites to orogenic and anorogenic settings.

Figure 1 shows the distribution of the major pegmatite provinces and districts in the world. In most cases, these are spatially related to orogenic belts associated with areas of crustal convergence, i.e., a compressional regime. Granitic pegmatites can also form in environments marked by tectonic quiescence, i.e., an extensional regime. Most of the large and mineralized pegmatites are associated with collisional orogens, in districts containing thousands of distinct pegmatitic bodies. Such voluminous pegmatite fields are lacking in non-collisional environments, as in the western part of the American continent and in the eastern part of the Australian continent, because a thickened continental crust is needed to create the heat and pressure necessary for melt generation (e.g., Tkachev, 2011). In Figure 1, granitic pegmatites are mainly classified according to the conventional NYF–LCT bimodal approach, although some provinces and districts are known to have hybrid pegmatites. From this literature analysis and the field experience of the authors in many of these provinces, it was possible to distinguish four groups of pegmatites (Table 1) to be discriminated by the mineralogical and geochemical signatures of the perthitic K-rich feldspar. The identification of distinctive features to distinguish among bodies or groups of pegmatites is quite challenging because exceptions are the rule. However, the relative proportions of the major minerals can be used as starting point for discrimination using only general "trends" to test our initial hypothesis (i.e., the usefulness of mineralogical and geochemical features of perthitic K-feldspar for pegmatite discrimination).

(Figure 1. The distribution of the major pegmatite provinces and districts in the world)

The main distinction is based on the proportion of hydrous minerals in the pegmatitic rocks. A first category, which we label "High-T, low-flux", consists of pegmatites with rare

162 micas or amphiboles (group I) and pegmatites that contain hydrous minerals (biotite) as minor
163 phases (group II). These are pegmatites derived from syenitic magmas, or hosted in granulitic
164 terranes without obvious genetic relationship to a parental pluton (anatectic pegmatites). Such
165 pegmatite-forming magmas are likely to have crystallized at a temperature largely above the
166 upper thermal stability of the ferroan hydrous phases, from a magma relatively poor in fluxing
167 components. A second category, which we label "Low-T, high-flux", consists of granitic
168 pegmatites that contain abundant micas (including muscovite). Two groups are further
169 distinguished by the abundance and diversity of phosphate minerals, which are much higher in
170 group IV than in group III. This bimodal partition parallels the NYF–LCT approach, but it is not
171 based on geochemical affiliations or index minerals.

172 The silica-poor pegmatites of group I contain in most cases two feldspars that have a
173 hypersolvus texture (Tuttle & Bowen, 1958); biotite and fayalite are rare, whereas quartz is
174 absent in some cases. They are common in rift settings associated with syenites and nepheline
175 syenites, as well as anatectic melts in high-grade metamorphic terranes, without a clear genetic
176 relationship to a parental pluton (Table 1). Phosphates are very rare, in comparison with types III
177 and IV, although accessory apatite and monazite do occur.

178 The silica-rich pegmatites of type II consist of quartz, two feldspars that have a subsolvus
179 texture, and biotite as major primary minerals (Table 1). They are typically found in anorogenic
180 environments, related to A-type melts, for example in the Grenville orogen of northeastern North
181 America and in southern Scandinavia, with an asymmetric structure, i.e., a linear orogen
182 bordered by two other linear orogens of very different age, one older and the other younger. The
183 Grenville orogen was a locus of repeated collisions of two crustal blocks over the period 1400–
184 1000 Ma, each followed by delamination and extension accompanying the diapiric rise of an

asthenospheric mantle (McLelland et al., 2010; Dickin et al., 2010). The juxtaposition of hot fertile mantle undergoing decompression-induced melting below the lowermost of the stacked crusts provided the setting for wholesale anatexis and production of relatively hot granitic magma. As in group I, pegmatites generally cannot be genetically linked to a parental pluton.

In contrast to group II, group III and IV are typically found in collisional orogens with a symmetrical structure, for instance, linear orogens ending with the collision of two cratons with similar geological structure and lithologies of Archean and Early Proterozoic age, initially as the product of subduction of an oceanic plate underneath a thickened continental crust. The resulting calc-alkaline magmas are metaluminous to peraluminous, and relatively oxidizing, except where the protolith is organic-matter-rich. The presence of a metasedimentary protoliths is responsible for phosphate enrichment. Typical examples (Fig. 1) are the Grenville-age pegmatites of Africa, such as in the Kibaride belt, like the Mwanza Sn-pegmatite and Manono Sn-Nb-Ta-pegmatite of southeastern Democratic Republic of Congo (Kokonyangi et al., 2006) and the Nb-Ta-Sn pegmatites of the Gatumba area in western Rwanda (Dewaele et al., 2011). In the same way, the Gascoin Complex in the Capricorn Orogen (West Australia) contains very rich rare-earth-element pegmatites (Jacobson et al., 2007) of Grenvillian age, such as the Nardoo Hills rare-element pegmatite (Sheppard et al., 2007), derived from crustal peraluminous melts. Thus, the African and West Australian pegmatites formed in symmetric orogens of Grenville age are typical LCT pegmatites, whereas the North American examples, as in the Pikes Peak district of Colorado (Simmons et al., 1980, 1987) and the south Scandinavian pegmatites, such as in Evje-Iveland, Froland, Glamsland, Arendal, Søndeled, Kragerø, Tørdal, Østfold-Halland districts (Müller et al. 2015), formed in an asymmetric orogen of the same age, have typically NYF affinity.

208 The silica-rich, P-poor pegmatites of group III contain quartz, two coexisting feldspars
209 and muscovite as major primary minerals, and minor phosphates. These pegmatites are
210 commonly formed during the late- to post-orogenic relaxation in an extensional environment,
211 typically in the form of long and regular tabular bodies, as the blue tourmaline-rich pegmatites in
212 Paraiba (Brazil) and in the Cooper Mountain and Casper Mountain districts in Wyoming, United
213 States of America (Harris and Hausel, 1986).
214 Pegmatites of the group IV are similar to those of the group III but are rich in phosphates
215 (Table 1). High-phosphorus pegmatites typically develop via fractionation of voluminous
216 granitic melts formed by melting of a thick crust in a syn- to late-orogenic setting. Typical
217 examples are most of the pegmatites of Minas Gerais in Brazil, formed during the Braziliano
218 Orogeny (Pedrosa-Soares et al., 2011).
219 **(Table 1. Main features of the four groups of pegmatites used in this work.)**
220
221 **4. Experimental procedure**
222 *4.1. Samples*
223 Samples of fresh megacrystic (blocky) perthitic K-rich feldspar having distinct (001) and
224 (010) cleavages were taken from the intermediate zone of selected pegmatite bodies of the four
225 groups of pegmatites. Table 2 provides details about the origin of the samples that we
226 investigated. As the content of impurities of feldspars changes from border to core in zoned
227 bodies of pegmatites, only blocky feldspars from the intermediate zone were sampled, in order
228 acquire a set of comparable data.
229 **(Table 2. Selected pegmatites, sample codes and some important geological features)**
230

231

232 *4.2. Methods*

233 *4.2.1. Polarized light optical microscopy (PLOM)*

234 The feldspar samples were studied using surface-polished thin sections of 30 and 300 μm
235 thickness mounted on standard glass slides parallel to the (001) cleavage. Surfaces were polished
236 up to an average roughness Ra value less than 0.5 μm. A Nikon Eclipse LV100 POL was used,
237 using 1x to 100x objectives that allow observations at five orders of magnitude in the same
238 petrographic preparation, resolving textural and microstructural features with size between 10^{-2}
239 and 10^{-7} m in the same area. Pristine areas without turbidity (i.e., fluid and mineral inclusions, as
240 well as particles of clay minerals resulting from hydrothermal alteration) were selected and
241 marked for the *in situ* trace-element analyses by LA-ICP-MS. The detail of the experimental
242 procedure for textural and microtextural characterization of the samples can be found in
243 Sánchez-Muñoz et al., (2012).

244

245 *4.2.2. Scanning electron microscopy and electron microprobe*

246 The microscopic observations using back-scattered electron imaging (BSE) were
247 acquired using an Inspect ESEM of the FEI Company (for details see Sánchez-Muñoz et al.
248 2012), and a field-emission scanning electron microscope (FE-SEM) also in the BSE modus,
249 using a FEI Nova NANOSEM 230, at 5 kV with a vCD detector at 5.2 mm from the sample. In
250 addition, electron microprobe analysis (EMPA) was used to visualize perthitic textures by
251 chemical mapping, using a SX-50 instrument at 15 kV and 50 nA (see Sánchez-Muñoz et al.,
252 2012 for details).

253

4.2.3. X-ray fluorescence (XRF)

The concentrations of major elements (Si, Al, K, Na, Ca, Fe, Mg, Mn and Ti) were established at the Technical Assistance Center in Earth Science Research of the Complutense University (Madrid, Spain) using a Bruker S2 Ranger energy-dispersive X-ray fluorescence (EDXRF) spectrometer equipped with a Pd anticathode X-ray tube of 50 W in a vacuum atmosphere. Sample preparation was made by the flux-fusion technique with 10 g flux [mix of $Li_2B_4O_7$ (99.5%) and LiI (0.5%)] and 0.5g sample at 1050ºC (maximum temperature), and pressed cylindrical pellets of 4 cm in diameter (9.5 g of dry sample and 0.5 g of Hoechst wax C micropowder as binding agent). Quantification was made with the software provided with the equipment (Spectra Plus/Bruker AXS) through empirical calibration of the system, by using six certified reference materials (NCS DC 71313, FKN, GA, GH, NIM-G and SY3). The limits of detection (%) are: SiO_2 0.23 and Al_2O_3 0.05 with fused beads, and Fe_2O_3 0.004, MnO 0.01, MgO 0.02, CaO 0.02, Na_2O 0.02, K_2O 0.03, TiO_2 0.01 and P_2O_5 0.003 to pressed cylindrical pellets. The chemical compositions was expressed as $Or_xAb_yAn_z$ (x+y+z = 100) (Supplementary Material Table SM1), with Or, Ab and An expressing the molar content of $KAlSi_3O_8$, $NaAlSi_3O_8$ and $CaAl_2Si_2O_8$ components.

4.2.4. Laser-ablation inductively coupled plasma mass spectrometry (LA-ICP-MS)

The analyses were performed at the Geological Survey of Norway, in Trondheim (Norway) on the double-focusing sector field mass spectrometer, model ELEMENT XR, from Thermo Scientific, which is combined with the excimer-based NewWave UP193FX laser probe. The analyses were done on the 300-μm-thick sections. The 193-nm laser had a repetition rate of 20 Hz, a spot size of 75 μm, and an energy fluence of 5.5 to 6.5 mJ/cm^2 on the sample surface. A

277 continuous raster ablation (laser speed 15 μm/s) on an area of approximately 300 × 150 μm was
278 applied. In all specimens, it was possible to select regions for analysis without turbidity, where
279 the separation between albite veins (microperthitic texture) is larger than the spatial resolution of
280 this technique. The size scale of the crypto- and microperthitic intergrowths of K- and Na-
281 feldspar is much smaller that the size of the ablation pits. However, no chemical changes are
282 expected during the exsolution process to produce such fine microtextures. The chemical
283 composition will not change at the scale of the sampled surface, i.e., exsolution took place in
284 "isochemical condition" at the size of the laser probe. Problems related to the dispersion of data
285 are related to albite veins and turbidity, not to fine perthitic textures.

286 For each sample, two analyses of the K-feldspar matrix and one of the Na-rich feldspar in
287 the veins of the perthite intergrowth were carried out. The isotope ^{29}Si was used as the internal
288 standard, applied to the concentration of Si determined by XRF. An Ar blank was run before
289 every sample and standard measurement to determine the background signal. In order to avoid
290 memory effects between samples, the background signal was subtracted from the instrumental
291 response of the standard before normalization against the internal standard. External
292 multistandard calibration was performed using five silicate glass reference materials produced by
293 the National Institute of Standards and Technology, USA (NIST SRM 610, 612, 614, 616, 1830)
294 and the certified reference material silica glass BCS CRM 313/1 from the Federal Institute for
295 Material Research and Testing in Germany. Certified, recommended, and proposed values for
296 these reference materials were taken from Jochum et al., (2011), Flem and Bédard, (2002) and
297 from the certificates of analysis where available. The limits of detection (LOD) are based upon
298 3x standard deviation (3σ) of 10 NIST SRM 616 measurements. The LODs for the individual
299 elements are: Li 0.14 ppm, P 5.01 ppm, Fe 0.88 ppm, Ga 0.26 ppm, Ge 0.04 ppm, Rb 0.02 ppm,

Sr 11.46 ppm, Y 0.01 ppm, Cs 0.01 ppm, Ba 0.53 ppm, La 0.012 ppm, Ce 0.007 ppm, Pr 0.004 ppm, Nd 0.009, Sm 0.009, Eu 0.004 ppm, Gd 0.009 ppm, Tb 0.005 ppm, Dy 0.007 ppm, Ho 0.008 ppm, Er 0.004 ppm, Tm 0.005 ppm, Yb 0.009 ppm, Lu 0.006 ppm, Tl 0.006 ppm, and Pb 0.16 ppm. Data provided in Tables 4 and 5, and Tables SM1 to SM5 (Supplementary Materials) represent a single value for Na-feldspar veins and the average of two analyses for K-feldspar in each sample.

5. Perthitic textures and twin patterns

The main features of the microstructures developed as a result of the monoclinic-to-triclinic inversion and recrystallization-induced twinning in the K-feldspar and the perthitic microtextures resulting from K–Na exsolution for the four categories of pegmatites are shown in Table 3. The nomenclature employed to describe the twin patterns and to identify microcline and orthoclase using Raman spectra, measured directly on the thin sections, is explained in detail in Sánchez-Muñoz et al., (2012). Figure 2 shows some typical features of the perthitic textures and twin patterns observed in the specimens studied, as well as examples of laser ablation pits created during the LA-ICP-MS analyses (see Electronic Appendix 1 for examples of the analytical area sampled in the K-rich feldspar regions of the specimens used in this work).

(Table 3. Petrographic features of samples selected by PLOM observations)

Pegmatite bodies of group I typically show first-generation twins of microcline, and albite veins in a wide range of sizes. Albite in fine mesoperthitic microtextures only occurs in the hypersolvus feldspars of this type, i.e., in samples S5C2 (Fig.2a), S10C12 and FH1. The coarsening and formation of large incoherent Na-feldspar veins in sample S5C2 and S10C12 is

limited to certain parts of the specimen, leaving vast areas with pristine character. Exsolution-induced textures are much finer that the width of the portions ablated by the laser. In the other samples of group II, albite veins of different sizes are formed that leave space for proper chemical analyses by the selected area method.

(Figure 2. Selected features of perthitic textures and twin patterns, showing the selected area for LA-ICP-MS analyses)

Extremely coarse veins of albite in large mesoperthitic textures, visible with the naked eye, occur in sample TL from a group-I pegmatite in Perth, Ontario, Canada, i.e., the type locality of perthite, where albite veins can have up to 2 millimeters wide, leaving region with microperthitic K-rich feldspars of the same width. Microcline perthites of group IV have albite veins of a similar size to that one, but the relative extent of the regions of microperthitic K-rich feldspars is greater than in mesoperthites (Fig. 2b).

First-generation twins in tartan and parquet configurations in microcline are also the most common feature in pegmatite bodies of group II (see Fig. 2a and Fig. 6 in Sánchez-Muñoz et al., 2012). These configurations commonly involve irrational twins, as well as diffuse cross-hatched microstructures. In some cases, one can observe several microtextures resulting from the recrystallization of Albite-twinned (A) and Pericline-twinned (P) microcline to single-orientation microcline. All examples studied in this category exhibit a subsolvus texture, in which perthitic grains contain albite veins narrower than 100 μm, as well as thin films of albite. Residual orthoclase with an intermediate degree of local order can be found in this group, as for instance in specimen WC1. The width of the areas between albite veins was sufficient to obtain LA-ICP-MS analyses without interference of these more altered zones (see Electronic Appendix 1).

346 Single-orientation microcline is the most characteristic microstructure in pegmatites of
347 group III, as well as intermediate steps in achieving that pattern (see Figure 10 in Sánchez-
348 Muñoz et al., 2012). The perthitic textures consist of albite veins ranging from a few
349 micrometers to tens of micrometers in width. Orthoclase can be found in some cases, specifically
350 where the K-rich feldspars of this category have a relatively high content of phosphorus, as in
351 specimen MMG2. The K-rich matrix with fine micro- and cryptoperthitic textures, located
352 between large albite veins, were also easily analyzed by LA-ICP-MS also in this case (see
353 Electronic Appendix 1).
354 The twin patterns of microcline in pegmatites of group IV are extremely variable, but
355 single-orientation microcline has not been found in any case. Perthites with orthoclase as a major
356 component (Fig. 2c) are common in these pegmatites, mainly because of the chemical effect of
357 impurities as kinetic hinderers (i.e., kinetic barriers to ordering), such as phosphorus (Sánchez-
358 Muñoz et al., 2012). Second-generation twins that arise by recrystallization and directed
359 coarsening of the first generation of twins or the recrystallization of orthoclase along interfaces
360 between the K-feldspar matrix and albite veins are very common (Fig. 2c). Twin coarsening of
361 polysynthetic patterns and chessboards are very common. Perthitic textures trend to be bimodal
362 in size, having fine films that are well preserved if orthoclase is not recrystallized into microcline
363 (Fig. 2d). These areas marked by minimum interaction with water, i.e., the exsolution process
364 was isochemical at the scale of the laser probe, were selected for LA-ICP-MS analysis.
365 Perthites formed mostly by large microcline twins (Fig. 2b) have also important
366 development of recrystallization units along interfaces with fine veins (Figs. 2e). It involves the
367 breaking of albite films into several parts (Figs. 2f, 2g) or the formation of zigzag interfaces
368 (serrated albite) related to mechanical polysynthetic A± twinning arising from tectonic stresses

(see Fig. 2 en Sánchez-Muñoz et al. 2006). Large veins arising from the coalescence of albite are the most frequently encountered feature, commonly showing also the last stages of coarsening resulting from interactions with fluids migrating along interfaces, giving rise to patch morphology. It was easy to find large albite veins to obtain the chemical composition in terms of minor and trace elements by LA-ICP-MS analysis (Fig. 2h).

Therefore, with the selected-area technique, it was possible to analyze pristine areas of micro and-cryptoperthitic K-rich feldspars, avoiding large and small albite veins, turbid areas with strong alteration, inclusions of other minerals (for instance, Fe-rich amphiboles in specimen S10C12), zones with a high rugosity from imperfect sample preparation, as well as cracks (see examples of these situations in the selected areas analyzed in Electronic Appendix 1). However, the LA-ICP-MS technique does not allow us to obtain chemical bulk compositions of the feldspars because the size of the laser probe is too small in comparison with the size of the textural elements in such heterogeneous textures of the perthitic and twinned feldspars. On the other hand, we were not interested in obtaining such global values but those in areas which are closer to the original composition of the mineral, having the minimum amount as possible of chemical losses by albite vein formation and water circulation at low temperatures along the interfaces.

6. Major elements

We present chemical composition the 31 samples in terms of major elements from XRF (Table SM1). The proportion of K-feldspar is higher that the proportion of Na-feldspar in all samples, as most samples has Na_2O content between 1.5 and 4.2 wt %. Specimen Et1317 has only 1.51 wt % of Na_2O and does not have large veins of albite, a typical characteristic of K-rich

394 feldspar of post-orogenic granites (Marmo, 1971), consistent with our group III. In samples
395 S5C5 and S10C12, the two constituents have similar proportions. These samples are also rich in
396 inclusions of amphibole that could not be separated when preparing the powders for bulk
397 chemical analysis, resulting in high Fe_2O_3 content.
398
399 **7. Minor and trace elements**
400 The structure of alkali feldspars consists of three-dimensionally linked SiO_4 and AlO_4
401 tetrahedral units. There are four spectroscopically non-equivalent tetrahedrally coordinated (T)
402 sites in each ring of tetrahedra, which are arranged in double crankshaft chains (Taylor, 1965).
403 The alkali A^{+} and alkaline earth A^{2+} elements are located at the M sites inside the irregular cavity
404 formed by the framework of tetrahedra; these ensure local electrostatic neutrality forming
405 medium-range order schemes (Sánchez-Muñoz et al., 2013). The Si and Al atoms of the
406 framework sites can be replaced by 5+, 4+ and 3+ cations such as P^{5+}, Ge^{4+}, Ga^{3+} and Fe^{3+},
407 during crystallization of the magma. Their concentration in the feldspar will reflect the
408 availability of these elements in the pegmatite-forming magma and the relevant partition-
409 coefficients. Similarly, K and Na atoms of the cavity M sites can be occupied by 1+, 2+ and 3+
410 cations, such as Li^{+}, Rb^{+}, Cs^{+}, Tl^{+}, Sr^{2+}, Ba^{2+}, Pb^{2+} and rare-earth elements as REE^{3+}, except for
411 Eu, which in reducing environments can be present as Eu^{2+}.
412 When *averaged values* for the four groups of pegmatites are considered, they are found to
413 be very different (Table 4). Lithium, Rb, Cs, Tl, Ge and P increase in concentration from group I
414 to IV, whereas Sr, Eu and Fe exhibit the contrary trend. Barium peaks in group II, a behaviour
415 also found in Ga, Y, La and Ce. Lead also peaks in group II, but its concentration is higher in

group III and IV than in I. Thus, the coherent pattern of distribution of these elements indicates that the selection of samples and pegmatites was appropriate to attain our objectives.

(Table 4. Average values of minor and trace elements in ppm (ppb for Y, La, Ce and Eu) of the K-rich feldspar and Na-feldspar in the four groups of pegmatites from LA-ICP-MS)

7.1. The M-site cations

No meaningful distinctions were observed in the concentrations of the alkalis and alkaline earths among the feldspars from different groups of pegmatites. Tables SM2 and SM3 and Figure SM1a and SM1b in Supplementary Materials show the correlations between the Rb content and other 1+ and 2+ elements occupying the M sites of K-rich feldspars. A tight linear relationship is found in the Rb-Tl diagram for K-rich feldspars, which becomes broader but still linear in the case of the Rb-Cs plot. The correlation is weakly developed in the Rb-Li plot. The fields are not well defined, and thus these diagrams are not useful for the discrimination of pegmatites. The contents of these elements in the albite veins of the perthitic microtexture are in most cases much lower than values in the K-feldspar matrix, indicating that important chemical changes must occur during exsolution and later growth of the albite veins. This effect is particularly strong in specimen TL1, with albite veins up to 2 mm wide, and also in specimens NH1, CM3, TC and BK2. In contrast to the Rb-A^+ plots, no well-defined trend can be observed in the correlation of Rb and 2+ elements also present at the M sites. Because of the high detection limit of Sr (11.5 ppm), the Rb-Sr plot is not of much use. Moreover, the contents of these elements in the Na-feldspar do not follow any particular behavior. In many cases, these elements are lost with albite formation, particularly in samples TL1 and CM3, as was found to be the case with the alkalis.

439

440 *7.2. Rare-earth elements*

441 Rare-earth elements are allocated to the M sites of the structure (Zhang et al., 2009).
442 Although La, Ce, Pr, Nd, Sm, Eu, Gd, Tb, Dy, Ho, Er, Tm, Yb, and Lu were sought in all
443 samples, only Y, La, Ce and Eu have concentrations sufficient to be measured with the
444 equipment used, particularly in feldspars of group-I and group-II pegmatites (Table SM4).
445 Interestingly, the REE are mainly concentrated in the Na-feldspar of the albite veins in the
446 perthitic microtexture, as shown in the REE patterns (Fig. SM2). The highest contents in most of
447 these elements are encountered in pegmatites of group I; these exhibit a pronounced Eu anomaly.
448 Only in one sample (specimen LL1 from the Lone Lode pegmatite in the Pikes Peak, Colorado,
449 USA) is there a sufficiently high concentration in the two feldspars to compare their REE
450 patterns. In this case, the total REE content is higher in the K-rich feldspar, but its positive Eu
451 anomaly is lower than in the Na-feldspar, and these anomalies are lower than in the sample C5S5
452 from a pegmatite of group I. Figure SM2c illustrates an example of a REE pattern in a group-III
453 pegmatite, where no Eu anomaly is found, and a very low total REE content is recorded, as well
454 as a small positive Sm anomaly. In most samples of group-IV pegmatites, the concentration of
455 REE is below the limit of detection.

456 These data only allow one to distinguish among the two first categories of pegmatites
457 (Fig. 3). In this graph, where Eu and Ce contents have the same scale, two fields represent well
458 the different geochemical affiliations. Pegmatites of group I exhibit Eu > Ce (pink field in Fig.
459 3), in contrast to pegmatites of group II, where in most cases, Eu < Ce (violet field in Fig. 3).
460 Similar REE contents to pegmatites of group II have been found in K-feldspar from the Evje-
461 Iveland and Froland pegmatite fields in southern Norway (Larsen, 2002). Only certain samples

462 from pegmatites of group III have a sufficient content of these elements to be shown in this plot,
463 and thus, they were not represented in Figure 3.

464 **(Figure 3. The Eu-Ce diagram)**

465

466 *7.3. The T-site cations*

467 Figure SM3 shows the measured concentrations of Ga and Ge in K-feldspar, using a plot
468 with the same values for both axes, and Table SM5 has the numerical values. The Ge-Ga graph
469 shows that pegmatites of group I can be clearly discriminated from the other types because they
470 show a lower content in Ge. The pegmatites of group II can be distinguished only partially from
471 the pegmatites of group III and IV (the two groups of LCT pegmatites) by means of the ratio
472 Ga/Ge. Note that in contrast with the behaviour of the M cations (including REE), there are no
473 sharp differences in most cases between the values of the K-feldspar matrix and the Na-feldspar
474 veins. The implication is that these elements remain where they are during the subsolidus
475 transformations (Si–Al ordering, transformation twinning and recrystallization twinning, as
476 described in Sánchez-Muñoz et al., 2012).

477 In sharp contrast with the previous graphs, the P-Fe plot of K-feldspars (Fig. 4) shows a
478 very good discrimination among the four groups of pegmatite (see Table 5 for numerical values).
479 The plot is constructed using the same log scale for both elements. The transversal line
480 expressing a Fe:P ratio equal to 1.0 perfectly separates the NYF pegmatites (group I in pink and
481 group II in violet) from the LCT pegmatites (group III in blue and group IV in green). The only
482 exception is sample CM3 from the Climax Mica pegmatite (sample CM, Fig. 4), which contains
483 rare-earth minerals and a strongly peraluminous character. It contains unusual large masses of
484 cordierite (Heinrich, 1950) and abundant secondary muscovite (Hanley et al., 1950). Pegmatites

485 of groups I and II are separated by a line starting at the origin (at a concentration of 1 ppm in the
486 two cations) and ending at P = 10^2 ppm and Fe = 10^4 ppm. In the same way, pegmatites of
487 groups III and IV can be separated by a similar line starting at the same point and ending at P =
488 10^4 ppm and Fe = 10^2 ppm. Sample Et1317 from East Transbaikalia (Russia) is an exception,
489 and extensive recrystallization has caused single-orientation microcline to form (PLOM
490 observations). Thus, a pegmatite belonging to group III is represented in the field of group IV.

491 **(Table 5. Fe and P contents in K- and Na-feldspars (ppm) by LA-ICP-MS**

492 **(Figure 4. The Fe-P diagram)**

493

494 **8. Implications**

495 Figure 4 shows that the four categories of pegmatite that we have defined can be
496 discriminated using the contents of P and Fe. Any pegmatitic body thus can presumably be
497 classified with this graph, independently of index minerals or the mineralization and economic
498 potential (see Dill, 2015 for a recent review of the ore geology of pegmatites). Thus a purely
499 petrochemical classification seems to be possible. This type of diagram is common in the
500 geological literature, e.g., discriminant diagrams are used to infer the tectonic setting of granitic
501 rocks, but the resulting shape and distribution of the chemical fields in plots are difficult to
502 interpret from the point of view of crystallochemical phenomena, as they result from statistical
503 studies from a data bank (Pearce et al., 1984). In our approach, we have selected a few
504 representative pegmatites to obtain high-quality trace-element data by selected-area chemical
505 analyses of pristine regions of K-rich feldspar (i.e. areas without turbidity, with crypto- and
506 microperthitic domains located between large Na-feldspar veins) using LA-ICP-MS. Thus,

507 conventional crystallochemical concepts can be employed to interpret the resulting radial fields
508 of Figure 4.

509 Starting from the high-temperature crystallization of a pegmatite-forming melt, the first-
510 formed alkali feldspar at the magmatic stage is sanidine, a disordered solid-solution with a
511 composition close to $(Na,K)AlSi_3O_8$ that incorporates other cations in the framework T and
512 cavity M sites as "chemical impurities". Goldsmith, (1953) explained the crystallization with the
513 Ostwald's rule of stages, i.e., the highest simplexity or most disordered stage should be the most
514 easily formed from a random liquid system. In this initial step, the concentration of the minor
515 and trace elements in feldspars depends mainly on their concentration in the melt, as well as on
516 pressure, temperature and oxygen fugacity at the time of crystal growth.

517 However, as temperature decreases after emplacement, the feldspar system evolves to
518 more equilibrated configurations by means of several processes, including atomic ordering,
519 phase separation and impurity exclusion. The transformation and recrystallization affecting the
520 sanidine solid-solution to produce orthoclase or microcline (or both) and albite (Sánchez-Muñoz
521 et al., 2012, 2013) involve a drastic decrease in the concentration of impurities. Thus, in most
522 cases, orthoclase has a higher content of minor and trace elements than microcline in the same
523 group of pegmatites, as shown by the circle in Figure 5. The trend shown by samples of each
524 population trending toward the origin in the diagram can be explained as a progressive loss of
525 impurities with its recrystallization of A± and P± twinned microcline first, and the development
526 of single-orientation microcline at later subsolidus stages.

527 Consequently, the concentrations that we measure in the feldspars are the result of two
528 effects: the composition of the original melt, which depends on the source lithologies (upper
529 mantle, lower crust, upper crust), and the extent of recrystallization, which mainly depends on

530 the tectonic setting and local geological conditions such as cooling rate, directed stresses [see
531 Černý et al., (2012) and Martin and De Vito, (2005) for detailed discussions]. The K-feldspar
532 records self-organized non-equilibrium twin patterns at the subsolidus stage and ambient
533 physical conditions in each tectonic setting (Sánchez-Muñoz et al., 2012). It is clear that the
534 original chemical signatures involving the framework (T) sites are not totally erased. However,
535 when hydrothermal and deuteric fluids interact with feldspars, dissolution-recrystallization
536 phenomena occur by catastrophic processes, typically at the last stages of vein perthite
537 formation, to give patches. Drastic chemical changes in bulk compositions are likely to occur in
538 fine-grained granitic rocks because of the interaction of hydrothermal and deuteric fluids with
539 feldspars at low temperatures.
540
541 **9. Conclusions**
542 Because of the large size of crystals and the exceptional textural heterogeneity of
543 pegmatites, it is not possible to use the standard methods of classification, like modal mineralogy
544 and bulk chemical compositions. An alternative approach is to use the geochemical features of
545 K-feldspar, an omnipresent mineral in pegmatites, to discriminate among different groups having
546 well-defined petrological features. With this objective, we have selected 31 samples of blocky
547 feldspars from pegmatites that can be grouped into four different categories according to the
548 amount of hydrous minerals, the presence or absence of quartz, and the abundance and
549 variability of phosphates minerals (Table 1). The trace-element diagrams based on cations at M
550 sites (M vs M and M vs T) were found to be of no use to discriminate among the four categories
551 in spite of average values in each population that are different. Elements located at the M site are
552 easily released from the mineral structure during the subsolidus and hydrothermal-deuteric

553 stages. However, the T vs T plots are useful to represent different pegmatites in well-separated
554 fields, as the T cations are much more firmly held in the structure. Specifically, the P–Fe plot,
555 with four radially distributed fields, is found to be very useful in the division of four previously
556 defined categories of pegmatite. Therefore, this methodology could be useful to help place the
557 classification of pegmatites on a more objective basis than has been possible so far.
558
559 **Acknowledgements**
560 We thank B. Ronald Frost of the University of Wyoming in Laramie for his assistance in
561 the field while sampling of Funny Hill pegmatite (specimen FH1) in Wyoming, USA, used in
562 this work; to Victor Ye. Zagorsky (1942-2015) and V.M. Makagon from Vinogradov Institute of
563 Geochemistry (Irkutsk, Russia) for samples ZAG and Et1317. We are grateful to an anonymous
564 reviewer for constructive suggestions and comments, and to the editor-in-Chief Nelson Eby, and
565 Skip Simmons for their help in improving the quality of this manuscript. The study was partially
566 financially supported by the project MAT2013-48009-C4-1-P.
567
568 **References**
569 Alfonso, P., 2003. Geochemistry of feldspars and muscovite in granitic pegmatite from Cap de
570 Creus Field, Catalonia, Spain. The Canadian Mineralogist 41, 103-116.
571 Beurlen, H., Da Silva, M.R.R., Thomas, R., Soares, D.R., and Olivier, P., 2008. Nb–Ta–(Ti–Sn)
572 oxide mineral chemistry as tracer of rare element granitic pegmatite fractionation in the
573 Borborema Province, Northeastern Brazil. Mineralium Deposita 43, 207-228.

574 Beurlen, H., Thomas, R., Rodrigues da Silva, M.R., Müller, A., Rhede, D., Soares, D.R., 2014.
575 Perspectives for Li- and Ta-mineralization in the Borborema pegmatite province, NE-Brazil: A
576 review. Journal of South American eath Sciences 56, 110-127.
577 Černý, P., Smith, J.V., Mason, R.A., Delaney, J.S., 1984. Geochemistry and petrology of
578 feldspar crystallization in the Vezna pegmatite, Czechoslovakia. The Canadian Mineralogist 22,
579 631-651.
580 Černý, P., Meintzer, R.E., Anderson, A.J., 1985. Extreme fractionation in rare-element granitic
581 pegmatites: selected examples of data and mechanisms. The Canadian Mineralogist 23, 381-421.
582 Černý, P. 1991. Fertile granites of Precambrian rare-element pegmatite fields: is geochemistry
583 controlled by tectonic setting or source lithologies? Precambrian Research 51, 429-468.
584 Černý, P., Ercit, T.S., 2005. The classification of granitic pegmatites revisited. The Canadian
585 Mineralogist 43, 2005–2026.
586 Černý, P., London, D., Novak, M., 2012. Granitic pegmatites as reflections of their sources.
587 Elements 8, 257–261.
588 Dewaele, S., Henjes-Kunst, F., Melcher, F., Sitnikova, M., Burgess, R., Gerdes, A., Alonso
589 Fernandez, M., De Clercq, F., Muchez, P., Lehmann, B., 2011. Late Neoproterozoic overprinting
590 of the cassiterite and columbite–tantalite bearing pegmatites of the Gatumba area, Rwanda
591 (Central Africa). Journal of African Earth Sciences 61, 10–26.
592 Dickin, A.P., McNutt, R.H., Martin, C., Guo, A., 2010. The extent of juvenile crust in the
593 Grenville Province: Nd isotope evidence. Geological Society of America Bulletin 122, 870-883.
594 Dill, H.G., 2015. Pegmatites and aplites: Their genetic and applied ore geology. Ore Geology
595 Reviews 69, 417-561.

596 Ercit, T.S., 2005. REE-enriched granitic pegmatites, in: Linnen, R.L., Samson, I.M. (Eds.), Rare-
597 element geochemistry and mineral deposits. Geological Association of Canada, Geological
598 Association of Canada, Short Course Notes 17, 175-199.
599 Fanton J.J., Arioli E.A., Moura O.J.M., 1978. Pegmatitos da região de Galiléia-Mendes Pimentel,
600 MG. In: SBG, Anais do XXX Congresso Brasileiro de Geologia, Recife, 1770-1781.
601 Flem B., Bédard L.P., 2002. Determination of Trace Elements in BCS CRM 313/1 (BAS) and
602 NIST SRM 1830 by Inductively Coupled Plasma-Mass Spectrometry and Instrumental Neutron
603 Activation Analysis. Journal of Geostandards and Geoanalysis, 26, 287-300.
604 Galliski, M.A., Márquez-Zavalía, M.F., Martínez, V., Roquet, M.B., 2011. Granitic pegmatites
605 of the San Luis Ranges. Field Trip Guidebook, 5th International Symposium on Granitic
606 Pegmatites. PEG2011. Argentina, pp. 44.
607 Ginsburg, A.I., Rodionov, G.G., 1960. On the depths of the granitic pegmatite formation.
608 Geologiya Rudnykh Mestorozhdenyi, Izd. Nauka, Moskva, l, pp. 45-54. (in Russian)
609 Ginsburg, A.I., 1984. The geological conditions of the location and the formation of granitic
610 pegmatites. 27Th International Geological Congress, 15: 245-260.
611 Goldsmith, J.R., 1953. A “simplexity principle” and its relations to “ease” of crystallization.
612 Journal of Geology 61, 439-451.
613 Hanley, J.B., Heinrich E.WM. and Page, L.R., 1950. Pegmatite investigations in Colorado,
614 Wyoming, and Utah 1942-1944. Geological Survey Professional Paper 227, 83p.
615 Hanson, S.L., Simmons, W.B., Webber, K.L., Falster, A.U., 1992. Rare-earth-element
616 mineralogy of granitic pegmatites in the Trout Creek Pass dictrict, Chaffee County, Colorado.
617 The Canadian Mineralogist 30, 673-686.

618 Harris, R.E., Hausel, W.D., 1986. Wyoming pegmatites. In: Colorado Pegmatite Symposium:
619 Colorado Chapter, Friends of Mineralogy, May 30th-June 2nd, p. 101-108.
620 Heinrich, E.W., 1950. Cordierite in pegmatite near Micanite, Colorado. American Mineralogist,
621 35, 173-184.
622 Jacobson, M.I., Calderwood, M.A., Grguric, B.A., 2007. Guidebook to the pegmatites of
623 Western Australia. Carlisle, Hesperian Press.
624 Jochum, K.P., Weis, U., Stoll, B., Kuzmin, D., Yang, Q., Raczek, I., Jacob, D.E., Stracke, A.,
625 Birbaum, K., Frick, D.A., Günther, D. and Enzweiler, J., 2011, Determination of reference
626 values for NIST SRM 610-617 glasses following ISO guidelines: Geostandards and
627 Geoanalytical Research, 35, p. 397–429.
628 Jolliff, B.L:, Papike, J.J., Shearer, C.K., 1992. Petrogenetic relationships between pegmatite and
629 granite based on geochemistry of muscovite in pegmatite wall zones, Black Hills, South Dakota,
630 USA. Ceochimica et Cosmochimica Acta 56, 1915-1939.
631 Jordt-Evangelista, H., Cesar-Mendes, J., Cosso Lima, A.L., 2000. Amazonitação em granito
632 resultante da intrusão de pegmatitos. Revista Brasileira de Geosciências 30, 693-698.
633 Kinnaird, J., Schneider, G., Nex, P., 2014. Namibian pegmatites and indsutrial minerals. 6-12
634 September. Post Conference Field Trips. 21st General Meeting of IMA South Africa 2014.
635 Kokonyangi, J.W., Kampunzu, A.B., Armtrong, R., Yoshida, M., Okudaira, T., Arima, M.
636 Ngulube, D.A., 2006. The Mesoproterozoic Kibaride belt (Katanga, SE D.R. Congo). Journal of
637 African Earth Sciences 46, 1–35.
638 Larsen, R.B., 2002. The distribution of rare-earth elements in K-feldspars as an indicator of
639 petrogenetic processes in granitic pegmatites: Examples from two pegmatite fields in Southern
640 Norway. The Canadian Mineralogist 40, 137-151.

641 London, D., 1990. Phosphorus in alkali feldspars of rare-element granitic pegmatites. The
642 Canadian Mineralogist 28, 771-786.
643 London, D., 1992. Phosphorus in S-type magmas: the P_2O_5 content of feldspars from
644 peraluminous granites, pegmatites, and rhyolites. American Mineralogist 77, 126–145.
645 London, D., 2014. A petrologic assessment of internal zonation in granitic pegmatites. Lithos
646 184-187, 74-104.
647 Lottermoser, B.G., Lu, J., 1997. Petrogenesis of rare-element pegmatites in the Olary Block,
648 South Australia, part 1. Mineralogy and chemical evolution. Mineralogy and Petrology 59, 1-19.
649 Marchal, K.L., Simmons, W.B., Falster, A.U., Webber, K.L., Roda-Robles, E., 2014.
650 Geochemistry, mineralogy, and evolution of Li-Al micas and feldspars from the Mount Mica
651 pegmatite, Maine, USA. The Canadian Mineralogist 52, 221-233.
652 Marmo, V., 1971. Granite petrology and the granite problem. Elsevier Publishing Company,
653 New York.
654 Martin, R.F., De Vito, C., 2005. The patterns of enrichment in felsic pegmatites ultimately
655 depend on tectonic setting. The Canadian Mineralogist 43, 2027-2048.
656 Martin, R.F., De Vito, C., 2014. The late-stage miniflood of Ca in granitic pegmatites: an open
657 system acid-reflux model involving plagioclase in the exocontact. The Canadian Mineralogist
658 52, 165-181.
659 Martin, R.F., De Vito, C., Pezzotta, F., 2008. Why is amazonitic K-feldspar an earmark of NYF-
660 type granitic pegmatites? Clues from hybrid pegmatites in Madagascar. American Mineralogist
661 93, 263-269.

McLelland, J.M., Selleck, B.W., Hamilton, M.A., Bickford, M.E., 2010. Late- to posttectonic setting of some major Proterozoic anorthosite–mangerite–charnockite–granite (AMCG) suites. The Canadian Mineralogist 48, 729-750.

Merino, E., Villaseca, C., Orejana, D., Jeffries, T., 2013. Gahnite, chrysoberyl and beryl co-occurrence as accessory minerals in a highly evolved peraluminous pluton: The Belvís de Monroy leucogranite (Cáceres, Spain). Lithos 179, 137-156.

Mitchell, R.H., Platt, R.G., 1978. Mafic mineralogy of ferroaugite syenite from the Coldwell alkaline complex, Ontario, Canada. Journal of Petrology 19, 627-651.

Mitchell, R.H., Platt, R.G., 1982. Mineralogy and Petrology of Nepheline Syenites from the Coldwell Alkaline Complex, Ontario, Canada. Journal of Petrology 23, 186-214.

Müller, A., Ihlen, P.M., 2012, Trace elements of pegmatitic quartz and their regional distribution in two pegmatite fields of Southern Norway. Maarten A. T. M. Broekmans (ed.), Proceedings of the 10th International Congress for Applied Mineralogy (ICAM), Springer-Verlag, Berlin Heidelberg.

Müller, A., Seltmann, R., Kober, B., Eklund, O., Jeffries, T., Kronz, A., 2008. Compositional zoning of rapakivi feldspars and coexisting quartz phenocrysts. The Canadian Mineralogist 46, 1417-1442.

Müller, A., Kearsley A., Spratt J., Seltmann R., 2012. Petrogenetic implications of magmatic garnet in granitic pegmatites from southern Norway. The Canadian Mineralogist 50, 1095-1115.

Müller, A., Snook, B., Ihlen, M.P., Beurlen, H., Breiter, K., 2013. Diversity of the quartz chemistry of NYF- and LCT-type pegmatites and its economic implications. Mineral Deposit Research for a High-Tech World. Proceedings of the 12th Biennial SGA Meeting, Vol. 4, 12–15 August 2013, Uppsala, Sweden, p. 1774–1776.

Müller, A., 2014. Chemistry of pegmatite quartz – a possible classification criterion for granitic pegmatites? Abstract Volume of the 21st General Meeting of the International Mineralogical Association 1 to 5 September 2014, Johannesburg, South Africa, p. 261.

Müller A., Ihlen P.M., Snook B., Larsen R., Flem B., Bingen B., Williamson B.J., 2015. The chemistry of quartz in granitic pegmatites of southern Norway: Petrogenetic and economic implications. Economic Geology 110, 137-157.

Neiva, A.M.R., 1995. Distribution of trace elements in feldspars granitic aplites and pegmatites from Alijó-Sanfins, northern Portugal. Mineralogical Magazine 59, 35-45.

Norton, J.J., Page, L.R., Brosbst, D.A., 1962. Geology of the Hugo pegmatite, Keystone, South Dakota. Geological Survey Professional Paper 297-P, 1-85.

Pearce, J.A., Harris, N.B.W., Tindle, A.G., 1984. Trace Element Discrimination Diagrams for the Tectonic Interpretation of Granitic Rocks. Journal of Petrology 25, 956-983.

Pedrosa-Soares, A.C., De Campos, C.P., Noce, C., Silva, L.C., Novo, T., Roncato, J., Medeiros, S., Castañeda, C., Queiroga, G., Dantas, E., Dussin, I., Alkmim, F., 2011, Late Neoproterozoic-Cambrian granitic magmatism in the Araçuaí orogen (Brazil), the Eastern Brazilian Pegmatite Province and related mineral resources. Geological Society, London, Special Publications 350, 25-51.

Ostrooumov, M., 2016. Amazonite: Mineralogy, crystal chemistry, and typomorphism. Amsterdam, Elsevier.

Oyarzábal, J., Galliski, M.A., Perino, E., 2009. Geochemistry of K-feldspar and Muscovite in Rare-element Pegmatites and Granites from the Totoral Pegmatite Field, San Luis, Argentina. Resource Geology 59, 315–329.

707 Palme, H., Jones, A., 2003. Solar system abundances of the elements, in: Meteorites, comets, and
708 planets. Treatise on Geochemistry, vol. 1, Amsterdam, Elsevier, pp. 41-61.
709 Payne, J.G., 1968. Geology and geochemistry of the Blue Mountain nepheline syenite. Canadian
710 Journal of Earth Sciences 5, 259-273.
711 Proctor, K., 1985. Gem pegmatites of Minas Gerais, Brazil: the tourmalines of the Governador
712 Valadares district. Gems and Gemology 21, 86-104.
713 Rino, S., Kon, Y., Sato, W., Maruyama, S., Santosh, M., Zhao, D., 2008. The Grenvillian and
714 Pan-African orogens: World's largest orogenies through geologic time, and their implications on
715 the origin of superplume. Gondwana Research 14, 51–72.
716 Rhodes, J.M., 1969. On the chemistry of potassium feldspars in granitic rocks. Chemical
717 Geology 4, 373-392.
718 Sabina, A.P., 1971. Rocks and Minerals for the Collector: Ottawa to North Bay, Ontario, Hull to
719 Waltham, Quebec. Geological Survey of Canada. paper 70-50. Canada. pp. 130.
720 Sabina, A.P., 1983. Rocks and Minerals for the Collector: Kingston, Ontario to Lac St-Jean,
721 Quebec. Geological Survey of Canada Miscellaneous Reports 32. Canada. pp. 130.
722 Sánchez-Muñoz, L., Correcher, V., Turrero, M.J., Cremades, A., García-Guinea, J., 2006.
723 Visualization of elastic strain fields by the spatial distribution of the blue luminescence in a
724 twinned microcline crystal. Physics and Chemistry of Minerals 33, 639-650.
725 Sánchez-Muñoz, L., García-Guinea, J., Zagorsky, V.Ye., de Moura, O.J.M., Modreski, P.J.,
726 2011a. K-feldspar minerals defined from their twin-structures: Application to a preliminary
727 classification of pegmatites. Asociación Geológica Argentina, Serie D, Publicación Especial 14,
728 175-178.

729 Sánchez-Muñoz, L., Modreski, P.J., Frost, B.R., 2011b. K-feldspar twin-structures from orogenic
730 and anorogenic granitic pegmatites in Central North America. Asociación Geológica Argentina,
731 Serie D, Publicación Especial 14, 179-183.
732 Sánchez-Muñoz, L., García-Guinea, J., Zagorsky, V.Ye., Juwono, T., Modreski, P.J., Cremades,
733 A., Van Tendeloo, G., De Moura, O.J.M., 2012. The evolution of twin patterns in perthitic K-
734 feldspar from granitic pegmatites. The Canadian Mineralogist 50, 989-1024.
735 Sánchez-Muñoz, L., Sanz, J., Sobrados, I., Gan, Z.-H., 2013. Medium-range order in disordered
736 K-feldspars by multinuclear NMR. American Mineralogist 98, 2112-2131.
737 Satterly, J. Hewitt, D.F., 1955. Some radioactive mineral occurrences in the Bancroft area.
738 Geological Circular nº 2 of the Ontario Department of Mines. Toronto, pp.76.
739 Scoates, J.S., Frost, C.D., Mitchell, J.N., Lindsley, D.H., Frost, B.R., 1996. A residual liquid
740 origin for monzonitic rocks in Proterozoic anorthosite complexes: The Sybille intrusion, Laramie
741 Anorthosite Complex, Wyoming. Geological Society of American Bulletin 108, 1357-1371.
742 Sheppard, S., Rasmussen, B., Muhling, J.R., Farrell, T.R., Fletcher, I.R., 2007. Grenvillian-aged
743 orogenesis in the Palaeoproterozoic Gascoyne Complex, Western Australia: 1030–950 Ma
744 reworking of the Proterozoic Capricorn Orogen. Journal of Metamorthic Geology 25, 477-494.
745 Shmakin, B.M., 1979. Composition and structural state of K-feldspars from some U.S.
746 pegmatites. American Mineralogist 64, 49-56.
747 Shearer, C.K., Papike, J.J., Laul, J.C., 1985. Chemistry of potassium feldspars from three zoned
748 pegmatites, Black Hills, South Dakota: Implications concerning pegmatite evolution.
749 Geochimica et Cosmochimica Acta 49, 663-673.
750 Simmons, W.B., Heinrich, E.W., 1980. Rare-earth pegmatites of the South Platte District,
751 Colorado. Colorado Geological survey, Resource Series 11, 131 p.

752 Simmons, W.B., Lee, M.T., Brewster, R.H., 1987. Geochemistry and evolution of the South
753 Platte granite-pegmatite system, Jefferson County, Colorado. Geochimica et Cosmochimica Acta
754 51, 455-471.
755 Simmons, W.B., Webber, K.L., 2008. Pegmatite genesis: state of the art. European Journal of
756 Mineralogy 20, 421-438.
757 Sweetapple, M.T., Collins, P.L.F., 2002. Genetic Framework for the Classification and
758 Distribution of Archean Rare Metal Pegmatites in the North Pilbara Craton, Western Australia.
759 Economic Geology 97, 873-895.
760 Tkachev, A.V., 2011. Evolution of metallogeny of granitic pegmatites associated with orogens
761 throughout geological time. From: Sial, A. N., Bettencourt, J. S., De Campos, C. P. & Ferreira,
762 V. P. (eds) Granite-Related Ore Deposits. Geological Society, London, Special Publications 350,
763 7–23.
764 Taylor, W.H., 1965. The Feldspars, in: Bragg W.L. and Claringbull G.F. (Eds.), Crystal
765 Structure of Minerals, London, Bell and Sons.
766 Utsunomiya, A.; Ota, T., Windley, B.F., Suzuki, N., Uchio, Y., Munekata, K., Maruyama, S.,
767 2007. History of the Pacific superplume: Implications for Pacific paleogeography since the late
768 Proterozoic, in: Yuen, D.A. et al. (Eds.), Superplumes. Springer, pp. 363-408.
769 Vetrin, V.R., Rodionov, N.V., 2009. Geology and Geochronology of Neoarchean Anorogenic
770 Magmatism of the Keivy Structure, Kola Peninsula. Petrology 17, 578-600.
771 Wagener, G.F., 1989. Systematic variation in the tin content of pegmatites in western central
772 Namibia. Journal of Geochemical Exploration 34, 1-19.
773 Walker, R.J., Hanson, G.N., Papike, J.J., Oneil, J.R., Laul, J.C., 1986. Internal evolution of the
774 Tin Mountain pegmatite, Black Hills, South-Dakota. American Mineralogist 71, 440-459.

775 Walker, E.E., Sutcliffe, R.H., Shaw, C.S.J., Shore, G.T., 1993. Preliminary Report on the
776 Petrology and Chemistry of the Rare Metal Occurrences Hosted by the Coldwell Alkaline
777 Complex. Ontario Geological Survey, Open File Report 5840, 20p.
778 Webber, K.L., Simmons, W.B., Falster, A.U., 1999. Biotite as a tectonic discriminant for
779 anorogenic and orogenic pegmatites. Canadian Mineralogist 37, 839-841.
780 Wise, M.A., 1999. Characterization and classification of NYF-type pegmatites. The Canadian
781 Mineralogist 37, 802-803.
782 Wise, M.A., 2013. The discrimination of LCT and NYF granitic pegmatites using mineral
783 chemistry: A pilot study. Abstracts PEG 2013 New Hampshire (USA): The 6th International
784 Symposium on Granitic Pegmatites. 156-157.
785 Zagorsky, V.Ye., Makagon, V.M., Shmakin, B.M., 2003. Systematics of granitic pegmatites.
786 Russian Geology and geophysics 44, 422-435.
787 Zhang, C., Yang, J., Lin, C., Li, C., Lin, J. 2009. Reduction of Eu^{3+} to Eu^{2+} in $MAl_2Si_2O_8$ (M =
788 Ca, Sr,Ba) in air condition. Journal of Solid State Chemistry 182, 1673-1678.
789

790 **Footnotes**

791 Figure 1. Map of the world showing the geological distribution of 123 pegmatite provinces and
792 districts, distinguishing between LCT and NYF suites, as well as some with hybrid affiliation.
793 The map of orogenic belts is based on Utsunomiya et al., (2007) and Rino et al., (2008). Legend:
794 1. Bighorn Mt. (WY, USA); 2. Copper Mt. (WY, USA); 3. South Pass (WY, USA); 4. Black
795 Hills (SD, UDistrict (Country); 5. Haystack Range (WY, USA); 6. Routt Plutonic Suite (CO,
796 USA); 7. Trout Creek Pass (CO, USA); 8. White Picacho (AZ, USA); 9. Mohave Co (AZ, USA);
797 10. Laramie Mt (WY, USA); 11. Berthoud Plutonic Suite (CO, USA); 12. Burro Mtn (NM,

USA); 13. Adirondack Highlands (NY, USA); 14. North New Mexico fields, (USA); 15. Rockford (AL, USA); 16. Kings Mountain (NC, USA); 17. Spruce Pine (NC); 18. Amelia (Virginia, USA); 19. New England districts (USA); 20. Brazil Lake (Nova Scotia, Canada); 21. Southern California (USA); 22. Cat Lake – Winnipeg River (Manitoba, Canada); 23. Wekusko Lake (Manitoba, Canada); 24. Yellowknife basin (NW Territories, Canada); 25. NW Ontario fields (Canada); 26. Superior Lake (ON, Canada); 27. Lac Simard (QC, Canada); 28. Preissac – Lacorne (QC, Canada); 29. Birch Portage – Hanson Lake (SK, Canada); 30. Granville Lake (Manitoba, Canada); 31. SW Grenville southern fields (ON, Canada); 32. SW Grenville northern fields (ON, Canada); 33. Mt Laurier and Gatineau fields (QC, Canada); 34. Lac Turgeon Johan Beetz (QC, Canada); 35. Pikes Peak (CO, USA); 36. Llano-Burnet (TX, USA); 37-37. Sveconorwegian Province in S Norway and SW Sweden (Evje-Iveland, Froland, Glamsland, Arendal, Søndeled, Kragerø, Tørdal, Østfold-Halland; 39. Uttö-Mysingen (Sweden); 40. Varuträsk (Sweden); 41. Bothnian Basin (Sweden); 42. Falun (Central Sweden); 43. Kemiö – Orijärvi (Finland); 44. Eräjärvi (Finland); 45. Seinäjorki (Finland); 46. Ladoga Lake (Russia - Finland); 47. Chupa-Ijona (Karelia, Russia); 48. Keivy Massif. Kola Peninsula (Russia); 49. Leinster (Ireland); 50. El Muerto pegmatites (Oaxacan Complex, Southern Mexico); 51. Borborema Province (RGN, PB, Brazil); 52. Eastern Brazilian Province (MG, BA, ES, Brazil); 53. Sta Maria de Itabira (MG, Brazil); 54. Damara province (Namibia); 55. Namaqualand (South Africa); 56. Kaapvaal (South Africa); 57. Natal districts (South Africa); 58. Panpean Pegmatite Province; 59. SW Nigeria province (Ago-Iwoye, Keffi, Nassarawa, Komu, Wamba districts); 60. Giraul (SW Angola); 61. Caxito (NW Angola); 62. Bikita, Zimbabwe; 63. Alto Ligonha, Mozambique; 64. Ruanda; 65. Burundi; 66. Kobokobo, Kamituga area, South Kivu (Congo); 67. Kapiri Mposhi, Zambia; 68. Lundazi, Zambia; 69. Chroma-Kalomo (Zambia) and Kamativi

(Zimbabwe); 70. Itremo, Madagascar; 71. Southeastern Desert province (Egypt); 72. Manono-Kittolo (Shaba, Congo); 73. Pilbara (WA, Australia); 74. Lake Moore - Dalgaranda (WA); 75. King Leopold (WA); 76. Greenbushes (WA); 77. Coolgardie – Norseman (WA); 78. Mukinbudin (WA); 79. Gascoyne (WA); 80. Mt. Isa (QNL); 81. Olary and Broken Hill, Curnamona province (SA-NSW); 82. Bihar mica belt (India); 83. Nellore mica belt (India); 84. Tamil Nadu belt (india); 85. Bastar-Malkagiri belt India); 86. Rajasthan belt (India); 87. Nuuk region (Greenland); 88. Gardar province (Greenland); 89. Volta Grande, Sao Joao de Rei (Brazil); 90. Strange Lake, Labrador, Canada ; 91.Alakha (Russia); 92. Kolmozero-Voronya (Kola Peninsula, Russia); 93. Yenisei Ridge (Russia); 94. Highland Complex (Sri Lanka); 95. Ghaha-Cote d'Ivore; 96. Bohemian-Moldanubicum belt; 97. Taimyr fold belt (Russia); 98. Altai belt (China, Kazakhstan, Russia); 99. Mongol-Okhotsk fold belt; 100. East Sayan Mt. (Siberi, Russia); 101. Southern Tuva (Kamar-Daba fold belt); 102. East Transbaikalia (Russia); 103. NW Baikal (Russia); 104. Mama-Chuya, North Baikal Highland (Rissia); 105. Iberian Peninsula; 106. Creus Cap (Spain); 107. Hagendorf-Pleystein (Babaria, Germany); 108. Paranesti (NE Greece); 109. Koralpe (Austria); 110. Afghanistan-Pakistan belt; 111. Little Nahanni (NW Territories, Canada); 112. Jiajika, Kangdi, (Sichuan province, China); 113. Nanping, China; 114. Cattlin CreeK –Cocanarup, Ravensthorpe, (WA); 115. Tak (Thailand); 116. Phuket (Thailand); 117. Lao Cai and Phu Tho (Northern Vietnam); 118. Kenticha (Ethiopia); 119. Nimnyr block, Central Aldan (Russia); 120. Middle Urals (Russia); 121. South Urals (Russia); 122. Southern Japan (Japan); 123 Central Alps.

Figure 2. Perthitic textures and twin patterns of the selected feldspars. a) BSE image by FE-SEM of the exsolution pattern of specimen S5C5, showing K-feldspar in white color and Na-feldspar

844 in black color. b) Optical micrograph taken with red plate of sample GcInt2, showing Albite
845 macrotwins in horizontal orientation in blue color close to albite veins in purple color. c) Optical
846 micrograph of a thick section of sample En19 showing many recrystallization units of low
847 microcline in A± and P± orientations from albite veins. The LA-ICP-MS pit visible in the center
848 of the image was placed mostly in clear orthoclase and intermediate microcline to avoid areas of
849 albite veins. d) BSE image of the K-rich orthoclase of c), showing Na-feldspar lamellae in black
850 color without extensive porosity. e) Optical image of a thick section of specimen GcInt2 showing
851 an area between large albite veins (not shown in the photo) with the selected-area for chemical
852 analyses that avoids irregular small albite patches and fine albite films. f) BSE image of an area
853 similar to that presented in e), with albite in black color. g) EMPA image of the albite films
854 broken by Albite recrystallization twinning from small albite veins in e). h) Optical image
855 showing an example of selected area for LS-ICP-MS analysis in a large albite vein in specimen
856 CM3.
857
858 Figure 3. Ce-Eu plot (ppb) with two fields, type I with Eu/Ce > 1.0, type II with Eu/Ce < 1.0.
859 Normalization values from Palme and Jones, (2005). Estimated uncertainties in the
860 measurements are indicated with crosses.
861
862 Figure 4. P-Fe plot by LA-ICP-MS measurements in a log-log scale of the 31 pegmatites, where
863 four radial fields can be differentiated for each type of pegmatites: group I (red squares in a pink
864 field), group II (dark violet lozenges in a violet field), group III (blue lozenges in a shy blue
865 field) and group IV (green squares in a clear green field). A circle marks the samples in each
866 population with a highest content of orthoclase. Sample CM is from a peraluminous pegmatite of

867 group II that is represented in the field of group III. Sample Et1317 is from a group III pegmatite
868 that is represented in the field of group IV pegmatites. The diagonal line separates NYF
869 pegmatites on the left side with Fe > P from LCT pegmatites on the right side with P > Fe.
870 Estimated uncertainties in the measurements are indicated with crosses.
871

The P-Fe diagram for K-feldspars: a preliminary approach in the discrimination of pegmatites

Luis Sánchez-Muñoz[a]*, Axel Müller[b,c], Sol López Andrés[d], Robert F. Martin[e], Peter J. Modreski[f], Odulio J.M. de Moura[g]

[a] Instituto de Cerámica y Vidrio – CSIC, Kelsen 5, E-28049 Madrid, Spain,*lsm@icv.csic.es

[b] Natural History Museum, University of Oslo, NO-0318 Oslo, Norway.

[c] Natural History Museum, London SW7 5BD, UK.

[d] Facultad de Ciencias Geológicas, Universidad Complutense de Madrid, E-28040, Spain.

[e] Earth and Planetary Science, McGill University, Montreal, Quebec, H3A 0E8, Canada.

[f] U.S. Geological Survey, Federal Center Denver, CO 80225-0046, USA.

[g] Governador Valadares, Minas Gerais, Brazil.

ABSTRACT

Pegmatites are extremely coarse-grained and heterogeneous rocks in which quantitative measurements of mineral proportions and chemical compositions of the whole rock are virtually impossible to acquire. Thus, conventional criteria such as bulk compositions and modal mineralogy used for the classifications of igneous rocks simply cannot be applied for pegmatites. An alternative is to use the mineralogical and chemical attributes of K-rich feldspars, the only mineral that is omnipresent in pegmatites. We have used this approach to test a possible discriminant among four groups of pegmatites on the basis of major petrological features, such as the abundance of quartz, feldspars, micas and phosphates. Group I is represented by relatively flux-poor, and silica-poor pegmatites, in most cases with hypersolvus feldspars, devoid of quartz and with minor biotite, which are common in rift settings as in the Coldwell Alkaline Complex

in northwestern Ontario, Canada. Group II comprises relatively flux-poor, silica-rich pegmatites with quartz, subsolvus feldspars and biotite as major primary minerals, typically occurring in the asymmetric collisional Grenville Orogeny. Group III comprises relatively flux-rich, silica-rich P-poor pegmatites with quartz, subsolvus feldspars, and muscovite as the major primary minerals. Finally, group IV consists of relatively flux-rich, silica-rich, P-rich pegmatites with the same previous major minerals as in group III but with abundant phosphates. Group III and IV are found in most symmetric collisional orogens, such as in the Eastern Brazilian Pegmatite Province as the result of the collision of cratons mainly formed by igneous and metamorphic rock of Archean and Early Proterozoic age. We have selected specimens of blocky perthitic K-rich feldspar from the inner part of thirty-one pegmatites belonging to these four categories occurring worldwide to cover a wide range of mineralogy, geological age, geotectonic setting and geographical positions. Concentrations of major elements (Si, Al, K, Na, Ca, Fe, Mg, Mn, Ti and P) were obtained by X-ray fluorescence (XRF), and those of minor and trace elements (P, Fe, Li, Ge, Ga, Rb, Sr, Ba, Tl, Pb, Y, Cs, Ba, La, Ce, Pr, Nd, Sm, Eu, Gd, Tb, Dy, Ho, Er, Tm, Yb, and Lu) were established by laser-ablation inductively coupled plasma - mass spectrometry (LA-ICP-MS), in areas free of coarse Na-feldspar veins or patches. We show that the four groups have very different average values of the minor and trace elements. However, only the cations occupying tetrahedral sites, particularly the Fe and P, are sufficiently immobile to show distinct differences among pegmatites. Hence, we propose a P-Fe diagram to discriminate among the four groups of pegmatites, as a possible criterion with which to classify pegmatites.

Keywords: K-feldspar, pegmatites, perthite, trace elements, LA-ICP-MS data, P-Fe diagram

1. Introduction

One of the challenges of studying any rock with a pegmatitic texture is the lack of information on bulk composition of an intrusive body, owing to the exceptionally coarse grain-size and textural heterogeneity. For these reasons, conventional schemes of classification of igneous rocks using modal proportions or bulk compositions are not applicable. Furthermore, in the case of pegmatites of granitic composition, the intrusive bodies are commonly zoned vertically and horizontally, such that modal proportions of essential minerals may show extreme variability and thus significant departures from the bulk composition of the pegmatite-forming magma. Yet there is a pressing need to classify granitic pegmatites, in order to properly assess their economic potential and the geological information they can provide, including the tectonic context of their emplacement.

Existing classifications are largely based on qualitative criteria applied mainly to mineralized pegmatites, and do not lead to broadly defined or accepted categories. After a brief review of these schemes of classifications, we present analytical results of representative alkali feldspar from 31 carefully evaluated pegmatite localities covering a wide range of mineralogy, age, geotectonic setting at the time of emplacement, and geographic position. These specimens have been characterized by selected-area chemical analysis using laser-ablation – inductively coupled plasma – mass spectrometry (LA–ICP–MS) in order to obtain the concentration of 33 minor elements in pristine areas of K-rich feldspar making up the blocky perthite from the voluminous intermediate zone of zoned bodies of granitic and syenitic pegmatites. Our simplified approach to a complex problem targets an essential mineral common to all pegmatites of granitic or syenitic composition, and yields several new insights that are useful to the

geologist mapping uncharted territory in a pegmatite district. Our aim in this research is to test whether the trace-element signature of K-rich feldspar can be used as a measurable criterion for pegmatite discrimination, and to suggest elements that are best suited to accomplish this purpose.

2. Brief review of the literature

Because of the exceptionally large size of some crystals and an overall textural heterogeneity (London, 2014), conventional schemes of classification, for example using quantitative estimates of modal mineralogy plotted in QAP and APF diagrams, are not possible. Likewise, an approach based of bulk chemical composition plotted in a TAS diagram cannot succeed. Several other criteria have been proposed. Index minerals have been applied, as well as characteristically enriched groups of elements, especially where tied into tectonic setting, for example using the S-I-A-M classification of granitic suites (Simmons and Webber, 2008). However, the recognition of key minerals commonly depends on the level of exposure in any zoned body of granitic pegmatite. Petrogenetic aspects and tectonic setting are difficult or impossible to evaluate from field observations, and their interpretation depends on current models, which evolve with time and increasing knowledge. Genetic classifications thus involve subjective criteria and interpretations. An easily and widely applicable classification should be based on objective (measurable) criteria only.

Most pegmatite investigators use a classification scheme based on the depth of pegmatite formation (pressure and temperature), inspired from the Russian literature (e.g., Ginsburg and Rodionov, 1960; Ginsburg, 1984) and refined by Petr Černý and co-authors (Černý, 1991; Černý and Ercit, 2005). In addition to the depth-zone classification of pegmatite classes (abyssal, muscovite, muscovite rare element, rare element, and miarolitic classes), Černý (1991)

93 established a geochemical subdivision of the rare-element class into three families: the Niobium–
94 Yttrium–Fluorine (NYF), the Lithium–Caesium–Tantalum (LCT) and the mixed NYF–LCT
95 family. Currently, however, the NYF–LCT subdivision has been applied to distinguish also
96 pegmatites of the other four depth-zone classes. The family classification is more widely used
97 than the depth-zone classification because it is useful for the study and description of pegmatites
98 having an economic interest, enriched in Li, Be, Sn, Nb, Ta and gemstones. Basically, the family
99 concept involves a bimodal approach for the discrimination between pegmatite-forming melts
100 derived from the middle and upper crust (i.e., with an LCT geochemical signature) and melts
101 arising from melting in the lower crust, in some cases with mantle contributions, i.e., with the
102 NYF geochemical signature. The NYF pegmatites have been subdivided into three groups,
103 peralkaline, metaluminous and peraluminous, based on the alumina saturation (Wise, 1999).
104 Numerous pegmatites have no temporal and obvious genetic relationship with a parental
105 pluton. In those cases, anatectic melts arising from ultrametamorphism in the deep crust can
106 evidently crystallize with a pegmatitic texture (Ercit, 2005; Müller et al., 2012; Müller et al.,
107 2015). In addition, bodies of pegmatite may well exhibit features of both NYF and LCT suites,
108 with the LCT overprinting the NYF assemblages. Such an overprint may be attributed to
109 hydrothermal activity involving an acidic fluid and contamination from the exocontact area
110 (Martin and De Vito, 2014), or it is a result of extreme, pegmatite-internal differentiation (e.g.
111 Müller et al., 2012). One must appreciate that not every mineral in granitic pegmatites
112 crystallized from a silicate magma; everything gets reworked to some degree after the magma
113 has crystallized, and especially so in large bodies.
114 It is important to note that many pegmatite occurrences do not contain rare minerals, and
115 a clear geochemical affiliation cannot be identified. Consequently, proposals for classification

have recently been suggested that focus on the rare elements and volatiles in addition to depth of emplacement (Zagorsky et al., 2003), the geochemistry of micas and feldspars (Webber et al., 1999; Wise, 2013), the trace element content of quartz (Müller et al., 2013; Müller, 2014), and the microtextural and microstructural characteristics of perthitic K-rich feldspars (Marmo, 1971; Sánchez-Muñoz et al., 2011a). The advantage of using feldspar for classification is that it is the only constituent that occurs in all types of pegmatites of the felsic composition, whereas quartz and micas can be absent. Actually, the presence of "amazonite" (blue-green variety of K-feldspar) in pegmatites has been considered a hallmark of pegmatites of the NYF family (Martin et al., 2008).

Although feldspars are heterogeneous minerals that are very sensitive to chemical changes during the subsolidus and hydrothermal-deuteric stages, the bulk chemical composition of feldspars is commonly used in the study of pegmatites. Previous studies have led to a better understanding of their variability, with applications in the exploration for rare elements (e.g., Alfonso, 2003; Černý et al., 1984; Černý et al., 1985; Larsen, 2002; London, 1990; London, 1992; Marchal et al., 2014; Müller et al., 2008; Neiva, 1995; Oyarzábal et al., 2009; Rhodes, 1969; Sánchez-Muñoz et al., 2011b; Shmakin, 1979; Shearer et al., 1985; Wise, 2013). However, most research has been done in pegmatites of the LCT affiliation, generally from a single province. In many cases, the samples selected for study have had a rather limited microtextural and microstructural characterization, without consideration of the location of the samples within zoned pegmatites, and in many cases using bulk data from powdered samples on the alkalis and the alkaline earths only.

3. The relation of pegmatites to orogenic and anorogenic settings.

Figure 1 shows the distribution of the major pegmatite provinces and districts in the world. In most cases, these are spatially related to orogenic belts associated with areas of crustal convergence, i.e., a compressional regime. Granitic pegmatites can also form in environments marked by tectonic quiescence, i.e., an extensional regime. Most of the large and mineralized pegmatites are associated with collisional orogens, in districts containing thousands of distinct pegmatitic bodies. Such voluminous pegmatite fields are lacking in non-collisional environments, as in the western part of the American continent and in the eastern part of the Australian continent, because a thickened continental crust is needed to create the heat and pressure necessary for melt generation (e.g., Tkachev, 2011). In Figure 1, granitic pegmatites are mainly classified according to the conventional NYF–LCT bimodal approach, although some provinces and districts are known to have hybrid pegmatites. From this literature analysis and the field experience of the authors in many of these provinces, it was possible to distinguish four groups of pegmatites (Table 1) to be discriminated by the mineralogical and geochemical signatures of the perthitic K-rich feldspar. The identification of distinctive features to distinguish among bodies or groups of pegmatites is quite challenging because exceptions are the rule. However, the relative proportions of the major minerals can be used as starting point for discrimination using only general "trends" to test our initial hypothesis (i.e., the usefulness of mineralogical and geochemical features of perthitic K-feldspar for pegmatite discrimination).

(Figure 1. The distribution of the major pegmatite provinces and districts in the world)

The main distinction is based on the proportion of hydrous minerals in the pegmatitic rocks. A first category, which we label "High-T, low-flux", consists of pegmatites with rare

micas or amphiboles (group I) and pegmatites that contain hydrous minerals (biotite) as minor phases (group II). These are pegmatites derived from syenitic magmas, or hosted in granulitic terranes without obvious genetic relationship to a parental pluton (anatectic pegmatites). Such pegmatite-forming magmas are likely to have crystallized at a temperature largely above the upper thermal stability of the ferroan hydrous phases, from a magma relatively poor in fluxing components. A second category, which we label "Low-T, high-flux", consists of granitic pegmatites that contain abundant micas (including muscovite). Two groups are further distinguished by the abundance and diversity of phosphate minerals, which are much higher in group IV than in group III. This bimodal partition parallels the NYF–LCT approach, but it is not based on geochemical affiliations or index minerals.

The silica-poor pegmatites of group I contain in most cases two feldspars that have a hypersolvus texture (Tuttle & Bowen, 1958); biotite and fayalite are rare, whereas quartz is absent in some cases. They are common in rift settings associated with syenites and nepheline syenites, as well as anatectic melts in high-grade metamorphic terranes, without a clear genetic relationship to a parental pluton (Table 1). Phosphates are very rare, in comparison with types III and IV, although accessory apatite and monazite do occur.

The silica-rich pegmatites of type II consist of quartz, two feldspars that have a subsolvus texture, and biotite as major primary minerals (Table 1). They are typically found in anorogenic environments, related to A-type melts, for example in the Grenville orogen of northeastern North America and in southern Scandinavia, with an asymmetric structure, i.e., a linear orogen bordered by two other linear orogens of very different age, one older and the other younger. The Grenville orogen was a locus of repeated collisions of two crustal blocks over the period 1400–1000 Ma, each followed by delamination and extension accompanying the diapiric rise of an

asthenospheric mantle (McLelland et al., 2010; Dickin et al., 2010). The juxtaposition of hot fertile mantle undergoing decompression-induced melting below the lowermost of the stacked crusts provided the setting for wholesale anatexis and production of relatively hot granitic magma. As in group I, pegmatites generally cannot be genetically linked to a parental pluton.

In contrast to group II, group III and IV are typically found in collisional orogens with a symmetrical structure, for instance, linear orogens ending with the collision of two cratons with similar geological structure and lithologies of Archean and Early Proterozoic age, initially as the product of subduction of an oceanic plate underneath a thickened continental crust. The resulting calc-alkaline magmas are metaluminous to peraluminous, and relatively oxidizing, except where the protolith is organic-matter-rich. The presence of a metasedimentary protoliths is responsible for phosphate enrichment. Typical examples (Fig. 1) are the Grenville-age pegmatites of Africa, such as in the Kibaride belt, like the Mwanza Sn-pegmatite and Manono Sn-Nb-Ta-pegmatite of southeastern Democratic Republic of Congo (Kokonyangi et al., 2006) and the Nb-Ta-Sn pegmatites of the Gatumba area in western Rwanda (Dewaele et al., 2011). In the same way, the Gascoin Complex in the Capricorn Orogen (West Australia) contains very rich rare-earth-element pegmatites (Jacobson et al., 2007) of Grenvillian age, such as the Nardoo Hills rare-element pegmatite (Sheppard et al., 2007), derived from crustal peraluminous melts. Thus, the African and West Australian pegmatites formed in symmetric orogens of Grenville age are typical LCT pegmatites, whereas the North American examples, as in the Pikes Peak district of Colorado (Simmons et al., 1980, 1987) and the south Scandinavian pegmatites, such as in Evje-Iveland, Froland, Glamsland, Arendal, Søndeled, Kragerø, Tørdal, Østfold-Halland districts (Müller et al. 2015), formed in an asymmetric orogen of the same age, have typically NYF affinity.

The silica-rich, P-poor pegmatites of group III contain quartz, two coexisting feldspars and muscovite as major primary minerals, and minor phosphates. These pegmatites are commonly formed during the late- to post-orogenic relaxation in an extensional environment, typically in the form of long and regular tabular bodies, as the blue tourmaline-rich pegmatites in Paraiba (Brazil) and in the Cooper Mountain and Casper Mountain districts in Wyoming, United States of America (Harris and Hausel, 1986).

Pegmatites of the group IV are similar to those of the group III but are rich in phosphates (Table 1). High-phosphorus pegmatites typically develop via fractionation of voluminous granitic melts formed by melting of a thick crust in a syn- to late-orogenic setting. Typical examples are most of the pegmatites of Minas Gerais in Brazil, formed during the Braziliano Orogeny (Pedrosa-Soares et al., 2011).

(Table 1. Main features of the four groups of pegmatites used in this work.)

4. Experimental procedure

4.1. Samples

Samples of fresh megacrystic (blocky) perthitic K-rich feldspar having distinct (001) and (010) cleavages were taken from the intermediate zone of selected pegmatite bodies of the four groups of pegmatites. Table 2 provides details about the origin of the samples that we investigated. As the content of impurities of feldspars changes from border to core in zoned bodies of pegmatites, only blocky feldspars from the intermediate zone were sampled, in order acquire a set of comparable data.

(Table 2. Selected pegmatites, sample codes and some important geological features)

231

232 *4.2. Methods*

233 *4.2.1. Polarized light optical microscopy (PLOM)*

234 The feldspar samples were studied using surface-polished thin sections of 30 and 300 μm
235 thickness mounted on standard glass slides parallel to the (001) cleavage. Surfaces were polished
236 up to an average roughness Ra value less than 0.5 μm. A Nikon Eclipse LV100 POL was used,
237 using 1x to 100x objectives that allow observations at five orders of magnitude in the same
238 petrographic preparation, resolving textural and microstructural features with size between 10^{-2}
239 and 10^{-7} m in the same area. Pristine areas without turbidity (i.e., fluid and mineral inclusions, as
240 well as particles of clay minerals resulting from hydrothermal alteration) were selected and
241 marked for the *in situ* trace-element analyses by LA-ICP-MS. The detail of the experimental
242 procedure for textural and microtextural characterization of the samples can be found in
243 Sánchez-Muñoz et al., (2012).

244

245 *4.2.2. Scanning electron microscopy and electron microprobe*

246 The microscopic observations using back-scattered electron imaging (BSE) were
247 acquired using an Inspect ESEM of the FEI Company (for details see Sánchez-Muñoz et al.
248 2012), and a field-emission scanning electron microscope (FE-SEM) also in the BSE modus,
249 using a FEI Nova NANOSEM 230, at 5 kV with a vCD detector at 5.2 mm from the sample. In
250 addition, electron microprobe analysis (EMPA) was used to visualize perthitic textures by
251 chemical mapping, using a SX-50 instrument at 15 kV and 50 nA (see Sánchez-Muñoz et al.,
252 2012 for details).

253

4.2.3. X-ray fluorescence (XRF)

The concentrations of major elements (Si, Al, K, Na, Ca, Fe, Mg, Mn and Ti) were established at the Technical Assistance Center in Earth Science Research of the Complutense University (Madrid, Spain) using a Bruker S2 Ranger energy-dispersive X-ray fluorescence (EDXRF) spectrometer equipped with a Pd anticathode X-ray tube of 50 W in a vacuum atmosphere. Sample preparation was made by the flux-fusion technique with 10 g flux [mix of $Li_2B_4O_7$ (99.5%) and LiI (0.5%)] and 0.5g sample at 1050ºC (maximum temperature), and pressed cylindrical pellets of 4 cm in diameter (9.5 g of dry sample and 0.5 g of Hoechst wax C micropowder as binding agent). Quantification was made with the software provided with the equipment (Spectra Plus/Bruker AXS) through empirical calibration of the system, by using six certified reference materials (NCS DC 71313, FKN, GA, GH, NIM-G and SY3). The limits of detection (%) are: SiO_2 0.23 and Al_2O_3 0.05 with fused beads, and Fe_2O_3 0.004, MnO 0.01, MgO 0.02, CaO 0.02, Na_2O 0.02, K_2O 0.03, TiO_2 0.01 and P_2O_5 0.003 to pressed cylindrical pellets. The chemical compositions was expressed as $Or_xAb_yAn_z$ (x+y+z = 100) (Supplementary Material Table SM1), with Or, Ab and An expressing the molar content of $KAlSi_3O_8$, $NaAlSi_3O_8$ and $CaAl_2Si_2O_8$ components.

4.2.4. Laser-ablation inductively coupled plasma mass spectrometry (LA-ICP-MS)

The analyses were performed at the Geological Survey of Norway, in Trondheim (Norway) on the double-focusing sector field mass spectrometer, model ELEMENT XR, from Thermo Scientific, which is combined with the excimer-based NewWave UP193FX laser probe. The analyses were done on the 300-µm-thick sections. The 193-nm laser had a repetition rate of 20 Hz, a spot size of 75 µm, and an energy fluence of 5.5 to 6.5 mJ/cm^2 on the sample surface. A

277 continuous raster ablation (laser speed 15 μm/s) on an area of approximately 300 × 150 μm was
278 applied. In all specimens, it was possible to select regions for analysis without turbidity, where
279 the separation between albite veins (microperthitic texture) is larger than the spatial resolution of
280 this technique. The size scale of the crypto- and microperthitic intergrowths of K- and Na-
281 feldspar is much smaller that the size of the ablation pits. However, no chemical changes are
282 expected during the exsolution process to produce such fine microtextures. The chemical
283 composition will not change at the scale of the sampled surface, i.e., exsolution took place in
284 "isochemical condition" at the size of the laser probe. Problems related to the dispersion of data
285 are related to albite veins and turbidity, not to fine perthitic textures.

286 For each sample, two analyses of the K-feldspar matrix and one of the Na-rich feldspar in
287 the veins of the perthite intergrowth were carried out. The isotope ^{29}Si was used as the internal
288 standard, applied to the concentration of Si determined by XRF. An Ar blank was run before
289 every sample and standard measurement to determine the background signal. In order to avoid
290 memory effects between samples, the background signal was subtracted from the instrumental
291 response of the standard before normalization against the internal standard. External
292 multistandard calibration was performed using five silicate glass reference materials produced by
293 the National Institute of Standards and Technology, USA (NIST SRM 610, 612, 614, 616, 1830)
294 and the certified reference material silica glass BCS CRM 313/1 from the Federal Institute for
295 Material Research and Testing in Germany. Certified, recommended, and proposed values for
296 these reference materials were taken from Jochum et al., (2011), Flem and Bédard, (2002) and
297 from the certificates of analysis where available. The limits of detection (LOD) are based upon
298 3x standard deviation (3σ) of 10 NIST SRM 616 measurements. The LODs for the individual
299 elements are: Li 0.14 ppm, P 5.01 ppm, Fe 0.88 ppm, Ga 0.26 ppm, Ge 0.04 ppm, Rb 0.02 ppm,

Sr 11.46 ppm, Y 0.01 ppm, Cs 0.01 ppm, Ba 0.53 ppm, La 0.012 ppm, Ce 0.007 ppm, Pr 0.004 ppm, Nd 0.009, Sm 0.009, Eu 0.004 ppm, Gd 0.009 ppm, Tb 0.005 ppm, Dy 0.007 ppm, Ho 0.008 ppm, Er 0.004 ppm, Tm 0.005 ppm, Yb 0.009 ppm, Lu 0.006 ppm, Tl 0.006 ppm, and Pb 0.16 ppm. Data provided in Tables 4 and 5, and Tables SM1 to SM5 (Supplementary Materials) represent a single value for Na-feldspar veins and the average of two analyses for K-feldspar in each sample.

5. Perthitic textures and twin patterns

The main features of the microstructures developed as a result of the monoclinic-to-triclinic inversion and recrystallization-induced twinning in the K-feldspar and the perthitic microtextures resulting from K–Na exsolution for the four categories of pegmatites are shown in Table 3. The nomenclature employed to describe the twin patterns and to identify microcline and orthoclase using Raman spectra, measured directly on the thin sections, is explained in detail in Sánchez-Muñoz et al., (2012). Figure 2 shows some typical features of the perthitic textures and twin patterns observed in the specimens studied, as well as examples of laser ablation pits created during the LA-ICP-MS analyses (see Electronic Appendix 1 for examples of the analytical area sampled in the K-rich feldspar regions of the specimens used in this work).

(Table 3. Petrographic features of samples selected by PLOM observations)

Pegmatite bodies of group I typically show first-generation twins of microcline, and albite veins in a wide range of sizes. Albite in fine mesoperthitic microtextures only occurs in the hypersolvus feldspars of this type, i.e., in samples S5C2 (Fig.2a), S10C12 and FH1. The coarsening and formation of large incoherent Na-feldspar veins in sample S5C2 and S10C12 is

limited to certain parts of the specimen, leaving vast areas with pristine character. Exsolution-induced textures are much finer that the width of the portions ablated by the laser. In the other samples of group II, albite veins of different sizes are formed that leave space for proper chemical analyses by the selected area method.

(Figure 2. Selected features of perthitic textures and twin patterns, showing the selected area for LA-ICP-MS analyses)

Extremely coarse veins of albite in large mesoperthitic textures, visible with the naked eye, occur in sample TL from a group-I pegmatite in Perth, Ontario, Canada, i.e., the type locality of perthite, where albite veins can have up to 2 millimeters wide, leaving region with microperthitic K-rich feldspars of the same width. Microcline perthites of group IV have albite veins of a similar size to that one, but the relative extent of the regions of microperthitic K-rich feldspars is greater than in mesoperthites (Fig. 2b).

First-generation twins in tartan and parquet configurations in microcline are also the most common feature in pegmatite bodies of group II (see Fig. 2a and Fig. 6 in Sánchez-Muñoz et al., 2012). These configurations commonly involve irrational twins, as well as diffuse cross-hatched microstructures. In some cases, one can observe several microtextures resulting from the recrystallization of Albite-twinned (A) and Pericline-twinned (P) microcline to single-orientation microcline. All examples studied in this category exhibit a subsolvus texture, in which perthitic grains contain albite veins narrower than 100 μm, as well as thin films of albite. Residual orthoclase with an intermediate degree of local order can be found in this group, as for instance in specimen WC1. The width of the areas between albite veins was sufficient to obtain LA-ICP-MS analyses without interference of these more altered zones (see Electronic Appendix 1).

346 Single-orientation microcline is the most characteristic microstructure in pegmatites of
347 group III, as well as intermediate steps in achieving that pattern (see Figure 10 in Sánchez-
348 Muñoz et al., 2012). The perthitic textures consist of albite veins ranging from a few
349 micrometers to tens of micrometers in width. Orthoclase can be found in some cases, specifically
350 where the K-rich feldspars of this category have a relatively high content of phosphorus, as in
351 specimen MMG2. The K-rich matrix with fine micro- and cryptoperthitic textures, located
352 between large albite veins, were also easily analyzed by LA-ICP-MS also in this case (see
353 Electronic Appendix 1).
354 The twin patterns of microcline in pegmatites of group IV are extremely variable, but
355 single-orientation microcline has not been found in any case. Perthites with orthoclase as a major
356 component (Fig. 2c) are common in these pegmatites, mainly because of the chemical effect of
357 impurities as kinetic hinderers (i.e., kinetic barriers to ordering), such as phosphorus (Sánchez-
358 Muñoz et al., 2012). Second-generation twins that arise by recrystallization and directed
359 coarsening of the first generation of twins or the recrystallization of orthoclase along interfaces
360 between the K-feldspar matrix and albite veins are very common (Fig. 2c). Twin coarsening of
361 polysynthetic patterns and chessboards are very common. Perthitic textures trend to be bimodal
362 in size, having fine films that are well preserved if orthoclase is not recrystallized into microcline
363 (Fig. 2d). These areas marked by minimum interaction with water, i.e., the exsolution process
364 was isochemical at the scale of the laser probe, were selected for LA-ICP-MS analysis.
365 Perthites formed mostly by large microcline twins (Fig. 2b) have also important
366 development of recrystallization units along interfaces with fine veins (Figs. 2e). It involves the
367 breaking of albite films into several parts (Figs. 2f, 2g) or the formation of zigzag interfaces
368 (serrated albite) related to mechanical polysynthetic A± twinning arising from tectonic stresses

(see Fig. 2 en Sánchez-Muñoz et al. 2006). Large veins arising from the coalescence of albite are the most frequently encountered feature, commonly showing also the last stages of coarsening resulting from interactions with fluids migrating along interfaces, giving rise to patch morphology. It was easy to find large albite veins to obtain the chemical composition in terms of minor and trace elements by LA-ICP-MS analysis (Fig. 2h).

Therefore, with the selected-area technique, it was possible to analyze pristine areas of micro and-cryptoperthitic K-rich feldspars, avoiding large and small albite veins, turbid areas with strong alteration, inclusions of other minerals (for instance, Fe-rich amphiboles in specimen S10C12), zones with a high rugosity from imperfect sample preparation, as well as cracks (see examples of these situations in the selected areas analyzed in Electronic Appendix 1). However, the LA-ICP-MS technique does not allow us to obtain chemical bulk compositions of the feldspars because the size of the laser probe is too small in comparison with the size of the textural elements in such heterogeneous textures of the perthitic and twinned feldspars. On the other hand, we were not interested in obtaining such global values but those in areas which are closer to the original composition of the mineral, having the minimum amount as possible of chemical losses by albite vein formation and water circulation at low temperatures along the interfaces.

6. Major elements

We present chemical composition the 31 samples in terms of major elements from XRF (Table SM1). The proportion of K-feldspar is higher that the proportion of Na-feldspar in all samples, as most samples has Na_2O content between 1.5 and 4.2 wt %. Specimen Et1317 has only 1.51 wt % of Na_2O and does not have large veins of albite, a typical characteristic of K-rich

feldspar of post-orogenic granites (Marmo, 1971), consistent with our group III. In samples S5C5 and S10C12, the two constituents have similar proportions. These samples are also rich in inclusions of amphibole that could not be separated when preparing the powders for bulk chemical analysis, resulting in high Fe_2O_3 content.

7. Minor and trace elements

The structure of alkali feldspars consists of three-dimensionally linked SiO_4 and AlO_4 tetrahedral units. There are four spectroscopically non-equivalent tetrahedrally coordinated (T) sites in each ring of tetrahedra, which are arranged in double crankshaft chains (Taylor, 1965). The alkali A^{+} and alkaline earth A^{2+} elements are located at the M sites inside the irregular cavity formed by the framework of tetrahedra; these ensure local electrostatic neutrality forming medium-range order schemes (Sánchez-Muñoz et al., 2013). The Si and Al atoms of the framework sites can be replaced by 5+, 4+ and 3+ cations such as P^{5+}, Ge^{4+}, Ga^{3+} and Fe^{3+}, during crystallization of the magma. Their concentration in the feldspar will reflect the availability of these elements in the pegmatite-forming magma and the relevant partition-coefficients. Similarly, K and Na atoms of the cavity M sites can be occupied by 1+, 2+ and 3+ cations, such as Li^{+}, Rb^{+}, Cs^{+}, Tl^{+}, Sr^{2+}, Ba^{2+}, Pb^{2+} and rare-earth elements as REE^{3+}, except for Eu, which in reducing environments can be present as Eu^{2+}.

When *averaged values* for the four groups of pegmatites are considered, they are found to be very different (Table 4). Lithium, Rb, Cs, Tl, Ge and P increase in concentration from group I to IV, whereas Sr, Eu and Fe exhibit the contrary trend. Barium peaks in group II, a behaviour also found in Ga, Y, La and Ce. Lead also peaks in group II, but its concentration is higher in

group III and IV than in I. Thus, the coherent pattern of distribution of these elements indicates that the selection of samples and pegmatites was appropriate to attain our objectives.

(Table 4. Average values of minor and trace elements in ppm (ppb for Y, La, Ce and Eu) of the K-rich feldspar and Na-feldspar in the four groups of pegmatites from LA-ICP-MS)

7.1. The M-site cations

No meaningful distinctions were observed in the concentrations of the alkalis and alkaline earths among the feldspars from different groups of pegmatites. Tables SM2 and SM3 and Figure SM1a and SM1b in Supplementary Materials show the correlations between the Rb content and other 1+ and 2+ elements occupying the M sites of K-rich feldspars. A tight linear relationship is found in the Rb-Tl diagram for K-rich feldspars, which becomes broader but still linear in the case of the Rb-Cs plot. The correlation is weakly developed in the Rb-Li plot. The fields are not well defined, and thus these diagrams are not useful for the discrimination of pegmatites. The contents of these elements in the albite veins of the perthitic microtexture are in most cases much lower than values in the K-feldspar matrix, indicating that important chemical changes must occur during exsolution and later growth of the albite veins. This effect is particularly strong in specimen TL1, with albite veins up to 2 mm wide, and also in specimens NH1, CM3, TC and BK2. In contrast to the Rb-A^{+} plots, no well-defined trend can be observed in the correlation of Rb and 2+ elements also present at the M sites. Because of the high detection limit of Sr (11.5 ppm), the Rb-Sr plot is not of much use. Moreover, the contents of these elements in the Na-feldspar do not follow any particular behavior. In many cases, these elements are lost with albite formation, particularly in samples TL1 and CM3, as was found to be the case with the alkalis.

439

440 *7.2. Rare-earth elements*

441 Rare-earth elements are allocated to the M sites of the structure (Zhang et al., 2009).
442 Although La, Ce, Pr, Nd, Sm, Eu, Gd, Tb, Dy, Ho, Er, Tm, Yb, and Lu were sought in all
443 samples, only Y, La, Ce and Eu have concentrations sufficient to be measured with the
444 equipment used, particularly in feldspars of group-I and group-II pegmatites (Table SM4).
445 Interestingly, the REE are mainly concentrated in the Na-feldspar of the albite veins in the
446 perthitic microtexture, as shown in the REE patterns (Fig. SM2). The highest contents in most of
447 these elements are encountered in pegmatites of group I; these exhibit a pronounced Eu anomaly.
448 Only in one sample (specimen LL1 from the Lone Lode pegmatite in the Pikes Peak, Colorado,
449 USA) is there a sufficiently high concentration in the two feldspars to compare their REE
450 patterns. In this case, the total REE content is higher in the K-rich feldspar, but its positive Eu
451 anomaly is lower than in the Na-feldspar, and these anomalies are lower than in the sample C5S5
452 from a pegmatite of group I. Figure SM2c illustrates an example of a REE pattern in a group-III
453 pegmatite, where no Eu anomaly is found, and a very low total REE content is recorded, as well
454 as a small positive Sm anomaly. In most samples of group-IV pegmatites, the concentration of
455 REE is below the limit of detection.

456 These data only allow one to distinguish among the two first categories of pegmatites
457 (Fig. 3). In this graph, where Eu and Ce contents have the same scale, two fields represent well
458 the different geochemical affiliations. Pegmatites of group I exhibit Eu > Ce (pink field in Fig.
459 3), in contrast to pegmatites of group II, where in most cases, Eu < Ce (violet field in Fig. 3).
460 Similar REE contents to pegmatites of group II have been found in K-feldspar from the Evje-
461 Iveland and Froland pegmatite fields in southern Norway (Larsen, 2002). Only certain samples

462 from pegmatites of group III have a sufficient content of these elements to be shown in this plot,
463 and thus, they were not represented in Figure 3.

464 **(Figure 3. The Eu-Ce diagram)**

465

466 *7.3. The T-site cations*

467 Figure SM3 shows the measured concentrations of Ga and Ge in K-feldspar, using a plot
468 with the same values for both axes, and Table SM5 has the numerical values. The Ge-Ga graph
469 shows that pegmatites of group I can be clearly discriminated from the other types because they
470 show a lower content in Ge. The pegmatites of group II can be distinguished only partially from
471 the pegmatites of group III and IV (the two groups of LCT pegmatites) by means of the ratio
472 Ga/Ge. Note that in contrast with the behaviour of the M cations (including REE), there are no
473 sharp differences in most cases between the values of the K-feldspar matrix and the Na-feldspar
474 veins. The implication is that these elements remain where they are during the subsolidus
475 transformations (Si–Al ordering, transformation twinning and recrystallization twinning, as
476 described in Sánchez-Muñoz et al., 2012).

477 In sharp contrast with the previous graphs, the P-Fe plot of K-feldspars (Fig. 4) shows a
478 very good discrimination among the four groups of pegmatite (see Table 5 for numerical values).
479 The plot is constructed using the same log scale for both elements. The transversal line
480 expressing a Fe:P ratio equal to 1.0 perfectly separates the NYF pegmatites (group I in pink and
481 group II in violet) from the LCT pegmatites (group III in blue and group IV in green). The only
482 exception is sample CM3 from the Climax Mica pegmatite (sample CM, Fig. 4), which contains
483 rare-earth minerals and a strongly peraluminous character. It contains unusual large masses of
484 cordierite (Heinrich, 1950) and abundant secondary muscovite (Hanley et al., 1950). Pegmatites

of groups I and II are separated by a line starting at the origin (at a concentration of 1 ppm in the two cations) and ending at P = 10^2 ppm and Fe = 10^4 ppm. In the same way, pegmatites of groups III and IV can be separated by a similar line starting at the same point and ending at P = 10^4 ppm and Fe = 10^2 ppm. Sample Et1317 from East Transbaikalia (Russia) is an exception, and extensive recrystallization has caused single-orientation microcline to form (PLOM observations). Thus, a pegmatite belonging to group III is represented in the field of group IV.

(Table 5. Fe and P contents in K- and Na-feldspars (ppm) by LA-ICP-MS

(Figure 4. The Fe-P diagram)

8. Implications

Figure 4 shows that the four categories of pegmatite that we have defined can be discriminated using the contents of P and Fe. Any pegmatitic body thus can presumably be classified with this graph, independently of index minerals or the mineralization and economic potential (see Dill, 2015 for a recent review of the ore geology of pegmatites). Thus a purely petrochemical classification seems to be possible. This type of diagram is common in the geological literature, e.g., discriminant diagrams are used to infer the tectonic setting of granitic rocks, but the resulting shape and distribution of the chemical fields in plots are difficult to interpret from the point of view of crystallochemical phenomena, as they result from statistical studies from a data bank (Pearce et al., 1984). In our approach, we have selected a few representative pegmatites to obtain high-quality trace-element data by selected-area chemical analyses of pristine regions of K-rich feldspar (i.e. areas without turbidity, with crypto- and microperthitic domains located between large Na-feldspar veins) using LA-ICP-MS. Thus,

507 conventional crystallochemical concepts can be employed to interpret the resulting radial fields
508 of Figure 4.

509 Starting from the high-temperature crystallization of a pegmatite-forming melt, the first-
510 formed alkali feldspar at the magmatic stage is sanidine, a disordered solid-solution with a
511 composition close to $(Na,K)AlSi_3O_8$ that incorporates other cations in the framework T and
512 cavity M sites as "chemical impurities". Goldsmith, (1953) explained the crystallization with the
513 Ostwald's rule of stages, i.e., the highest simplexity or most disordered stage should be the most
514 easily formed from a random liquid system. In this initial step, the concentration of the minor
515 and trace elements in feldspars depends mainly on their concentration in the melt, as well as on
516 pressure, temperature and oxygen fugacity at the time of crystal growth.

517 However, as temperature decreases after emplacement, the feldspar system evolves to
518 more equilibrated configurations by means of several processes, including atomic ordering,
519 phase separation and impurity exclusion. The transformation and recrystallization affecting the
520 sanidine solid-solution to produce orthoclase or microcline (or both) and albite (Sánchez-Muñoz
521 et al., 2012, 2013) involve a drastic decrease in the concentration of impurities. Thus, in most
522 cases, orthoclase has a higher content of minor and trace elements than microcline in the same
523 group of pegmatites, as shown by the circle in Figure 5. The trend shown by samples of each
524 population trending toward the origin in the diagram can be explained as a progressive loss of
525 impurities with its recrystallization of A± and P± twinned microcline first, and the development
526 of single-orientation microcline at later subsolidus stages.

527 Consequently, the concentrations that we measure in the feldspars are the result of two
528 effects: the composition of the original melt, which depends on the source lithologies (upper
529 mantle, lower crust, upper crust), and the extent of recrystallization, which mainly depends on

530 the tectonic setting and local geological conditions such as cooling rate, directed stresses [see
531 Černý et al., (2012) and Martin and De Vito, (2005) for detailed discussions]. The K-feldspar
532 records self-organized non-equilibrium twin patterns at the subsolidus stage and ambient
533 physical conditions in each tectonic setting (Sánchez-Muñoz et al., 2012). It is clear that the
534 original chemical signatures involving the framework (T) sites are not totally erased. However,
535 when hydrothermal and deuteric fluids interact with feldspars, dissolution-recrystallization
536 phenomena occur by catastrophic processes, typically at the last stages of vein perthite
537 formation, to give patches. Drastic chemical changes in bulk compositions are likely to occur in
538 fine-grained granitic rocks because of the interaction of hydrothermal and deuteric fluids with
539 feldspars at low temperatures.
540
541 **9. Conclusions**
542 Because of the large size of crystals and the exceptional textural heterogeneity of
543 pegmatites, it is not possible to use the standard methods of classification, like modal mineralogy
544 and bulk chemical compositions. An alternative approach is to use the geochemical features of
545 K-feldspar, an omnipresent mineral in pegmatites, to discriminate among different groups having
546 well-defined petrological features. With this objective, we have selected 31 samples of blocky
547 feldspars from pegmatites that can be grouped into four different categories according to the
548 amount of hydrous minerals, the presence or absence of quartz, and the abundance and
549 variability of phosphates minerals (Table 1). The trace-element diagrams based on cations at M
550 sites (M vs M and M vs T) were found to be of no use to discriminate among the four categories
551 in spite of average values in each population that are different. Elements located at the M site are
552 easily released from the mineral structure during the subsolidus and hydrothermal-deuteric

553 stages. However, the T vs T plots are useful to represent different pegmatites in well-separated
554 fields, as the T cations are much more firmly held in the structure. Specifically, the P–Fe plot,
555 with four radially distributed fields, is found to be very useful in the division of four previously
556 defined categories of pegmatite. Therefore, this methodology could be useful to help place the
557 classification of pegmatites on a more objective basis than has been possible so far.
558
559 **Acknowledgements**
560 We thank B. Ronald Frost of the University of Wyoming in Laramie for his assistance in
561 the field while sampling of Funny Hill pegmatite (specimen FH1) in Wyoming, USA, used in
562 this work; to Victor Ye. Zagorsky (1942-2015) and V.M. Makagon from Vinogradov Institute of
563 Geochemistry (Irkutsk, Russia) for samples ZAG and Et1317. We are grateful to an anonymous
564 reviewer for constructive suggestions and comments, and to the editor-in-Chief Nelson Eby, and
565 Skip Simmons for their help in improving the quality of this manuscript. The study was partially
566 financially supported by the project MAT2013-48009-C4-1-P.
567
568 **References**
569 Alfonso, P., 2003. Geochemistry of feldspars and muscovite in granitic pegmatite from Cap de
570 Creus Field, Catalonia, Spain. The Canadian Mineralogist 41, 103-116.
571 Beurlen, H., Da Silva, M.R.R., Thomas, R., Soares, D.R., and Olivier, P., 2008. Nb–Ta–(Ti–Sn)
572 oxide mineral chemistry as tracer of rare element granitic pegmatite fractionation in the
573 Borborema Province, Northeastern Brazil. Mineralium Deposita 43, 207-228.

574 Beurlen, H., Thomas, R., Rodrigues da Silva, M.R., Müller, A., Rhede, D., Soares, D.R., 2014.
575 Perspectives for Li- and Ta-mineralization in the Borborema pegmatite province, NE-Brazil: A
576 review. Journal of South American eath Sciences 56, 110-127.
577 Černý, P., Smith, J.V., Mason, R.A., Delaney, J.S., 1984. Geochemistry and petrology of
578 feldspar crystallization in the Vezna pegmatite, Czechoslovakia. The Canadian Mineralogist 22,
579 631-651.
580 Černý, P., Meintzer, R.E., Anderson, A.J., 1985. Extreme fractionation in rare-element granitic
581 pegmatites: selected examples of data and mechanisms. The Canadian Mineralogist 23, 381-421.
582 Černý, P. 1991. Fertile granites of Precambrian rare-element pegmatite fields: is geochemistry
583 controlled by tectonic setting or source lithologies? Precambrian Research 51, 429-468.
584 Černý, P., Ercit, T.S., 2005. The classification of granitic pegmatites revisited. The Canadian
585 Mineralogist 43, 2005–2026.
586 Černý, P., London, D., Novak, M., 2012. Granitic pegmatites as reflections of their sources.
587 Elements 8, 257–261.
588 Dewaele, S., Henjes-Kunst, F., Melcher, F., Sitnikova, M., Burgess, R., Gerdes, A., Alonso
589 Fernandez, M., De Clercq, F., Muchez, P., Lehmann, B., 2011. Late Neoproterozoic overprinting
590 of the cassiterite and columbite–tantalite bearing pegmatites of the Gatumba area, Rwanda
591 (Central Africa). Journal of African Earth Sciences 61, 10–26.
592 Dickin, A.P., McNutt, R.H., Martin, C., Guo, A., 2010. The extent of juvenile crust in the
593 Grenville Province: Nd isotope evidence. Geological Society of America Bulletin 122, 870-883.
594 Dill, H.G., 2015. Pegmatites and aplites: Their genetic and applied ore geology. Ore Geology
595 Reviews 69, 417-561.

596 Ercit, T.S., 2005. REE-enriched granitic pegmatites, in: Linnen, R.L., Samson, I.M. (Eds.), Rare-
597 element geochemistry and mineral deposits. Geological Association of Canada, Geological
598 Association of Canada, Short Course Notes 17, 175-199.
599 Fanton J.J., Arioli E.A., Moura O.J.M., 1978. Pegmatitos da região de Galiléia-Mendes Pimentel,
600 MG. In: SBG, Anais do XXX Congresso Brasileiro de Geologia, Recife, 1770-1781.
601 Flem B., Bédard L.P., 2002. Determination of Trace Elements in BCS CRM 313/1 (BAS) and
602 NIST SRM 1830 by Inductively Coupled Plasma-Mass Spectrometry and Instrumental Neutron
603 Activation Analysis. Journal of Geostandards and Geoanalysis, 26, 287-300.
604 Galliski, M.A., Márquez-Zavalía, M.F., Martínez, V., Roquet, M.B., 2011. Granitic pegmatites
605 of the San Luis Ranges. Field Trip Guidebook, 5th International Symposium on Granitic
606 Pegmatites. PEG2011. Argentina, pp. 44.
607 Ginsburg, A.I., Rodionov, G.G., 1960. On the depths of the granitic pegmatite formation.
608 Geologiya Rudnykh Mestorozhdenyi, Izd. Nauka, Moskva, l, pp. 45-54. (in Russian)
609 Ginsburg, A.I., 1984. The geological conditions of the location and the formation of granitic
610 pegmatites. 27Th International Geological Congress, 15: 245-260.
611 Goldsmith, J.R., 1953. A “simplexity principle” and its relations to “ease” of crystallization.
612 Journal of Geology 61, 439-451.
613 Hanley, J.B., Heinrich E.WM. and Page, L.R., 1950. Pegmatite investigations in Colorado,
614 Wyoming, and Utah 1942-1944. Geological Survey Professional Paper 227, 83p.
615 Hanson, S.L., Simmons, W.B., Webber, K.L., Falster, A.U., 1992. Rare-earth-element
616 mineralogy of granitic pegmatites in the Trout Creek Pass dictrict, Chaffee County, Colorado.
617 The Canadian Mineralogist 30, 673-686.

618 Harris, R.E., Hausel, W.D., 1986. Wyoming pegmatites. In: Colorado Pegmatite Symposium:
619 Colorado Chapter, Friends of Mineralogy, May 30th-June 2nd, p. 101-108.
620 Heinrich, E.W., 1950. Cordierite in pegmatite near Micanite, Colorado. American Mineralogist,
621 35, 173-184.
622 Jacobson, M.I., Calderwood, M.A., Grguric, B.A., 2007. Guidebook to the pegmatites of
623 Western Australia. Carlisle, Hesperian Press.
624 Jochum, K.P., Weis, U., Stoll, B., Kuzmin, D., Yang, Q., Raczek, I., Jacob, D.E., Stracke, A.,
625 Birbaum, K., Frick, D.A., Günther, D. and Enzweiler, J., 2011, Determination of reference
626 values for NIST SRM 610-617 glasses following ISO guidelines: Geostandards and
627 Geoanalytical Research, 35, p. 397–429.
628 Jolliff, B.L:, Papike, J.J., Shearer, C.K., 1992. Petrogenetic relationships between pegmatite and
629 granite based on geochemistry of muscovite in pegmatite wall zones, Black Hills, South Dakota,
630 USA. Ceochimica et Cosmochimica Acta 56, 1915-1939.
631 Jordt-Evangelista, H., Cesar-Mendes, J., Cosso Lima, A.L., 2000. Amazonitação em granito
632 resultante da intrusão de pegmatitos. Revista Brasileira de Geosciências 30, 693-698.
633 Kinnaird, J., Schneider, G., Nex, P., 2014. Namibian pegmatites and indsutrial minerals. 6-12
634 September. Post Conference Field Trips. 21st General Meeting of IMA South Africa 2014.
635 Kokonyangi, J.W., Kampunzu, A.B., Armtrong, R., Yoshida, M., Okudaira, T., Arima, M.
636 Ngulube, D.A., 2006. The Mesoproterozoic Kibaride belt (Katanga, SE D.R. Congo). Journal of
637 African Earth Sciences 46, 1–35.
638 Larsen, R.B., 2002. The distribution of rare-earth elements in K-feldspars as an indicator of
639 petrogenetic processes in granitic pegmatites: Examples from two pegmatite fields in Southern
640 Norway. The Canadian Mineralogist 40, 137-151.

641 London, D., 1990. Phosphorus in alkali feldspars of rare-element granitic pegmatites. The
642 Canadian Mineralogist 28, 771-786.
643 London, D., 1992. Phosphorus in S-type magmas: the P_2O_5 content of feldspars from
644 peraluminous granites, pegmatites, and rhyolites. American Mineralogist 77, 126–145.
645 London, D., 2014. A petrologic assessment of internal zonation in granitic pegmatites. Lithos
646 184-187, 74-104.
647 Lottermoser, B.G., Lu, J., 1997. Petrogenesis of rare-element pegmatites in the Olary Block,
648 South Australia, part 1. Mineralogy and chemical evolution. Mineralogy and Petrology 59, 1-19.
649 Marchal, K.L., Simmons, W.B., Falster, A.U., Webber, K.L., Roda-Robles, E., 2014.
650 Geochemistry, mineralogy, and evolution of Li-Al micas and feldspars from the Mount Mica
651 pegmatite, Maine, USA. The Canadian Mineralogist 52, 221-233.
652 Marmo, V., 1971. Granite petrology and the granite problem. Elsevier Publishing Company,
653 New York.
654 Martin, R.F., De Vito, C., 2005. The patterns of enrichment in felsic pegmatites ultimately
655 depend on tectonic setting. The Canadian Mineralogist 43, 2027-2048.
656 Martin, R.F., De Vito, C., 2014. The late-stage miniflood of Ca in granitic pegmatites: an open
657 system acid-reflux model involving plagioclase in the exocontact. The Canadian Mineralogist
658 52, 165-181.
659 Martin, R.F., De Vito, C., Pezzotta, F., 2008. Why is amazonitic K-feldspar an earmark of NYF-
660 type granitic pegmatites? Clues from hybrid pegmatites in Madagascar. American Mineralogist
661 93, 263-269.

McLelland, J.M., Selleck, B.W., Hamilton, M.A., Bickford, M.E., 2010. Late- to posttectonic setting of some major Proterozoic anorthosite–mangerite–charnockite–granite (AMCG) suites. The Canadian Mineralogist 48, 729-750.

Merino, E., Villaseca, C., Orejana, D., Jeffries, T., 2013. Gahnite, chrysoberyl and beryl co-occurrence as accessory minerals in a highly evolved peraluminous pluton: The Belvís de Monroy leucogranite (Cáceres, Spain). Lithos 179, 137-156.

Mitchell, R.H., Platt, R.G., 1978. Mafic mineralogy of ferroaugite syenite from the Coldwell alkaline complex, Ontario, Canada. Journal of Petrology 19, 627-651.

Mitchell, R.H., Platt, R.G., 1982. Mineralogy and Petrology of Nepheline Syenites from the Coldwell Alkaline Complex, Ontario, Canada. Journal of Petrology 23, 186-214.

Müller, A., Ihlen, P.M., 2012, Trace elements of pegmatitic quartz and their regional distribution in two pegmatite fields of Southern Norway. Maarten A. T. M. Broekmans (ed.), Proceedings of the 10th International Congress for Applied Mineralogy (ICAM), Springer-Verlag, Berlin Heidelberg.

Müller, A., Seltmann, R., Kober, B., Eklund, O., Jeffries, T., Kronz, A., 2008. Compositional zoning of rapakivi feldspars and coexisting quartz phenocrysts. The Canadian Mineralogist 46, 1417-1442.

Müller, A., Kearsley A., Spratt J., Seltmann R., 2012. Petrogenetic implications of magmatic garnet in granitic pegmatites from southern Norway. The Canadian Mineralogist 50, 1095-1115.

Müller, A., Snook, B., Ihlen, M.P., Beurlen, H., Breiter, K., 2013. Diversity of the quartz chemistry of NYF- and LCT-type pegmatites and its economic implications. Mineral Deposit Research for a High-Tech World. Proceedings of the 12th Biennial SGA Meeting, Vol. 4, 12–15 August 2013, Uppsala, Sweden, p. 1774–1776.

Müller, A., 2014. Chemistry of pegmatite quartz – a possible classification criterion for granitic pegmatites? Abstract Volume of the 21st General Meeting of the International Mineralogical Association 1 to 5 September 2014, Johannesburg, South Africa, p. 261.

Müller A., Ihlen P.M., Snook B., Larsen R., Flem B., Bingen B., Williamson B.J., 2015. The chemistry of quartz in granitic pegmatites of southern Norway: Petrogenetic and economic implications. Economic Geology 110, 137-157.

Neiva, A.M.R., 1995. Distribution of trace elements in feldspars granitic aplites and pegmatites from Alijó-Sanfins, northern Portugal. Mineralogical Magazine 59, 35-45.

Norton, J.J., Page, L.R., Brosbst, D.A., 1962. Geology of the Hugo pegmatite, Keystone, South Dakota. Geological Survey Professional Paper 297-P, 1-85.

Pearce, J.A., Harris, N.B.W., Tindle, A.G., 1984. Trace Element Discrimination Diagrams for the Tectonic Interpretation of Granitic Rocks. Journal of Petrology 25, 956-983.

Pedrosa-Soares, A.C., De Campos, C.P., Noce, C., Silva, L.C., Novo, T., Roncato, J., Medeiros, S., Castañeda, C., Queiroga, G., Dantas, E., Dussin, I., Alkmim, F., 2011, Late Neoproterozoic-Cambrian granitic magmatism in the Araçuaí orogen (Brazil), the Eastern Brazilian Pegmatite Province and related mineral resources. Geological Society, London, Special Publications 350, 25-51.

Ostrooumov, M., 2016. Amazonite: Mineralogy, crystal chemistry, and typomorphism. Amsterdam, Elsevier.

Oyarzábal, J., Galliski, M.A., Perino, E., 2009. Geochemistry of K-feldspar and Muscovite in Rare-element Pegmatites and Granites from the Totoral Pegmatite Field, San Luis, Argentina. Resource Geology 59, 315–329.

707 Palme, H., Jones, A., 2003. Solar system abundances of the elements, in: Meteorites, comets, and
708 planets. Treatise on Geochemistry, vol. 1, Amsterdam, Elsevier, pp. 41-61.
709 Payne, J.G., 1968. Geology and geochemistry of the Blue Mountain nepheline syenite. Canadian
710 Journal of Earth Sciences 5, 259-273.
711 Proctor, K., 1985. Gem pegmatites of Minas Gerais, Brazil: the tourmalines of the Governador
712 Valadares district. Gems and Gemology 21, 86-104.
713 Rino, S., Kon, Y., Sato, W., Maruyama, S., Santosh, M., Zhao, D., 2008. The Grenvillian and
714 Pan-African orogens: World's largest orogenies through geologic time, and their implications on
715 the origin of superplume. Gondwana Research 14, 51–72.
716 Rhodes, J.M., 1969. On the chemistry of potassium feldspars in granitic rocks. Chemical
717 Geology 4, 373-392.
718 Sabina, A.P., 1971. Rocks and Minerals for the Collector: Ottawa to North Bay, Ontario, Hull to
719 Waltham, Quebec. Geological Survey of Canada. paper 70-50. Canada. pp. 130.
720 Sabina, A.P., 1983. Rocks and Minerals for the Collector: Kingston, Ontario to Lac St-Jean,
721 Quebec. Geological Survey of Canada Miscellaneous Reports 32. Canada. pp. 130.
722 Sánchez-Muñoz, L., Correcher, V., Turrero, M.J., Cremades, A., García-Guinea, J., 2006.
723 Visualization of elastic strain fields by the spatial distribution of the blue luminescence in a
724 twinned microcline crystal. Physics and Chemistry of Minerals 33, 639-650.
725 Sánchez-Muñoz, L., García-Guinea, J., Zagorsky, V.Ye., de Moura, O.J.M., Modreski, P.J.,
726 2011a. K-feldspar minerals defined from their twin-structures: Application to a preliminary
727 classification of pegmatites. Asociación Geológica Argentina, Serie D, Publicación Especial 14,
728 175-178.

729 Sánchez-Muñoz, L., Modreski, P.J., Frost, B.R., 2011b. K-feldspar twin-structures from orogenic
730 and anorogenic granitic pegmatites in Central North America. Asociación Geológica Argentina,
731 Serie D, Publicación Especial 14, 179-183.
732 Sánchez-Muñoz, L., García-Guinea, J., Zagorsky, V.Ye., Juwono, T., Modreski, P.J., Cremades,
733 A., Van Tendeloo, G., De Moura, O.J.M., 2012. The evolution of twin patterns in perthitic K-
734 feldspar from granitic pegmatites. The Canadian Mineralogist 50, 989-1024.
735 Sánchez-Muñoz, L., Sanz, J., Sobrados, I., Gan, Z.-H., 2013. Medium-range order in disordered
736 K-feldspars by multinuclear NMR. American Mineralogist 98, 2112-2131.
737 Satterly, J. Hewitt, D.F., 1955. Some radioactive mineral occurrences in the Bancroft area.
738 Geological Circular nº 2 of the Ontario Department of Mines. Toronto, pp.76.
739 Scoates, J.S., Frost, C.D., Mitchell, J.N., Lindsley, D.H., Frost, B.R., 1996. A residual liquid
740 origin for monzonitic rocks in Proterozoic anorthosite complexes: The Sybille intrusion, Laramie
741 Anorthosite Complex, Wyoming. Geological Society of American Bulletin 108, 1357-1371.
742 Sheppard, S., Rasmussen, B., Muhling, J.R., Farrell, T.R., Fletcher, I.R., 2007. Grenvillian-aged
743 orogenesis in the Palaeoproterozoic Gascoyne Complex, Western Australia: 1030–950 Ma
744 reworking of the Proterozoic Capricorn Orogen. Journal of Metamorthic Geology 25, 477-494.
745 Shmakin, B.M., 1979. Composition and structural state of K-feldspars from some U.S.
746 pegmatites. American Mineralogist 64, 49-56.
747 Shearer, C.K., Papike, J.J., Laul, J.C., 1985. Chemistry of potassium feldspars from three zoned
748 pegmatites, Black Hills, South Dakota: Implications concerning pegmatite evolution.
749 Geochimica et Cosmochimica Acta 49, 663-673.
750 Simmons, W.B., Heinrich, E.W., 1980. Rare-earth pegmatites of the South Platte District,
751 Colorado. Colorado Geological survey, Resource Series 11, 131 p.

752 Simmons, W.B., Lee, M.T., Brewster, R.H., 1987. Geochemistry and evolution of the South
753 Platte granite-pegmatite system, Jefferson County, Colorado. Geochimica et Cosmochimica Acta
754 51, 455-471.
755 Simmons, W.B., Webber, K.L., 2008. Pegmatite genesis: state of the art. European Journal of
756 Mineralogy 20, 421-438.
757 Sweetapple, M.T., Collins, P.L.F., 2002. Genetic Framework for the Classification and
758 Distribution of Archean Rare Metal Pegmatites in the North Pilbara Craton, Western Australia.
759 Economic Geology 97, 873-895.
760 Tkachev, A.V., 2011. Evolution of metallogeny of granitic pegmatites associated with orogens
761 throughout geological time. From: Sial, A. N., Bettencourt, J. S., De Campos, C. P. & Ferreira,
762 V. P. (eds) Granite-Related Ore Deposits. Geological Society, London, Special Publications 350,
763 7–23.
764 Taylor, W.H., 1965. The Feldspars, in: Bragg W.L. and Claringbull G.F. (Eds.), Crystal
765 Structure of Minerals, London, Bell and Sons.
766 Utsunomiya, A.; Ota, T., Windley, B.F., Suzuki, N., Uchio, Y., Munekata, K., Maruyama, S.,
767 2007. History of the Pacific superplume: Implications for Pacific paleogeography since the late
768 Proterozoic, in: Yuen, D.A. et al. (Eds.), Superplumes. Springer, pp. 363-408.
769 Vetrin, V.R., Rodionov, N.V., 2009. Geology and Geochronology of Neoarchean Anorogenic
770 Magmatism of the Keivy Structure, Kola Peninsula. Petrology 17, 578-600.
771 Wagener, G.F., 1989. Systematic variation in the tin content of pegmatites in western central
772 Namibia. Journal of Geochemical Exploration 34, 1-19.
773 Walker, R.J., Hanson, G.N., Papike, J.J., Oneil, J.R., Laul, J.C., 1986. Internal evolution of the
774 Tin Mountain pegmatite, Black Hills, South-Dakota. American Mineralogist 71, 440-459.

Walker, E.E., Sutcliffe, R.H., Shaw, C.S.J., Shore, G.T., 1993. Preliminary Report on the Petrology and Chemistry of the Rare Metal Occurrences Hosted by the Coldwell Alkaline Complex. Ontario Geological Survey, Open File Report 5840, 20p.

Webber, K.L., Simmons, W.B., Falster, A.U., 1999. Biotite as a tectonic discriminant for anorogenic and orogenic pegmatites. Canadian Mineralogist 37, 839-841.

Wise, M.A., 1999. Characterization and classification of NYF-type pegmatites. The Canadian Mineralogist 37, 802-803.

Wise, M.A., 2013. The discrimination of LCT and NYF granitic pegmatites using mineral chemistry: A pilot study. Abstracts PEG 2013 New Hampshire (USA): The 6th International Symposium on Granitic Pegmatites. 156-157.

Zagorsky, V.Ye., Makagon, V.M., Shmakin, B.M., 2003. Systematics of granitic pegmatites. Russian Geology and geophysics 44, 422-435.

Zhang, C., Yang, J., Lin, C., Li, C., Lin, J. 2009. Reduction of Eu^{3+} to Eu^{2+} in $MAl_2Si_2O_8$ (M = Ca, Sr,Ba) in air condition. Journal of Solid State Chemistry 182, 1673-1678.

Footnotes

Figure 1. Map of the world showing the geological distribution of 123 pegmatite provinces and districts, distinguishing between LCT and NYF suites, as well as some with hybrid affiliation. The map of orogenic belts is based on Utsunomiya et al., (2007) and Rino et al., (2008). Legend: 1. Bighorn Mt. (WY, USA); 2. Copper Mt. (WY, USA); 3. South Pass (WY, USA); 4. Black Hills (SD, UDistrict (Country); 5. Haystack Range (WY, USA); 6. Routt Plutonic Suite (CO, USA); 7. Trout Creek Pass (CO, USA); 8. White Picacho (AZ, USA); 9. Mohave Co (AZ, USA); 10. Laramie Mt (WY, USA); 11. Berthoud Plutonic Suite (CO, USA); 12. Burro Mtn (NM,

USA); 13. Adirondack Highlands (NY, USA); 14. North New Mexico fields, (USA); 15. Rockford (AL, USA); 16. Kings Mountain (NC, USA); 17. Spruce Pine (NC); 18. Amelia (Virginia, USA); 19. New England districts (USA); 20. Brazil Lake (Nova Scotia, Canada); 21. Southern California (USA); 22. Cat Lake – Winnipeg River (Manitoba, Canada); 23. Wekusko Lake (Manitoba, Canada); 24. Yellowknife basin (NW Territories, Canada); 25. NW Ontario fields (Canada); 26. Superior Lake (ON, Canada); 27. Lac Simard (QC, Canada); 28. Preissac – Lacorne (QC, Canada); 29. Birch Portage – Hanson Lake (SK, Canada); 30. Granville Lake (Manitoba, Canada); 31. SW Grenville southern fields (ON, Canada); 32. SW Grenville northern fields (ON, Canada); 33. Mt Laurier and Gatineau fields (QC, Canada); 34. Lac Turgeon Johan Beetz (QC, Canada); 35. Pikes Peak (CO, USA); 36. Llano-Burnet (TX, USA); 37-37. Sveconorwegian Province in S Norway and SW Sweden (Evje-Iveland, Froland, Glamsland, Arendal, Søndeled, Kragerø, Tørdal, Østfold-Halland; 39. Uttö-Mysingen (Sweden); 40. Varuträsk (Sweden); 41. Bothnian Basin (Sweden); 42. Falun (Central Sweden); 43. Kemiö – Orijärvi (Finland); 44. Eräjärvi (Finland); 45. Seinäjorki (Finland); 46. Ladoga Lake (Russia - Finland); 47. Chupa-Ijona (Karelia, Russia); 48. Keivy Massif. Kola Peninsula (Russia); 49. Leinster (Ireland); 50. El Muerto pegmatites (Oaxacan Complex, Southern Mexico); 51. Borborema Province (RGN, PB, Brazil); 52. Eastern Brazilian Province (MG, BA, ES, Brazil); 53. Sta Maria de Itabira (MG, Brazil); 54. Damara province (Namibia); 55. Namaqualand (South Africa); 56. Kaapvaal (South Africa); 57. Natal districts (South Africa); 58. Panpean Pegmatite Province; 59. SW Nigeria province (Ago-Iwoye, Keffi, Nassarawa, Komu, Wamba districts); 60. Giraul (SW Angola); 61. Caxito (NW Angola); 62. Bikita, Zimbabwe; 63. Alto Ligonha, Mozambique; 64. Ruanda; 65. Burundi; 66. Kobokobo, Kamituga area, South Kivu (Congo); 67. Kapiri Mposhi, Zambia; 68. Lundazi, Zambia; 69. Chroma-Kalomo (Zambia) and Kamativi

(Zimbabwe); 70. Itremo, Madagascar; 71. Southeastern Desert province (Egypt); 72. Manono-Kittolo (Shaba, Congo); 73. Pilbara (WA, Australia); 74. Lake Moore - Dalgaranda (WA); 75. King Leopold (WA); 76. Greenbushes (WA); 77. Coolgardie – Norseman (WA); 78. Mukinbudin (WA); 79. Gascoyne (WA); 80. Mt. Isa (QNL); 81. Olary and Broken Hill, Curnamona province (SA-NSW); 82. Bihar mica belt (India); 83. Nellore mica belt (India); 84. Tamil Nadu belt (india); 85. Bastar-Malkagiri belt India); 86. Rajasthan belt (India); 87. Nuuk region (Greenland); 88. Gardar province (Greenland); 89. Volta Grande, Sao Joao de Rei (Brazil); 90. Strange Lake, Labrador, Canada ; 91.Alakha (Russia); 92. Kolmozero-Voronya (Kola Peninsula, Russia); 93. Yenisei Ridge (Russia); 94. Highland Complex (Sri Lanka); 95. Ghaha-Cote d'Ivore; 96. Bohemian-Moldanubicum belt; 97. Taimyr fold belt (Russia); 98. Altai belt (China, Kazakhstan, Russia); 99. Mongol-Okhotsk fold belt; 100. East Sayan Mt. (Siberi, Russia); 101. Southern Tuva (Kamar-Daba fold belt); 102. East Transbaikalia (Russia); 103. NW Baikal (Russia); 104. Mama-Chuya, North Baikal Highland (Rissia); 105. Iberian Peninsula; 106. Creus Cap (Spain); 107. Hagendorf-Pleystein (Babaria, Germany); 108. Paranesti (NE Greece); 109. Koralpe (Austria); 110. Afghanistan-Pakistan belt; 111. Little Nahanni (NW Territories, Canada); 112. Jiajika, Kangdi, (Sichuan province, China); 113. Nanping, China; 114. Cattlin CreeK –Cocanarup, Ravensthorpe, (WA); 115. Tak (Thailand); 116. Phuket (Thailand); 117. Lao Cai and Phu Tho (Northern Vietnam); 118. Kenticha (Ethiopia); 119. Nimnyr block, Central Aldan (Russia); 120. Middle Urals (Russia); 121. South Urals (Russia); 122. Southern Japan (Japan); 123 Central Alps.

Figure 2. Perthitic textures and twin patterns of the selected feldspars. a) BSE image by FE-SEM of the exsolution pattern of specimen S5C5, showing K-feldspar in white color and Na-feldspar

in black color. b) Optical micrograph taken with red plate of sample GcInt2, showing Albite macrotwins in horizontal orientation in blue color close to albite veins in purple color. c) Optical micrograph of a thick section of sample En19 showing many recrystallization units of low microcline in A± and P± orientations from albite veins. The LA-ICP-MS pit visible in the center of the image was placed mostly in clear orthoclase and intermediate microcline to avoid areas of albite veins. d) BSE image of the K-rich orthoclase of c), showing Na-feldspar lamellae in black color without extensive porosity. e) Optical image of a thick section of specimen GcInt2 showing an area between large albite veins (not shown in the photo) with the selected-area for chemical analyses that avoids irregular small albite patches and fine albite films. f) BSE image of an area similar to that presented in e), with albite in black color. g) EMPA image of the albite films broken by Albite recrystallization twinning from small albite veins in e). h) Optical image showing an example of selected area for LS-ICP-MS analysis in a large albite vein in specimen CM3.

Figure 3. Ce-Eu plot (ppb) with two fields, type I with Eu/Ce > 1.0, type II with Eu/Ce < 1.0. Normalization values from Palme and Jones, (2005). Estimated uncertainties in the measurements are indicated with crosses.

Figure 4. P-Fe plot by LA-ICP-MS measurements in a log-log scale of the 31 pegmatites, where four radial fields can be differentiated for each type of pegmatites: group I (red squares in a pink field), group II (dark violet lozenges in a violet field), group III (blue lozenges in a shy blue field) and group IV (green squares in a clear green field). A circle marks the samples in each population with a highest content of orthoclase. Sample CM is from a peraluminous pegmatite of

867 group II that is represented in the field of group III. Sample Et1317 is from a group III pegmatite
868 that is represented in the field of group IV pegmatites. The diagonal line separates NYF
869 pegmatites on the left side with Fe > P from LCT pegmatites on the right side with P > Fe.
870 Estimated uncertainties in the measurements are indicated with crosses.
871

Figure 1

Click here to download high resolution image

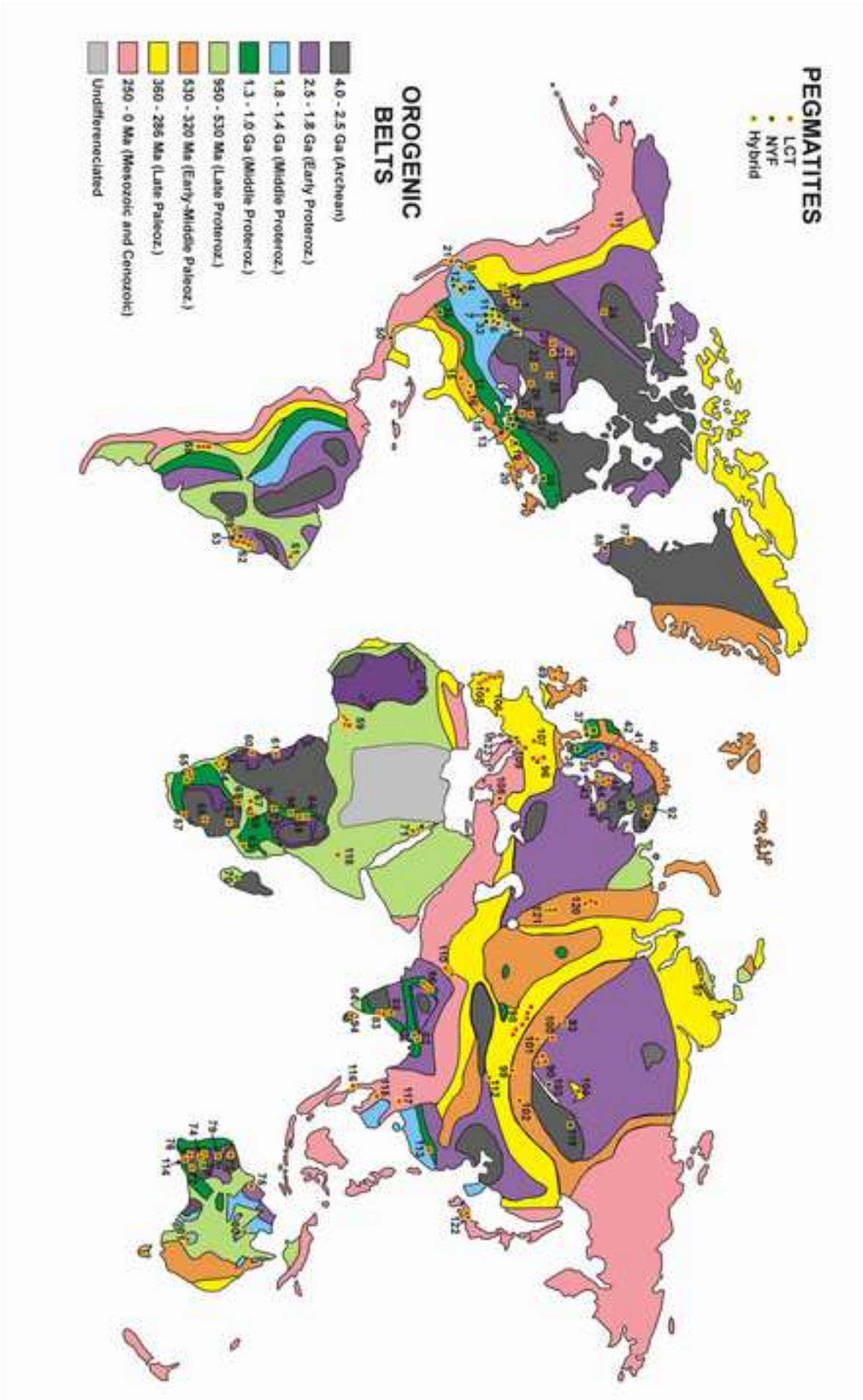

Figure 2

Click here to download high resolution image

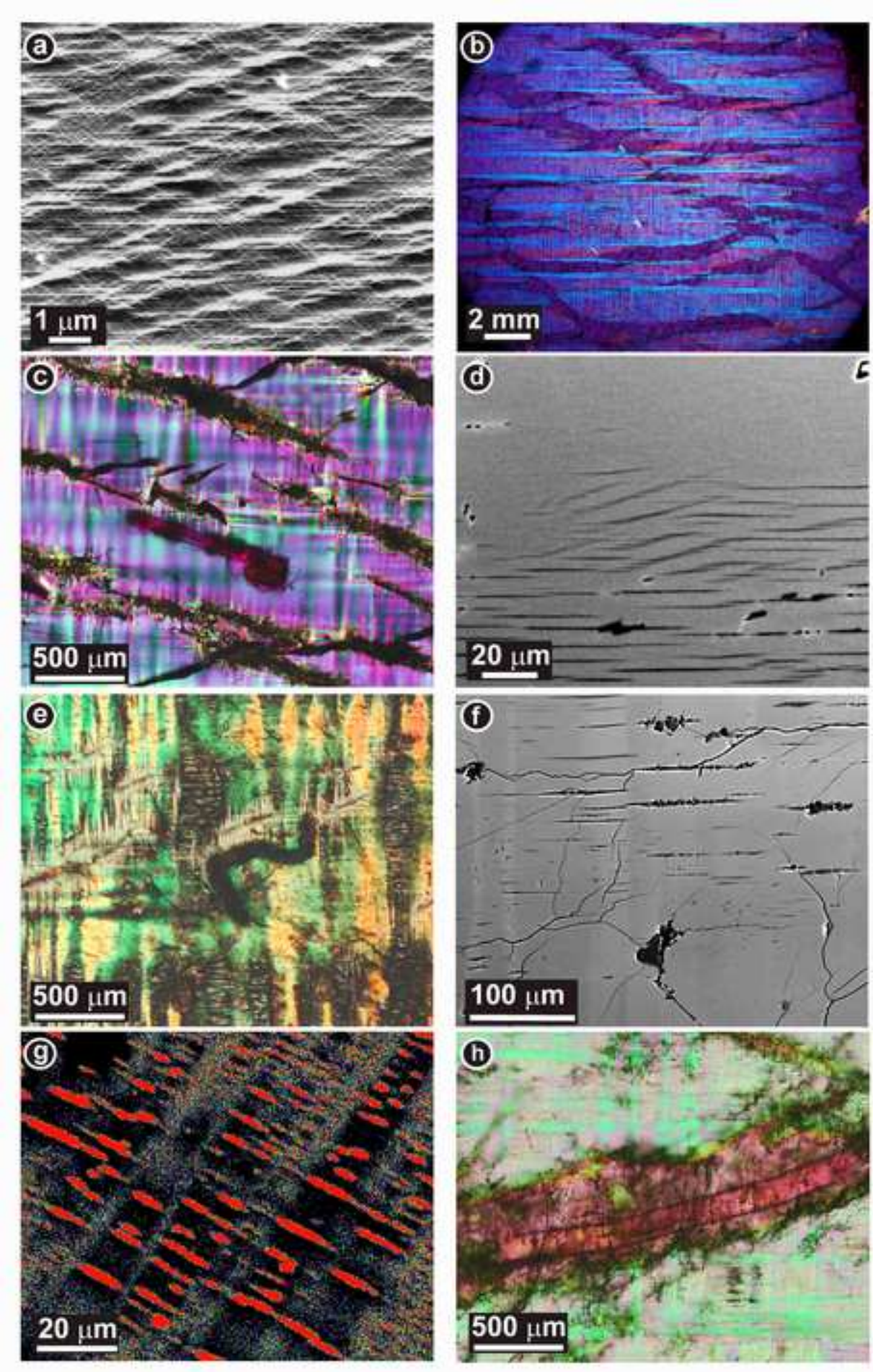

Figure 3

Click here to download high resolution image

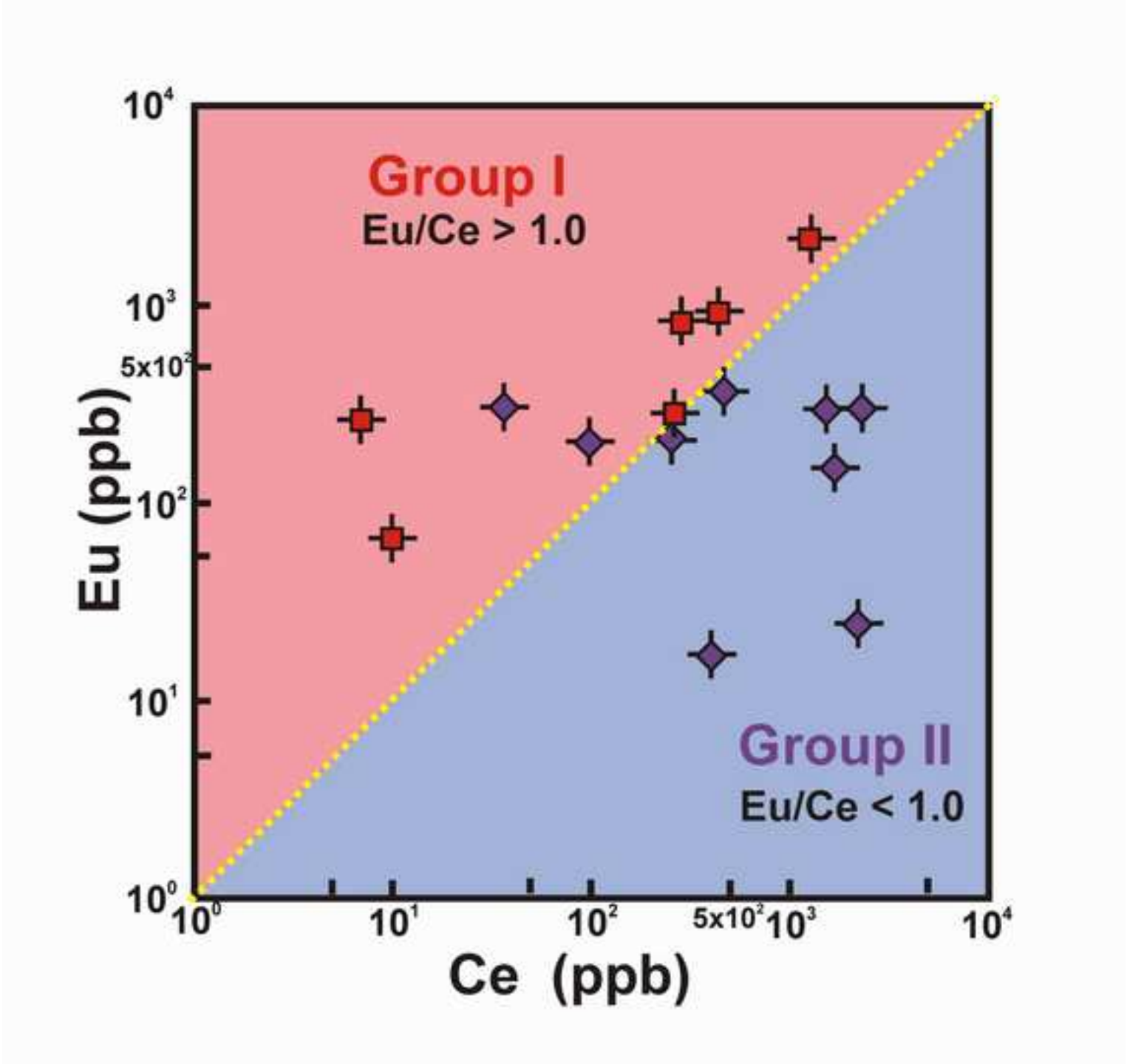

Figure 4

Click here to download high resolution image

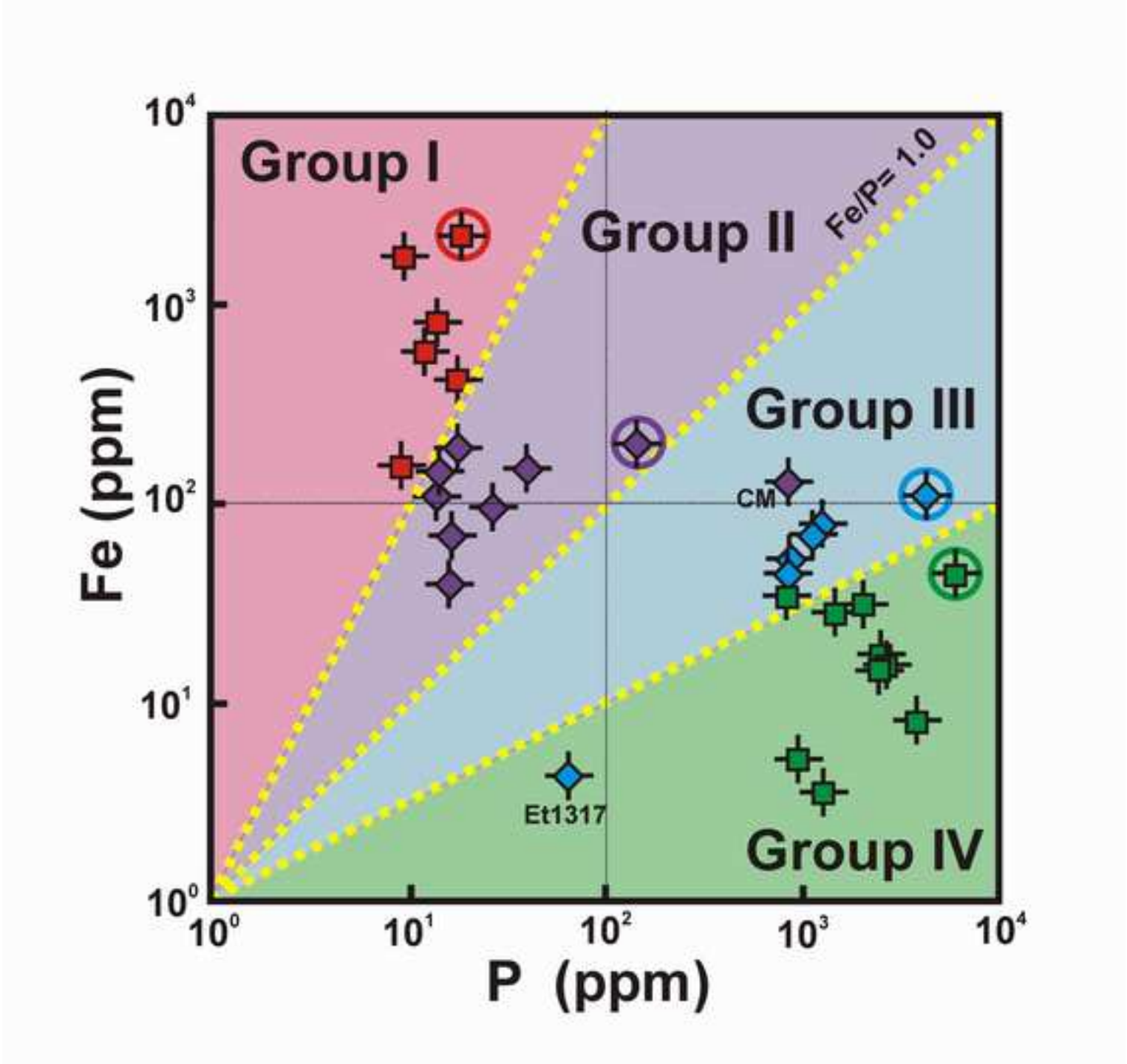

Figure 1

Click here to download high resolution image

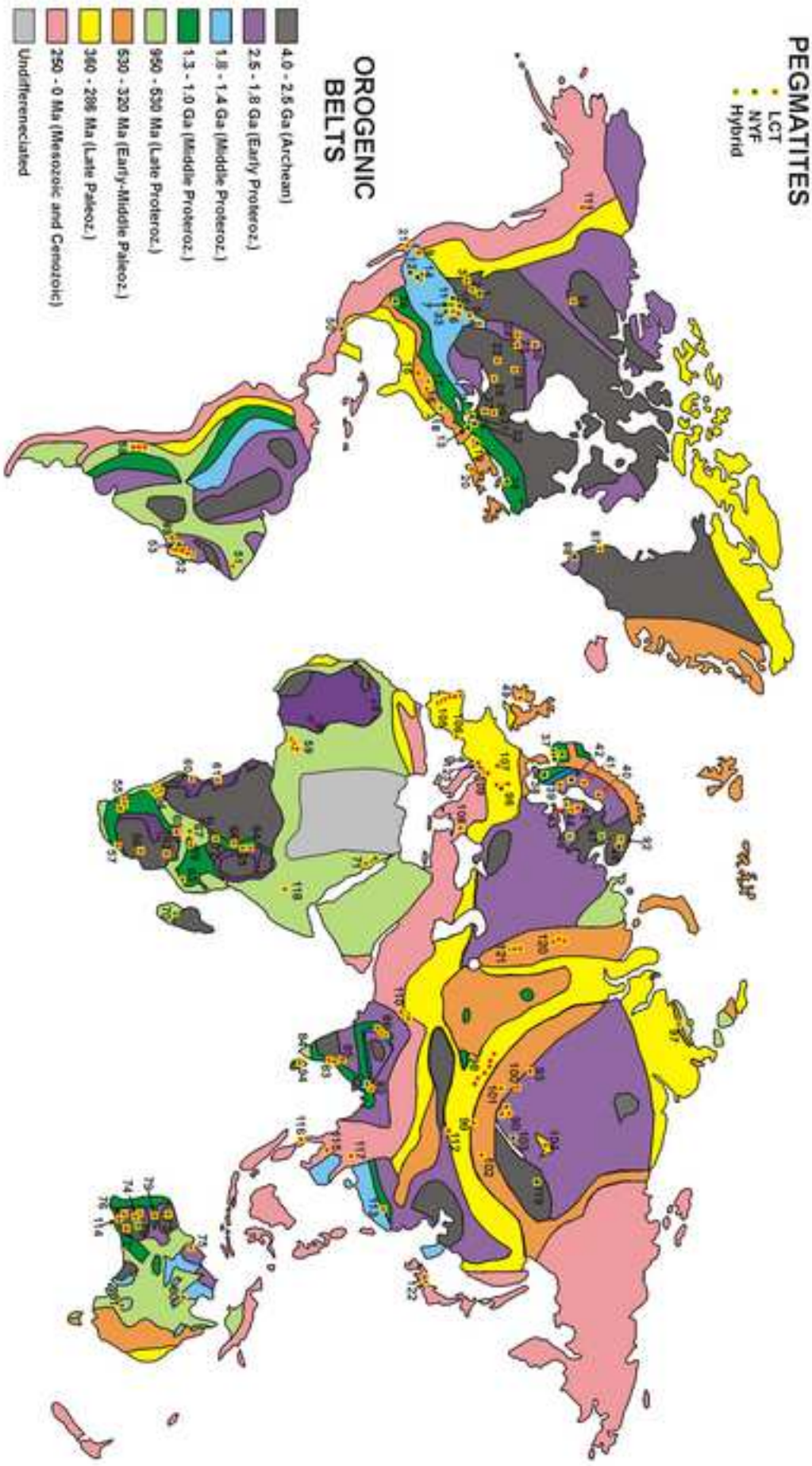

Figure 2

Click here to download high resolution image

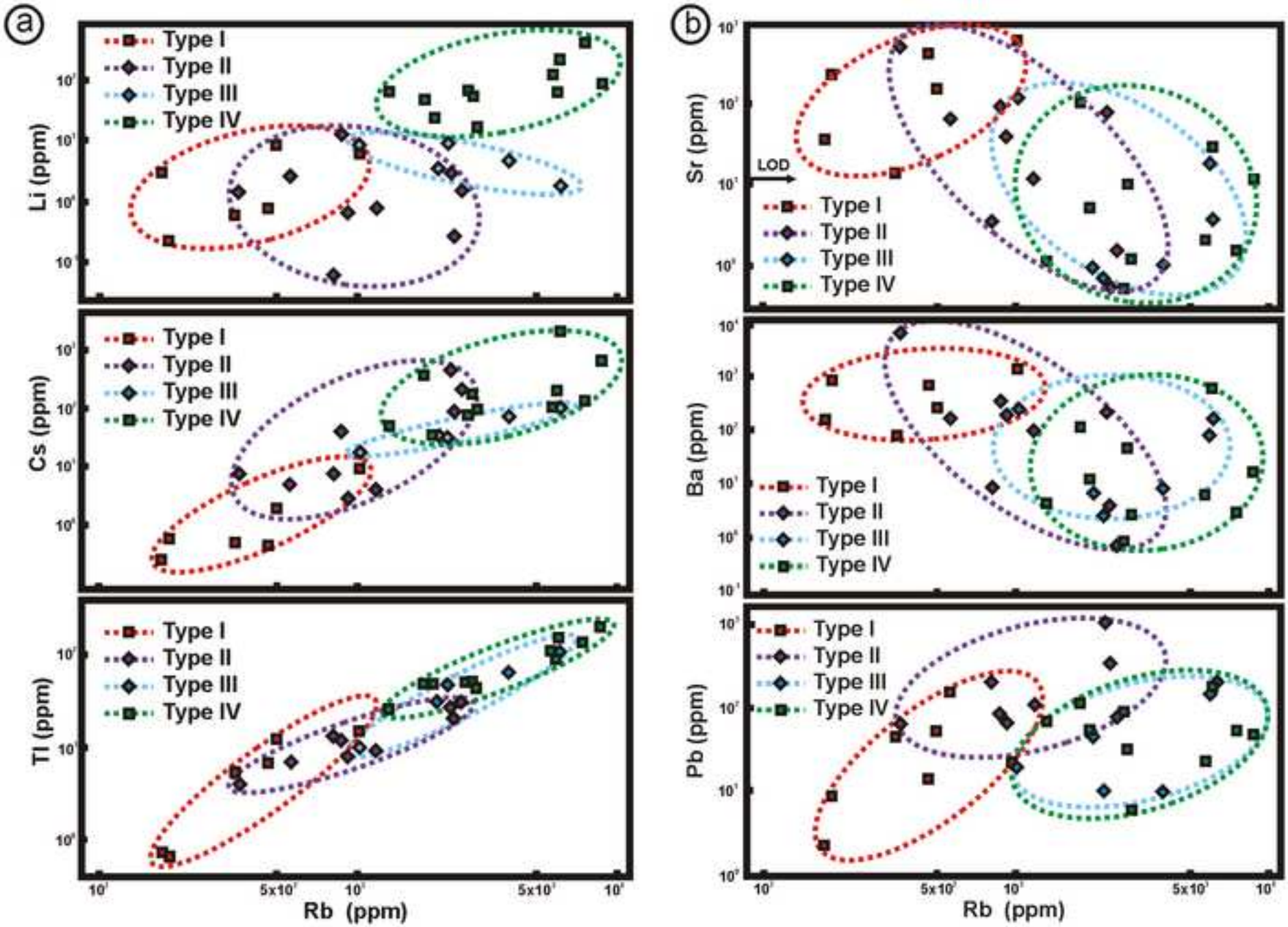

Figure 3

Click here to download high resolution image

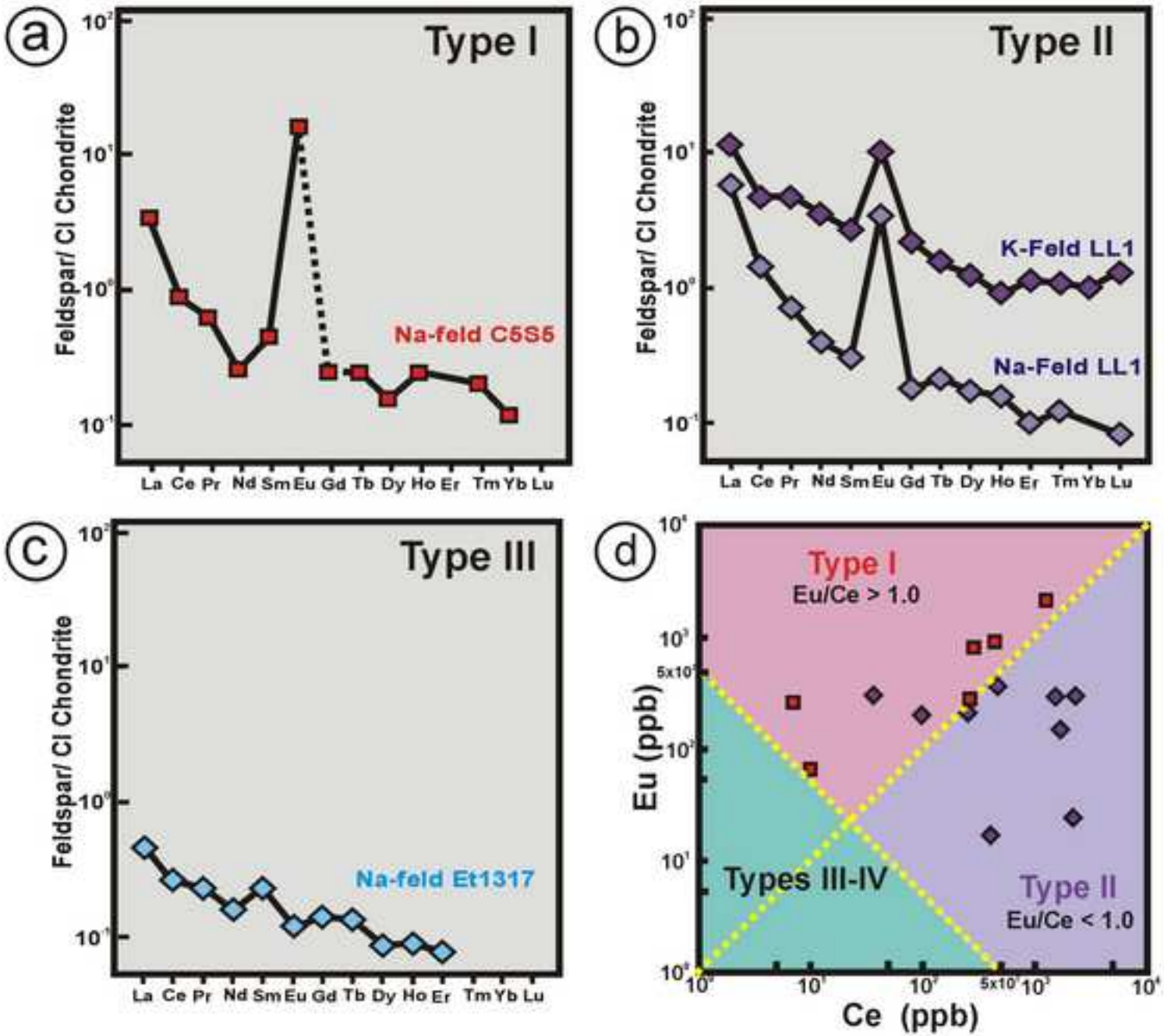

Figure 4

Click here to download high resolution image

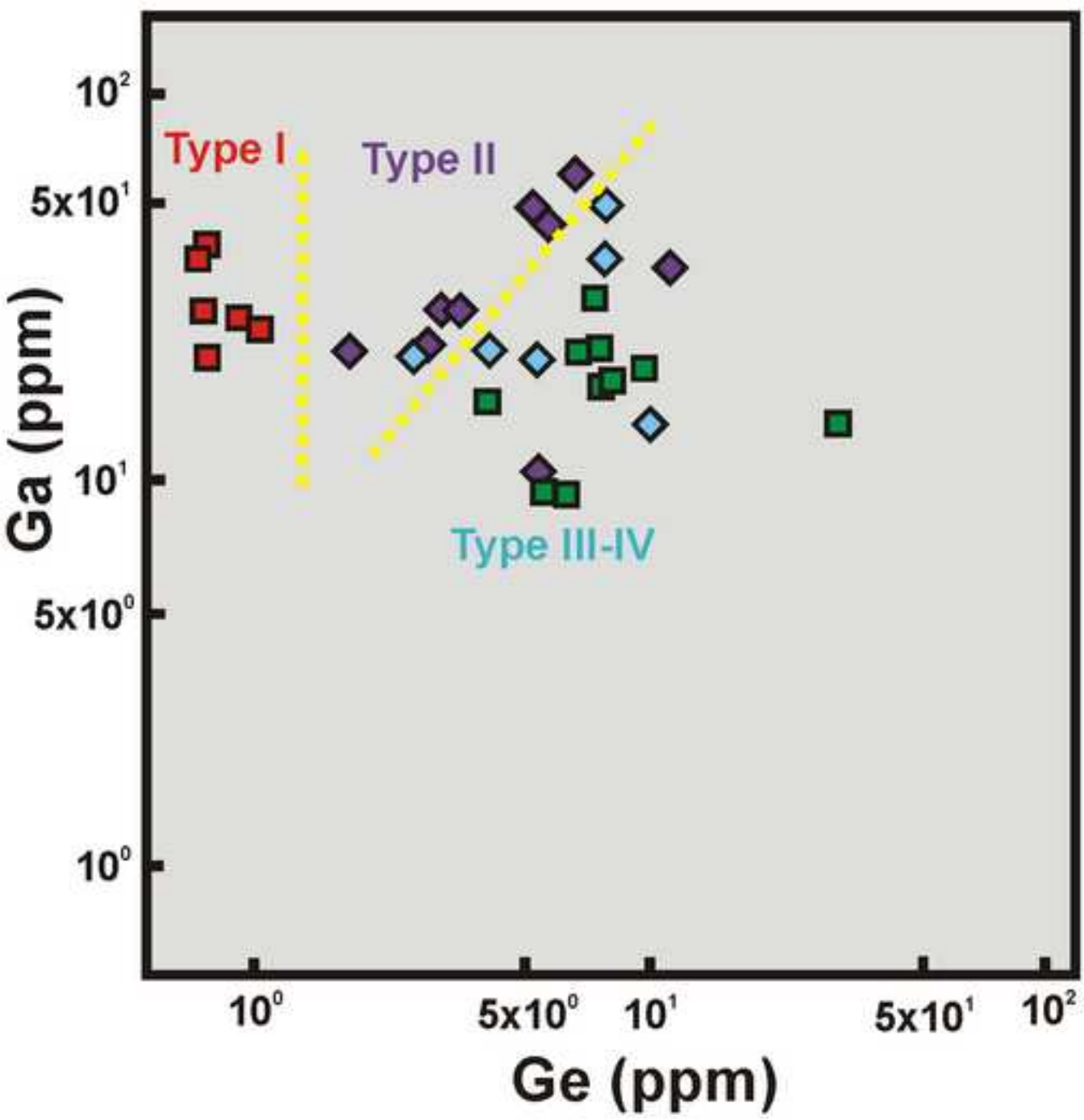

Figure 5

Click here to download high resolution image

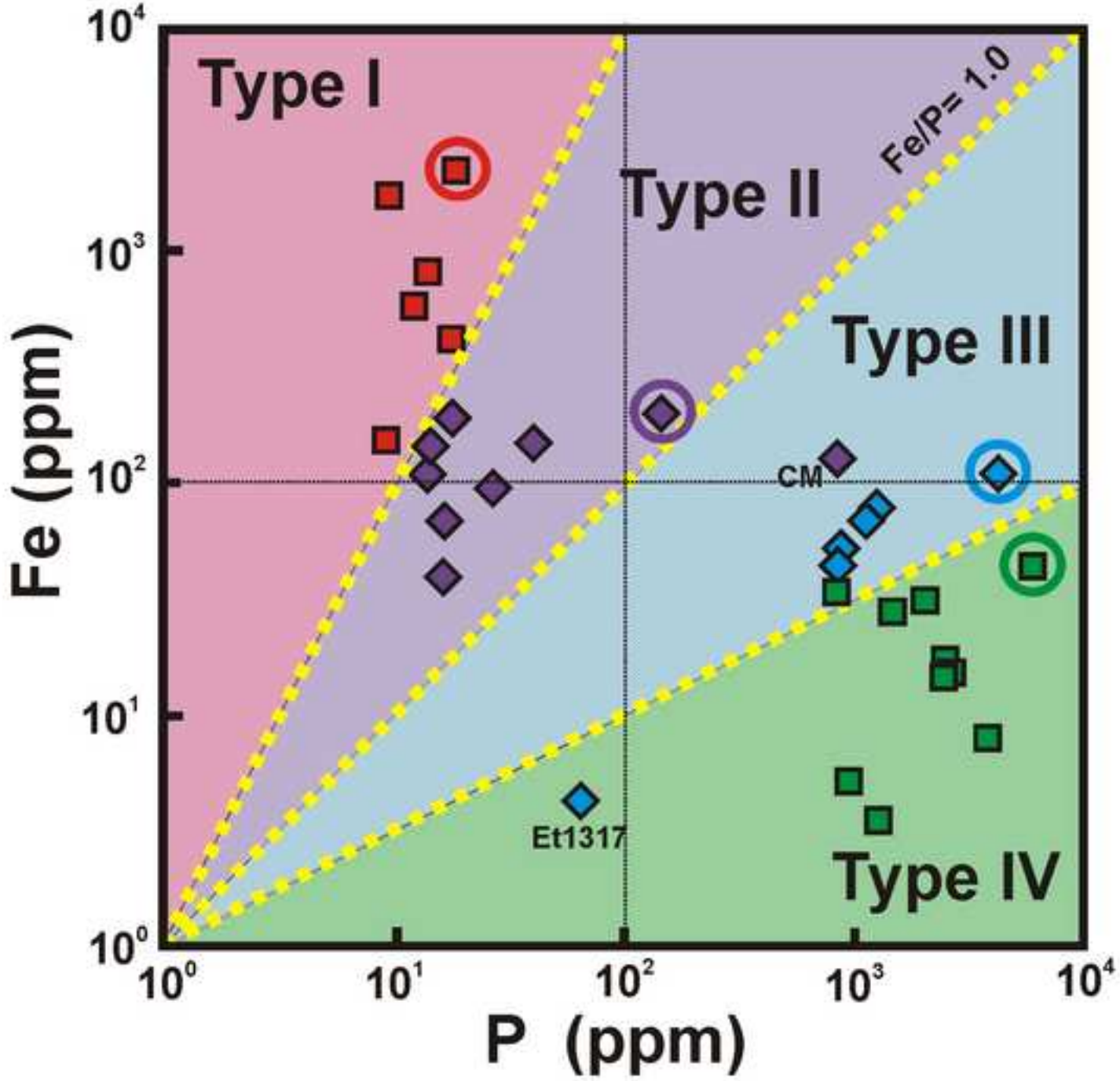

Table 1
Click here to download Table: Table 1.rtf

Table 1. Main features of the four groups of pegmatite used in this work

	"High-T, low-flux" pegmatites		"Low-T, high-flux" pegmatites	
Features	Group I, silica-poor	Group II silica-rich	Group III silica-rich, low-phosphorus	Group IV silica-rich, high-phosphorus
Quartz	In graphic textures, but may be absent (feldspathoids)	Core zone, prominent graphic textures	Mainly core, also graphic textures	Mainly core and external zone, minor graphic textures
Feldspars	Hypersolvus (and subsolvus)	Subsolvus, common amazonite	Subsolvus, very rare amazonite	Subsolvus, very rare amazonite
Hydrous minerals	Rare (amphiboles, biotite)	Biotite	Muscovite	Muscovite and and lepidolite
Phosphates	Absent to very rare (apatite and monazite)		Common	Abundant, primary and secondary
Plutonism	Subvolcanic alkali complexes to mesozonal plutons, some anatectic	Mesozonal granitic plutons, commonly of anatectic origin	Epizonal to mesozonal, spatially and genetically related to granitic plutons in most cases	
Geotectonic environment	Anorogenic alkaline complexes (rift)	Anorogenic, asymmetric orogens	Post-orogenic and extensional environment (tabular bodies)	Syncollisional symmetric orogens, compressive environments

Table 2
Click here to download Table: Table 2.rtf

Table 2. Selected pegmatites, sample codes and some important geological features

Pegmatite	Sample	Minerals, elements	Age (Ga)	Related rocks	References
		Group I			
Coldwell Complex, Center I	S5C5	Fergusonite REE, Nb	1.0	Syenites	Mitchell and Platt (1978, 1982)
Coldwell Complex Center II Ontario, Canada	S10C12	Natrolite Zr	1.0	Nepheline syenites	Walker et al. (1993)
Nephton mine Ontario, Canada	NH1	Corundum, nepheline cancrinite	1.0	Nepheline syenites	Payne (1968)
Perth “type locality” Ontario, Canada	TL1	Biotite Fe	1.0	-	Sabina (1963)
Funny Hill Wyoming, USA	FH1	Fayalite (?) REE, Nb	1.4	Syenites	Scoates et al. (1996)
Canada Radium Ontario, Canada	CR1	Uraninite REE, U	1.0	-	Satterly and Hewitt (1955)
		Group II			
Lone Lode Colorado, USA	LL1	Euxenite REE, Nb, F	1.0	Granitoids	Simmons and Heinrich (1980)
G.L. Gole Ontario, Canada	GL1	Fergusonite REE, Fe, U	1.0	-	Sabina (1971)
Roscoe Beryl Colorado, USA	RC3	Fergusonite REE, Fe, Be	1.4 (?)	-	Sánchez-Muñoz et al. (2011b)
Lavra da Generosa Minas Gerais, Brazil	GEN27	Euxenite REE, Nb, Fe, Be	1.0	Granitoids	Jordt-Evangelista et al. (2000)
Climax Mica Colorado, USA	CM3	Euxenite (?), cordierite P, B, REE (?)	1.4 (?)	-	Heinrich (1950)
White Cloud Colorado, USA	WC1	Fergusonite REE, U, F	1.0	Granitoids	Simmons et al. (1987)
Mt. Ploskaya Kola Peninsula, Russia	ZAG	Fergusonite REE, U, F, Pb	1.7	-	Vetrin and Rodionov (2009)
La Elsa San Luis Ranges, Argentina	LE3	Tourmaline B, F, Fe	0.38	Granitoids	Galliski et al. (2011)
Clora May Colorado, USA	CLM	Euxenite REE, Fe	1.7	Granitoids	Hanson et al. (1992)

Group III					
Capoeira mine Paraíba, Brazil	CAP1	Tourmaline Be, Ta	0.52	Granitoids	Beurlen et al. (2008, 2014)
Pippingarra WA, Australia	PPgInt2	Beryl	2.9	Granitoids	Sweetapple and Collins (2002); Jacobson (2007)
Maggie SA, Australia	MMG2	Beryl	1.6	Granitoids	Lottermoser and Lu (1997)
Etyka East Transbaikalia, Russia	Et1317	Tantalite (amazonite) Ta, Li, F	0.14	Granites	Ostrooumov (2016)
Beckers mine Namibia	BK2	Tourmaline Li	1.4	Granitoids	Kinnaird et al. (2014)
Casper mine Wyoming, USA	TC	Muscovite	2.65	Granitoids	Harris and Hausel (1986)
Group IV					
Golconda III Minas Gerais, Brazil	GcInt2	Tourmaline Be, Li	0.58	Granitoids	Proctor (1985)
Independencia Argentina San Luis Range, Argentina	IA1	Albite Li, Be, Nb–Ta	~0.46	Granitoids	Galliski et al. (2011)
Proberyl Minas Gerais, Brazil	En19	Beryl Be, Li	0.58	Granitoids	Fanton et al. (1978)
Tip Top South Dakota, USA	TT1	Amblygonite, triphylite Be, Li	1.7	Granitoids	Shearer et al. (1985)
Hugo South Dakota, USA	HG3	Spodumene, amblygonite Li, Be	1.7	Granitoids	Norton et al. (1962)
Rubicon mine Namibia	RU1	Petalite, amblygonite Li. Be, Cs,	~0.5	Granitoids	Kinnaird et al. (2014)
Tin Mountain South Dakota, USA	TM2	Spodumene, cassiterite Li, Be, Cs, Sn, Nb–Ta	1.7	Granitoids	Walker et al. (1986)
La Isla Belvis de Monroy, Spain	FB34	Amblygonite B, Li	0.3	Granitoids	Merino et al. (2013)
Uis mine Namibia	UI1	Cassiterite Sn	~0.5	Granitoids	Kinnaird et al. (2014), Wagener (1989)
Etta mine South Dakota, USA	ETT1	Spodumene Li, Be, Cs, Nb–Ta	1.7	Granitoids	Jolliff et al. (1992)

Table 3
Click here to download Table: Table 3.rtf

Table 3. Petrographic features of samples selected on the basis of PLOM observations

Sample	K-feldspar	Albite
	Group I	
S5C2	Untwinned low microcline	Fine lozenge mesoperthite
S10C12	Untwinned low microcline	Fine lozenge mesoperthite
NH1	First-generation parquet microcline diffuse cross-hatched microcline	Small, medium and large veins
TL1	First-generation parquet microcline	Very large veins (grading into patches)
FH1	First-generation ±A/±P needle twins and extinction waves from interfaces with albite veins	Films, lozenges, veins of various sizes
CR1	First-generation parquet microcline partially transformed into single-orientation microcline	Small, medium and large veins
	Group II	
LL1	Large mainly ±P* needle twins, thin ±A–A*/±P–P* twins from Na-veins (residual orthoclase)	Veins of variable size in transition to patches
GL1	Coarsened first-generation microcline	Fine veins
RC3	Diffuse very fine twinning replaced by polysynthetic ±A twins from large Na-veins	Fine veins to patches
GEN27	Residual parquet microcline transformed into large ±A/±P and large needle twins, in transition to single-orientation microcline	Veins of variable size in transition to patches
CM3	Coarse parquet twinning grading to single-orientation microcline	Veins of multiple size
WC1	Orthoclase transformed into ±A>A*/±P>P* microcline twins from Na-veins, extinction waves	Films in orthoclase, veins of multiple size
ZAG	Fine first-generation twins, tartan and parquet microcline	Films transformed into fine veins, large veins with (110) interfaces
LE3	Tartan and parquet microcline with ±A/±P large polysynthetic twins	Films transformed into fine veins, large veins grading to patches
CLM	Single-orientation microcline with homogeneous optical extinction, residual very fine ±A twins	Fine films transformed into small veins, medium spindle veins, large irregular veins
	Group III	
CAP1	Single-orientation microcline with homogeneous optical extinction, residual large ±A twins	Fine films transformed into small veins, and large veins
PPgInt2	Single-orientation microcline with homogeneous optical extinction, residual large ±A twins	Fine films transformed into small veins, and large veins
MMG2	Orthoclase with minor irregular microcline as extinction waves	Fine films transformed into small veins to patches, and large veins to patches
Et1317	Large ±A twins and single-orientation microcline	Fine films and medium-size albite transformed into small veins and patches
BK2	First-generation microcline partially transformed into single-orientation microcline	Films and veins partially transformed into patches
TC	Single-orientation microcline with homogeneous optical extinction, residual first-generation twins	Fine films transformed into small veins, medium spindle veins, large irregular veins
	Group IV	
GcInt2	Large needle and polysynthetic ±A twins from interfaces, residual ±P twins, and chessboards	Serrated films transformed into veins to patches, and large veins partially transformed into patches
IA1	Orthoclase with minor irregular microcline as extinction waves from interfaces	Residual films and veins transformed into patches
En19	Orthoclase with ±A/±P microcline twins from interfaces with veins	Fine films and large veins, locally transformed into patches
TT1	Large needle and polysynthetic ±A twins and chessboards to single-orientation microcline	Serrated films transformed into small veins, large veins partially transformed into patches

HG3	First-generation ±A–A*/±P–P* needle and polysynthetic twins, large needle and polysynthetic ±A/±P twins with chessboards	Serrated films transformed into small veins and large veins
RU1	Orthoclase with many ±A/±P microcline twins from interfaces with large veins	Fine films and large veins, locally transformed into patches
TM2	Large needle and polysynthetic ±A twins and chessboards to single-orientation microcline	Serrated films transformed into small veins, large veins partially transformed into patches
FB34	Mostly orthoclase, with little development of microcline from interfaces with large veins	Fine films and irregular large veins, partially transformed into patches
UI1	Mostly orthoclase, with little development of microcline from interfaces with large vein-patches	Very irregular and large veins strongly transformed into patches
ETT1	Extended parquet microcline with some coarsening to large ±A/±P twins	Serrated films and large veins of albite

Note: ±A refers to left- and right-handed Albite twins, respectively, and ±P refers to left- and right-handed Pericline twins, respectively. The * is used to indicate irrational twins.

Table 4
Click here to download Table: Table 4.rtf

Table 4. Average concentrations of minor and trace elements in K-feldspar and albite in the four groups of pegmatite

	Group I		Group II		Group III		Group IV	
	Kfs	Ab	Kfs	Ab	Kfs	Ab	Kfs	Ab
Li ppm	3.19	0.64	2.42	1.44	15.19	9.16	108.56	54.92
Rb	443.6	252.7	1314.8	761.1	3502	3812.6	4112.8	3193.1
Cs	2.12	1.3	89.3	41.1	75.9	243.4	381.7	522.8
Tl	6.66	2.94	14.32	8.01	56.76	57.04	85.91	64.17
Sr	243	133	87	82	56	36	<11.5	<11.5
Ba	557.1	200.2	833.7	927.7	84.3	74.5	81.0	34.3
Pb	23	12.3	234.1	109.5	71.9	91.5	65.4	44.1
Y ppb	<10	82	91	452	<10	61	<10	24
La	777	705	1365	955	100	235	15	18
Ce	379	266	998	674	74	418	<7	10
Eu	728	548	207	115	5	55	17	10
Ge ppm	0.8	0.9	4.9	4.8	6.2	6.0	9.3	8.8
Ga	29.5	29.6	33.6	34.1	27.5	26.9	17.6	18.5
Fe	1040	1059	128	105	60	172	20	43
P	13	13	125	123	1385	1150	2368	1587

Concentrations acquired by LA–ICP–MS. Symbols used: Kfs: K-feldspar, Ab: albite.

Table 5
Click here to download Table: Table 5.rtf

Table 5. Concentrations of Fe and P in K-feldspar and albite in the four groups of pegmatite specimens

Sample	Iron		Phosphorus	
	Kfs	Ab	Kfs	Ab
Group I				
S5C5	2375	3037	18	16
S10C12	860	1004	14	15
NH1	155	122	9	12
TL1	1830	1121	9	10
FH1	427	574	18	11
CR1	594	497	12	13
Group II				
LL1	208	203	144	143
GL1	113	205	14	8
RC3	196	78	18	14
GEN27	40	78	16	15
CM3	130	10	835	820
WC1	98	80	27	20
ZAG	148	150	14	13
LE	154	100	39	42
CLM	69	39	16	34
Group III				
CAP1	80	9	1191	871
PPgInt2	53	39	853	68
MMG2	111	153	4259	3345
Et1317	4	146	64	55
BK2	70	655	1110	1054
TC	44	31	834	898
Group IV				
GcInt2	34	14	835	386
IA1	17	109	2483	1203
En19	3	151	1271	745
Et1317	31	58	2025	567
BK2	14	14	2411	1473
RU1	28	6	1465	1324
TM2	15	11	2532	2202
FB34	44	54	5969	5060
UI1	8	2	3746	2476
ETT1	5	9	947	431

Concentrations acquired by LA–ICP–MS. Symbols used: Kfs: K-feldspar, Ab: albite.

Table 1
Click here to download Table: Table 1.docx

Table 1. Main features of the four types of pegmatites used in this work.

	"High-T, low-flux" pegmatites		"Low-T, high flux" pegmatites	
Features	Type I, silica-poor	Type II, silica-rich	Type III, silica-rich and low-P	Type IV, silica-rich and high-P
Quartz	Mainly graphic textures, but it can be absent (feldspathoids)	Core and extended development of graphic textures	Mainly core, also graphic textures	Mainly core and external zone, minor graphic textures
Feldspars	Hypersolvus (and subsolvus)	Subsolvus, common amazonite	Subsolvus rare amazonite	Subsolvus, very rare amazonite
Hydrated minerals	Very rare (in some cases amphiboles, biotite)	Biotite	Muscovite	Muscovite and lepidolite
Phosphates	Absent to very rare (apatite and monazite)		Common	Abundant and many different minerals
Plutonism	Subvolcanic alkali complexes to mesozonal plutons, some anatectic origin	Mesozonal granitic plutons and common anatectic origin	From epizonal to mesozonal granitic, in most cases spatially and genetically related to granitic plutonism	
Geotectonic environment	Anorogenic alkaline complexes (rift)	Anorogenic and asymmetric orogens	Post-orogenic and extensive environment (tabular bodies)	Syncollisional symmetric orogens and compressive environments

Table 2
Click here to download Table: Table 2.docx

Table 2. Selected pegmatites, sample codes and some important geological features.

	Pegmatite	Sample	Minerals - Elements	Age	Related rocks	References
Type I	Coldwell Complex Center I ON, Canada	S5C5	Fergusonite REE, Nb	1.0 Ga	Syenites	Mitchell and Platt, 1978, Mitchell and Platt, 1982; Walker et al., 1993
	Coldwell Complex Center II ON, Canada	S10C12	Natrolite Zr	1.0 Ga	Nepheline syenites	
	Nephton mine ON, Canada	NH1	Corundum, Nepheline, Cancrinite	1.0 Ga	Nepheline syenites	Payne, 1968
	Perth "type locality" ON, Canada	TL1	Biotite Fe	1.0 Ga	-	Sabina, 1983
	Funny Hill WY, USA	FH1	Fayalite (?) REE-Nb	1.4 Ga	Syenites	Scoates et al., 1996
	Canada Radium ON, Canada	CR1	Uraninite REE-U	1.0 Ga	-	Satterly and Hewitt, 1955
Type II	Lone Lode CO, USA	LL1	Euxenite REE, Nb, F	1.0 Ga	Granitoids	Simmons and Heinrich, 1980
	G.L. Gole ON, Canada	GL1	Fergusonite REE, Fe, U	1.0 Ga	-	Sabina, 1971
	Roscoe Beryl CO, USA	RC3	Fergusonite REE, Fe, Be	1.4 Ga (?)	-	Sánchez-Muñoz et al., 2011b
	Lavra da Generosa Minas Gerais, Brazil	GEN27	Euxenite REE, Nb, Fe, Be	1.0 Ga	Granitoids	Jordt-Evangelista et al., 2000
	Climax Mica CO, USA	CM3	Euxenite (?) Cordierite P, B, REE (?)	1.4 Ga (?)	-	Heinrich, 1950
	White Cloud CO, USA	WC1	Fergusonite REE-U, F	1.0 Ga	Granitoids	Simmons et al., 1987
	Ploskaya Mt. Kola Peninsula, Russia	ZAG	Fergusonite, REE, U, F, Pb	1.7 Ga	-	Vetrin and Rodionov, 2009
	La Elsa San Luis Ranges, Argentina	LE3	Tourmaline B, F, Fe	0.38 Ga	Granitoids	Galliski et al., 2011
	Clora May CO, USA	CLM	Euxenite REE, Fe	1.7 Ga	Granitoids	Hanson et al., 1992
Type III	Capoeira mine Paraiba, Brazil	CAP1	Tourmaline Be, Ta	0.52 Ga	Granitoids	Beurlen et al., 2008, Beurlen et al., 2014
	Pippingarra WA, Australia	PPgInt2	Beryl	2.9 Ga	Granitoids	Sweetapple and Collins, 2002; Jacobson, 2007
	Maggie SA, Australia	MMG2	Beryl	1.6 Ga	Granitoids	Lottermoser and Lu, 1997
	Etyka East Transbaikalia, Russia	Et1317	Tantalite (amazonite) Ta, Li, F	0.14 Ga	Granites	Ostrooumov, 2016
	Beckers mine Namibia	BK2	Tourmaline Li	1.4 Ga	Granitoids	Kinnaird et al., 2014
	Casper mine WY, USA	TC	Muscovite	2.65 Ga	Granitoids	Harris and Hausel, 1986
Type IV	Golconda III Minas Gerais, Brasil	GcInt2	Tourmaline Be, Li	0.58 Ga	Granitoids	Proctor, 1985
	Independencia Argentina San Luis Range, Argentina	IA1	Albite Li, Be, Nb-Ta	~0.46 Ga	Granitoids	Galliski et al., 2011
	Proberyl Minas Gerais, Brasil	En19	Beryl Be, Li	0.58 Ga	Granitoids	Fanton et al., 1978
	Tip Top SD, USA	TT1	Amblygonite, triphylite Be, Li	1.7 Ga	Granitoids	Shearer et al., 1985
	Hugo SD, USA	HG3	Spodumene, amblygonite Li, Be	1.7 Ga	Granitoids	Norton et al., 1962
	Rubicon mine Namibia	RU1	Petalite, amblygonite Li. Be, Cs,	~0.5 Ga	Granitoids	Kinnaird et al., 2014
	Tin Mountain SD, USA	TM2	Spodumene, cassiterite Li, Be, Cs, Sn, Nb-Ta	1.7 Ga	Granitoids	Walker et al., 1986
	La Isla	FB34	Amblygonite	0.3 Ga	Granitoids	Merino et al., 2013

	Belvis de Monroy, Spain		B, Li			
	Uis mine Namibia	UI1	Cassiterite Sn	~0.5 Ga	Granitoids	Kinnaird et al., 2014, Wagener, 1989
	Etta mine (SD, USA)	ETT1	Spodumene Li, Be, Cs, Nb-Ta	1.7 Ga	Granitoids	Jolliff et al., 1992

Table 3
Click here to download Table: Table 3.docx

Table 3. Petrographic features of samples selected by PLOM observations.

	Sample	K-feldspar	Na-feldspar
Type I	S5C2	Untwinned low microcline	Fine lozenge mesoperthite
	S10C12	Untwinned low microcline	Fine lozenge mesoperthite
	NH1	First generation parquet microcline and diffuse crosshatched microcline	Small, medium and large veins
	TL1	First generation parquet microcline	Very large veins (partially into patches)
	FH1	First generation ±A/±P needle twins and extinction waves from interfaces with albite veins	Films, lozenges, veins of multiple sizes
	CR1	First generation parquet microcline partially transformed into single orientation microcline	Small, medium and large veins
Type II	LL1	Large mainly ±P* needle twins, thin ±A-A*/±P-P* twins from Na-veins (residual orthoclase)	Veins of multiple size in transition to patches
	GL1	Coarsened first generation microcline	Fine veins
	RC3	Diffuse very fine twinning replaced by polysynthetic ±A twins from large Na-veins	Fine and large veins to patches
	GEN27	Residual parquet microcline transformed into large ±A/±P needle twins, in transition to single-orientation microcline	Veins of multiple size in transition to patches
	CM3	Coarse parquet twinning in transition to single-orientation microcline	Veins of multiple size
	WC1	Orthoclase transformed into ±A>A*/±P>P* microcline twins from Na-veins, extinction waves	Films in orthoclase, veins of multiple size
	ZAG	Fine first generation twins, tartan and parquet microcline	Films transformed into fine veins, large veins with (110) interfaces
	LE3	Tartan and parquet microcline with ±A/±P large polysynthetic twins	Films transformed into fine veins, large veins in transition to patches
	CLM	Single-orientation microcline with homogeneous optical extinction, residual very fine ±A twins	Fine films transformed into small veins, medium spindle veins, large irregular veins
Type III	CAP1	Single-orientation microcline with homogeneous optical extinction, residual large ±A twins	Fine films transformed into small veins, and large veins
	PPgInt2	Single-orientation microcline with homogeneous optical extinction, residual large ±A twins	Fine films transformed into small veins, and large veins
	MMG2	Orthoclase with minor irregular microcline as extinction waves	Fine films transformed into small veins to patches, and large veins to patches
	Et1317	Large ±A twins and single-orientation microcline	Fine films and medium size albite transformed into small veins and patches
	BK2	First generation microcline partially transformed into single orientation microcline	Films and veins partially transformed into patches
	TC	Single-orientation microcline with homogeneous optical extinction, residual first generation twins	Fine films transformed into small veins, medium spindle veins, large irregular veins
Type IV	GcInt2	Large needle and polysynthetic ±A twins from interfaces, residual ±P twins, and chessboards	Serrated films transformed into veins to patches, and large veins partially transformed into patches
	IA1	Orthoclase with minor irregular microcline as extinction waves from interfaces	Residual films and veins transformed into patches
	En19	Orthoclase with ±A-±P microcline twins from interfaces with veins	Fine films and large veins, locally transformed into patches
	TT1	Large needle and polysynthetic ±A twins and chessboards to single-orientation microcline	Serrated films transformed into veins and large veins, partially transformed into patches
	HG3	First generation ±A-A*/±P-P* needle and polysynthetic twins, large needle and polysynthetic ±A/±P twins with chessboards	Serrated films transformed into small veins and large veins
	RU1	Orthoclase with many ±A-±P microcline twins from interfaces with large veins	Fine films and large veins, locally transformed into patches

Note: ±A are left- and right-handed Albite twins, ±P are left- and right-handed Pericline twins, the * is used for irrational twins.

Table 4

Click here to download Table: Table 4.docx

Table 4. Bulk chemical analyses of the thirty-two samples by XRF (wt. %)

Sample	SiO_2	Al_2O_3	Fe_2O_3	MnO	MgO	CaO	Na_2O	K_2O	TiO_2	P_2O_5	$Or_xAb_yAn_z$
S5C5	66.74	18.60	2.87	0.06	0.47	0.44	4.66	6.34	0.04	0.02	$Or_{55.4}Ab_{40.7}An_{3.9}$
S10C12	67.44	19.77	0.25	0.00	0.05	0.50	4.34	7.59	0.06	0.00	$Or_{61.1}Ab_{34.9}An_{4.0}$
NH1	65.17	18.59	0.09	0.00	0.00	0.42	2.57	13.13	0.02	0.01	$Or_{81.5}Ab_{16.0}An_{2.6}$
TL1	67.13	18.86	0.32	0.00	0.00	0.39	3.73	9.52	0.05	0.01	$Or_{69.8}Ab_{27.3}An_{2.9}$
FH1	66.48	18.88	0.11	0.00	0.00	0.41	2.45	11.70	0.01	0.02	$Or_{80.4}Ab_{16.8}An_{2.8}$
CR1	65.39	18.71	0.20	0.00	0.00	0.46	2.56	12.58	0.08	0.01	$Or_{80.6}Ab_{16.4}An_{3.0}$
LL1	67.50	19.38	0.10	0.01	0.00	0.43	2.42	10.09	0.02	0.05	$Or_{78.0}Ab_{18.7}An_{3.3}$
GL1	65.01	18.80	0.09	0.00	0.00	0.62	2.13	12.98	0.35	0.01	$Or_{82.5}Ab_{13.6}An_{3.9}$
RC3	66.37	18.83	0.07	0.00	0.00	0.39	2.83	11.49	0.01	0.01	$Or_{78.1}Ab_{19.2}An_{2.7}$
GEN27	65.67	18.75	0.06	0.01	0.00	0.38	2.45	12.66	0.01	0.02	$Or_{81.7}Ab_{15.8}An_{2.4}$
CM3	66.09	19.10	0.05	0.01	0.00	0.37	2.70	11.53	0.01	0.15	$Or_{79.0}Ab_{18.5}An_{2.5}$
WC1	67.67	19.09	0.03	0.01	0.00	0.37	2.62	10.17	0.01	0.03	$Or_{77.3}Ab_{19.9}An_{2.8}$
ZAG	65.32	18.55	0.07	0.00	0.00	0.40	2.10	13.53	0.02	0.02	$Or_{84.4}Ab_{13.1}An_{2.5}$
LE3	65.20	18.74	0.06	0.01	0.00	0.42	2.19	13.34	0.02	0.02	$Or_{83.6}Ab_{13.7}An_{2.6}$
CLM1	65.99	18.85	0.04	0.01	0.00	0.42	2.12	12.53	0.02	0.02	$Or_{83.2}Ab_{14.1}An_{2.8}$
CAP1	66.65	19.21	0.03	0.00	0.00	0.43	1.94	11.54	0.01	0.02	$Or_{83.0}Ab_{13.9}An_{3.0}$
PPgInt2	66.25	19.29	0.05	0.00	0.00	0.41	2.62	11.24	0.01	0.13	$Or_{78.8}Ab_{18.4}An_{2.9}$
MMG2	64.12	19.28	0.10	0.01	0.00	0.44	2.61	12.75	0.02	0.69	$Or_{80.7}Ab_{16.5}An_{2.8}$
Et1317	65.14	18.03	0.03	0.00	0.00	0.44	1.49	14.82	0.02	0.03	$Or_{88.5}Ab_{8.9}An_{2.6}$
BK2	65.86	18.95	0.10	0.01	0.00	0.37	2.18	12.36	0.01	0.17	$Or_{82.9}Ab_{14.6}An_{2.5}$
TC	67.05	19.32	0.06	0.01	0.00	0.36	2.27	10.77	0.01	0.13	$Or_{80.3}Ab_{17.0}An_{2.8}$
GcInt2	66.18	18.94	0.03	0.00	0.00	0.41	2.16	12.11	0.01	0.16	$Or_{82.5}Ab_{14.7}An_{2.8}$
IA1	65.40	19.35	0.05	0.00	0.00	0.40	2.53	11.89	0.01	0.38	$Or_{80.2}Ab_{17.1}An_{2.7}$
En19	65.76	19.06	0.03	0.00	0.00	0.48	1.84	12.56	0.05	0.23	$Or_{84.4}Ab_{12.4}An_{3.2}$
TT1	64.35	19.16	0.05	0.00	0.00	0.43	2.43	13.26	0.01	0.28	$Or_{82.2}Ab_{15.1}An_{2.7}$
HG3	65.68	19.26	0.05	0.01	0.00	0.44	2.53	11.71	0.01	0.33	$Or_{79.8}Ab_{17.2}An_{3.0}$
RU1	67.04	19.42	0.04	0.01	0.00	0.40	1.97	10.88	0.01	0.23	$Or_{82.1}Ab_{14.9}An_{3.0}$
TM2	64.92	19.10	0.03	0.00	0.00	0.43	2.25	12.70	0.02	0.55	$Or_{55.4}Ab_{14.6}An_{2.8}$
FB34	64.11	19.94	0.03	0.00	0.00	0.40	2.39	12.72	0.01	0.40	$Or_{82.0}Ab_{15.4}An_{2.6}$
UI1	64.90	19.36	0.04	0.01	0.00	0.44	2.31	12.26	0.01	0.68	$Or_{81.7}Ab_{15.4}An_{2.9}$
ETT1	65.32	18.78	0.04	0.00	0.00	0.40	2.07	13.20	0.01	0.17	$Or_{84.2}Ab_{13.2}An_{2.6}$

Table 5

Click here to download Table: Table 5.docx

Table 5. Average values of minor and trace elements in ppm and ppb (only for Y, La, Ce and Eu) of the K- and Na-feldspars in the types of pegmatites by LA-ICP-MS.

	Type I		Type II		Type III		Type IV	
	K-feldsp.	Na-feldsp.	K-feldsp.	Na-feldsp.	K-feldsp.	Na-feldsp.	K-feldsp.	Na-feldsp.
Li	3.19	0.64	2.42	1.44	15.19	9.16	108.56	54.92
Rb	443.6	252.7	1314.8	761.1	3502	3812.6	4112.8	3193.1
Cs	2.12	1.3	89.3	41.1	75.9	243.4	381.7	522.8
Tl	6.66	2.94	14.32	8.01	56.76	57.04	85.91	64.17
Sr	243	133	87	82	56	36	< 11.46	< 11.46
Ba	557.1	200.2	833.7	927.7	84.3	74.5	81.0	34.3
Pb	23	12.3	234.1	109.5	71.9	91.5	65.4	44.1
Y	< 10	82	91	452	< 10	61	< 10	24
La	777	705	1365	955	100	235	15	18
Ce	379	266	998	674	74	418	< 7	10
Eu	728	548	207	115	5	55	17	10
Ge	0.8	0.9	4.9	4.8	6.2	6.0	9.3	8.8
Ga	29.5	29.6	33.6	34.1	27.5	26.9	17.6	18.5
Fe	1040	1059	128	105	60	172	20	43
P	13	13	125	123	1385	1150	2368	1587

Table 6
Click here to download Table: Table 6.docx

Table 6. Alkalis and thallium contents in K- and Na-feldspars (ppm) by LA-ICP-MS

	Sample	Rubidium (Rb)		Lithium (Li)		Cesium (Cs)		Thallium (Tl)	
		K-feldsp.	Na-feldsp.	K-feldsp.	Na-feldsp.	K-feldsp.	Na-feldsp.	K-feldsp.	Na-feldsp.
Type I	S5C5	176.5	172.9	2.96	0.36	0.24	0.30	0.72	0.65
	S10C12	188.8	199.6	0.23	0.6	0.58	0.94	0.64	0.70
	NH1	488.4	3.7	8.29	0.00	1.87	0.03	12.04	0.09
	TL1	452.3	0.0	0.76	0.28	0.43	0.00	6.69	0.00
	FH1	388.3	436.4	0.58	0.17	0.49	1.69	5.25	6.57
	CR1	1017.2	703.4	6.33	2.41	9.10	4.69	14.63	9.62
Type II	LL1	919.8	499.8	0.63	1.00	2.77	1.69	7.85	4.39
	GL1	350.7	365.8	1.38	2.03	7.57	8.11	3.94	3.68
	RC3	805.9	1047.2	0.06	0.23	7.24	43.64	13.19	14.08
	GEN27	2358.4	2064.3	0.26	0.34	84.44	61.62	19.95	18.40
	CM3	552.8	1.46	2.51	0.34	8.56	0.20	6.85	0.03
	WC1	1181.8	114.8	0.79	2.41	4.0	1.26	8.86	1.06
	ZAG	2284.4	1420.5	2.75	0.25	440.4	163.6	25.77	15.95
	LE	868.1	865.0	11.84	6.16	39.53	47.4	11.87	9.53
	CLM	2511.8	470.9	1.53	0.56	207.11	42.2	30.59	4.99
Type III	CAP1	3828.7	6014.1	4.63	4.29	73.01	559.2	63.67	85.14
	PPgInt2	2223.0	2710	8.98	0.6	49.32	298.9	47.15	50.33
	MMG2	1022.0	940.4	8.21	8.69	17.06	13.21	9.84	9.43
	Et1317	6052.1	6037.8	1.76	1.42	101.43	93.75	102.77	98.42
	BK2	5857.8	7160.4	64.03	39.62	198.73	494.7	86.31	98.71
	TC	2028.1	12.99	3.53	0.34	34.28	0.5	30.81	0.23
Type IV	GcInt2	2664.3	2482.6	61.22	26.26	75.4	194.3	49.59	37.4
	IA1	1326.0	514.5	63.33	3.98	49.32	67.1	25.60	8.87
	En19	5982.8	3535.3	217.11	6.20	2138.5	696.0	149.83	76.39
	Et1317	2757.8	3071	54.22	57.38	170.3	1135.3	50.11	48.70
	BK2	1967.7	12.93	23.59	2.27	33.8	1.26	49.04	0.23
	RU1	7447.8	6292.1	400.13	111.70	136.5	168.1	136.54	95.6
	TM2	8682.0	7644.8	86.29	88.23	650.4	591.0	198.6	205.1
	FB34	2881.0	1691.1	16.22	14.50	95.5	1691.1	42.57	25.26
	UI1	5611.63	5033.4	117.17	218.34	99.9	186.9	109.63	98.4
	ETT1	1807.11	1653.7	46.29	20.31	367.7	497.1	47.57	45.73

Table 7
Click here to download Table: Table 7.docx

Table 7. Alkaline earth and lead contents in K- and Na-feldspars (ppm) by LA-ICP-MS

	Sample	Barium (Ba)		Strontium (Sr)		Lead (Pb)	
		K-feldsp.	Na-feldsp.	K-feldsp.	Na-feldsp.	K-feldsp.	Na-feldsp.
Type I	S5C5	155.4	200.4	36	41	2.1	2.2
	S10C12	818.2	842.4	231	270	8.4	12.4
	NH1	256.2	14.8	156	54	49.8	5.0
	TL1	685.9	3.75	418	198	13.8	1.0
	FH1	76.1	107.4	14	15	44.2	43.2
	CR1	1351	32.5	605	219	19.4	10.3
Type II	LL1	188.3	113.5	39	24	64.7	38.9
	GL1	6487.3	7501.5	502	546	61.1	62.3
	RC3	8.0	15.0	< 11.46	< 11.46	200.7	158.3
	GEN27	4.0	3.92	< 11.46	< 11.46	331.6	257.6
	CM3	162.3	8.86	65	30	150.2	19.1
	WC1	96.8	65.9	11	< 11.46	105.9	36.3
	ZAG	211.2	265.7	78	72	1031.7	338.0
	LE	344.6	373.7	93	63	83.2	61.2
	CLM	0.7	1.29	< 11.46	< 11.46	77.9	13.7
Type III	CAP1	8.0	15.1	< 11.46	< 11.46	9.5	12.5
	PPgInt2	2.5	3.3	< 11.46	< 11.46	10.2	14.8
	MMG2	244.3	138.8	123	193	19.0	21.3
	Et1317	166.3	149.2	< 11.46	< 11.46	190.7	303.8
	BK2	78.2	128.9	211	24	157.1	191.4
	TC	6.7	12.0	< 11.46	< 11.46	45.0	3.1
Type IV	GcInt2	0.8	< 0.53	< 11.46	< 11.46	86.7	67.9
	IA1	4.2	47.6	< 11.46	84	67.4	25.3
	En19	603.6	97.2	29	21	179.7	107.4
	Et1317	47.2	41.1	< 11.46	< 11.46	30.5	44.9
	BK2	12.2	33.7	< 11.46	< 11.46	50.9	5.7
	RU1	2.9	1.3	< 11.46	< 11.46	52.1	44.8
	TM2	16.2	12.8	< 11.46	< 11.46	47.8	50.5
	FB34	2.6	18.9	< 11.46	12	5.8	44.1
	UI1	6.17	10.2	< 11.46	< 11.46	22.1	23.5
	ETT1	113.84	80.3	104	35	111.1	27.2

Table 8
Click here to download Table: Table 8.docx

Table 8. Rare-earth elements contents in K- and Na-feldspars (ppb) by LA-ICP-MS

	Sample	Yttrium (Y)		Lanthanum (La)		Cerium (Ce)		Europium (Eu)	
		K-feldsp.	Na-feldsp.	K-feldsp.	Na-feldsp.	K-feldsp.	Na-feldsp.	K-feldsp.	Na-feldsp.
Type I	S5C5	< 10	190	520	809	284	543	777	925
	S10C12	< 10	< 10	2827	2219	1256	609	2103	1805
	NH1	< 10	< 10	< 12	12	7	12	258	66
	TL1	10	19	25	< 12	10	8	64	17
	FH1	< 0.01	108	368	541	272	316	273	265
	CR1	15	175	922	649	445	110	892	212
Type II	LL1	758	1152	2586	1431	1507	915	291	200
	GL1	34	79	101	181	37	44	297	298
	RC3	< 10	111	1934	1397	1677	1115	151	61
	GEN27	26	199	706	1663	404	1018	17	18
	CM3	< 10	99	229	229	250	140	215	56
	WC1	< 10	279	2645	2661	2341	2257	301	127
	ZAG	< 10	203	244	165	98	62	203	36
	LE	< 10	151	784	463	459	302	369	184
	CLM	< 10	1793	3060	406	2209	219	24	54
Type III	CAP1	< 10	17	50	24	28	< 7	< 4	< 4
	PPgInt2	13	23	272	150	243	92	< 4	< 4
	MMG2	< 10	255	29	898	19	2020	9	97
	Et1317	21	56	18	113	20	168	4	13
	BK2	< 10	14	177	134	68	53	4	< 4
	TC	< 10	< 10	57	92	65	178	6	< 4
Type IV	GcInt2	< 10	< 10	< 12	< 12	< 7	< 7	< 4	< 4
	IA1	< 10	42	19	107	9	45	16	17
	En19	< 10	22	14	17	< 7	13	17	13
	Et1317	< 10	< 10	12	< 12	< 7	< 7	15	13
	BK2	< 10	36	34	21	19	< 7	34	21
	RU1	< 10	20	< 12	< 12	< 7	8	< 4	< 4
	TM2	< 10	< 10	12	< 12	< 7	< 7	12	< 4
	FB34	< 10	122	60	32	35	38	60	32
	UI1	< 10	< 10	< 12	< 12	< 7	< 7	< 4	< 4
	ETT1	< 10	< 10	< 12	< 12	< 7	< 7	16	< 4

Table 9
Click here to download Table: Table 9.docx

Table 9. Ge, Ga, Fe and P contents in K- and Na-feldspars (ppm) by LA-ICP-MS

	Sample	Germanium (Ge)		Gallium (Ga)		Iron (Fe)		Phosphorus (P)	
		K-feldsp.	Na-feldsp.	K-feldsp.	Na-feldsp.	K-feldsp.	Na-feldsp.	K-feldsp.	Na-feldsp.
Type I	S5C5	0.7	0.7	37.3	34.8	2375	3037	18	16
	S10C12	0.9	0.8	26.2	22.8	860	1004	14	15
	NH1	0.8	0.8	20.8	20.9	155	122	9	12
	TL1	0.8	0.8	40.6	40.7	1830	1121	9	10
	FH1	1.0	1.2	24.5	23.5	427	574	18	11
	CR1	0.7	0.9	27.3	35.1	594	497	12	13
Type II	LL1	3.3	3.4	27.5	25.7	208	203	144	143
	GL1	1.8	1.8	21.4	20.3	113	205	14	8
	RC3	3.0	3.2	27.4	29.4	196	78	18	14
	GEN27	5.6	5.1	45.6	59.0	40	78	16	15
	CM3	5.3	5.1	10.4	12.2	130	10	835	820
	WC1	5.1	5.1	50.8	53.4	98	80	27	20
	ZAG	5.6	6.3	61.5	40	148	150	14	13
	LE	2.8	2.7	22.4	20.8	154	100	39	42
	CLM	11.3	11	35.3	45.8	69	39	16	34
Type III	CAP1	5.2	5.3	20.3	22.7	80	9	1191	871
	PPgInt2	2.6	2.5	20.8	21.8	53	39	853	680
	MMG2	10.1	9.4	14.0	12.8	111	153	4259	3345
	Et1317	7.8	7.1	51.3	44.7	4	146	64	55
	BK2	7.8	8.2	37.1	35.5	70	655	1110	1054
	TC	3.9	3.8	21.5	23.8	44	31	834	898
Type IV	GcInt2	7.4	7.7	21.8	19.2	34	14	835	386
	IA1	6.2	5.1	9.2	10.3	17	109	2483	1203
	En19	30.2	27.1	14.0	16.2	3	151	1271	745
	Et1317	8.0	8.4	17.7	21.5	31	58	2025	567
	BK2	3.9	4.3	15.9	20.9	14	14	2411	1473
	RU1	7.4	7.5	29.4	29.7	28	6	1465	1324
	TM2	9.8	9.4	19.5	22.2	15	11	2532	2202
	FB34	7.7	5.5	17.6	10.4	44	54	5969	5060
	UI1	6.6	6.7	21.5	25.1	8	2	3746	2476
	ETT1	5.4	6.2	9.2	10	5	9	947	431

Figure SM1

Click here to download Background dataset for online publication only: figure SM1.JPG

Figure SM2

Click here to download Background dataset for online publication only: figure SM2.JPG

Figure SM3

Click here to download Background dataset for online publication only: figure SM3.JPG

Table SM1

Click here to download Background dataset for online publication only: Table SM1.docx

Table SM2

Click here to download Background dataset for online publication only: Table SM2.docx

Table SM3

Click here to download Background dataset for online publication only: Table SM3.docx

Table SM4

Click here to download Background dataset for online publication only: Table SM4.docx

Table SM5

Click here to download Background dataset for online publication only: Table SM5.docx

Electronic Appendix 1

Click here to download Background dataset for online publication only: ELECTRONIC APPENDIX 1 optical images.pdf